

**ANALYSIS DESIGN AND DEVELOPMENT OF HAPTIC
INTERFACE FOR HYDRAULIC MANIPULATOR**

**A thesis submitted to the
*University of Petroleum & Energy Studies***

**For the award of
DOCTOR OF PHILOSOPHY
in
*Electrical and Electronics Engineering***

BY

Meera C S

March 2020

SUPERVISOR

Dr. Mukul Kumar Gupta



**Department of Electrical and Electronics
University of Petroleum & Energy Studies
Dehradun-248007: Uttarakhand**

**“ANALYSIS DESIGN AND DEVELOPMENT OF HAPTIC
INTERFACE FOR HYDRAULIC MANIPULATOR”**

**A thesis submitted to the
*University of Petroleum & Energy Studies***

**For the award of
DOCTOR OF PHILOSOPHY
in
*Electrical and Electronics Engineering***

BY

**Meera C S
(SAP ID- 500056860)**

March 2020

Supervisor

Dr Mukul Kumar Gupta
Assistant Professor- Selection Grade
Department of Electrical and Electronics
University of Petroleum and Energy Studies



UNIVERSITY WITH A PURPOSE

**Department of Electrical and Electronics
School of Engineering
University of Petroleum & Energy Studies
Dehradun-248007: Uttarakhand**

March 2020

DECLARATION

I declare that the thesis entitled “**Analysis Design and Development of Haptic Interface for Hydraulic Manipulator**” has been prepared by me under the guidance of **Dr. Mukul Kumar Gupta**, Assistant Professor (Selection Grade) of Department of Electrical and Electronics, University of Petroleum & Energy Studies (UPES). No part of this thesis has formed the basis for the award of any degree or fellowship previously.



Meera C S

Department of Electrical and Electronics,
School of Engineering
University of Petroleum & Energy Studies
Dehradun-248007: Uttarakhand

DATE: **19/8/2020**

CERTIFICATE

I certify that **Meera C S** has prepared her thesis entitled “**Analysis Design and Development of Haptic Interface for Hydraulic Manipulator**”, for the award of PhD degree of the University of Petroleum & Energy Studies, under my guidance. She has carried out the work at the Department of Electrical and Electronics, University of Petroleum & Energy Studies.



Supervisor

Dr. Mukul Kumar Gupta

Assistant Professor- Selection Grade

Department of Electrical and Electronics

University of Petroleum and Energy Studies

Date: **19/8/2020**

ABSTRACT

Sense of touch is one of the important faculties that humans possess. The haptic devices engineer touch based physical interaction and can be used to enhance safety in operational tasks. The operation of mini excavators and small backhoes hold high fatality rates from instability and overturning. The research focuses on transference of the environmental perception to operators and reducing mis-judgement that leads to the accidents through force reflection.

A novel haptic framework is proposed to reduce the errors in operation and alleviate learning. A virtual backhoe simulator is used to evaluate the performance of the system. A complete mathematical model of the 4 degrees of freedom backhoe mechanism, assumed as a robotic planar manipulator is derived. This model is used to develop an insight into the dynamic behavior and joint torques in the system. The digging forces are complex and hence difficult to predict. An observer-based control system is developed to estimate the loading torques to maintain the fidelity in backhoe operation.

An innovative method of actuation is presented for haptic feedback in the proposed interface. The interaction transparency is maintained through rendering force feedback analogous to loading torque of the backhoe. The technical evaluation of the proposed device is carried out in different loading environments developed in dynamic virtual simulator. The kinesthetic feedback from the interface improves the operator awareness of system limitation and also maintains learning and ergonomics. Extensive human subject experiments are presented to validate the operator assistance system in loading operations. The study has resulted in a new haptic framework that can be used in a variety of manipulators where safety and efficiency of operation is critical.

ACKNOWLEDGMENT

I would like to thank all of the people who encouraged and supported me as I was undertaking this research. Firstly, I would like to thank my advisor Dr. Mukul Kumar Gupta for his continuous guidance and encouragement. Working under your mentorship has been a privilege and inspiration. I would like to thank Dr. Santhakumar Mohan for the invaluable advice and motivation for my research. His support for my PhD work has been invaluable.

A special thanks to Associate Dean Research Dr. Jitendra Kumar Pandey for supporting me throughout the journey. I would like to mention my gratitude to the HOD and the faculty colleagues, Electrical and Electronics Engineering department for the motivation and cooperation. A special thanks to group members of Centre for Robotics and Control, IIT Indore for their insightful comments during various discussions. I would like to acknowledge in-house Bosch Centre of Excellence and Robotics and Sensors lab at UPES Dehradun where I have carried out my experiments.

Many thanks go to Dr. R. Gowri, Dr. N.Prasanthi , Dr. Amit Kumar Mondal and Dr. Deepak Bharadwaj for encouraging me at various stages of research work. Special thanks go to Ms. Aslesha Bodavula for being a great friend and for the long walks. I would like to express my thanks to my friends and colleagues: Caneon Kurien, Debajyothi Bose, Siva Prasanna, Varnita Verma, Shikhar Purohit, Ravi Kumar Patel, Krishnamoorthy and Balaji for the insightful discussions and invaluable support throughout my Ph.D. journey. It has been a pleasure working with all of you. Thanks to my loving friends Ms. Kamala Mahadevan and Ms. Laxmi SV for being there for me when I needed support. Thanks go to Durga Dutt and Rohit Sankaria for the technical support. Special thanks to Alex, Kashyap, Vineeth and Adarsh for the support in my journey.

I would like to express my gratitude to my parents Chitra Sreedhar and Sunil S for their endless love and encouragement. I would also like to give a big thank you to my grandparents, Indira Devi, Vijaya Kumari, SSPRS Rao and SSP Devi to always

boosts my confidence. I am grateful to my in laws, P. Satyanarayana and P.Lalita for always being so understanding. Finally, I want to thank my beloved husband, Swami Sairam for being the source motivation throughout my research. Without your continued support I could never have accomplished so much.

To my family

TABLE OF CONTENTS

DECLARATION	III
CERTIFICATE	IV
ABSTRACT	V
ACKNOWLEDGMENT	VI
CHAPTER 1: INTRODUCTION	1
1.1 MINI EXCAVATION MACHINERIES	1
1.2 MOTIVATION	4
1.3 THESIS SCOPE AND PROPOSED APPROACHES	5
1.4 PRINCIPLE CONTRIBUTIONS	6
1.5 THESIS OVERVIEW	7
CHAPTER 2: LITERATURE REVIEW	9
2.1 OVERVIEW	9
2.2 HAPTIC INTERFACES IN EXCAVATION	11
2.4 SIMULATOR TEST BED	19
2.5 SUMMARY	22
CHAPTER 3: MODELLING OF ROBOTIC BACKHOE	23
3.1 BACKHOE KINEMATICS.....	23
3.1.1 FOREWARD KINEMATICS	24
3.1.2 INVERSE KINEMATICS	26
3.1.3 RELATION BETWEEN JOINT SPACE VARIABLES TO CYLINDER SPACE VARIABLES	28
3.2 BUCKET FORCE TO LOADING TORQUE.....	31
3.3 BACKHOE DYNAMICS	32
3.5 SUMMARY	33
CHAPTER 4: CONTROL OF ROBOTIC BACKHOE	35
4.1. LOADING TORQUE ESTIMATION	35
4.2 DESIGN OF THE CONTROL SYSTEM	37
4.3 SOIL TOOL INTERACTION MODEL	40
4.3 SIMULATION STUDY AND RESULTS	42

4.4 CO-SIMULATION ANALYSIS AND RESULTS	47
4.5 SUMMARY	52
CHAPTER 5: INTUITIVE JOYSTICK INTERFACE	53
5.1 INITIAL DESIGN	53
5.2 HAPTIC INTERFACES IN EXCAVATION	55
5.3 HAPTIC JOYSTICK	56
5.3.1 DESIGN AND CONSTRUCTION	57
5.3.2 VARIABLE STIFFNESS ACTUATION	60
5.4 ANALYSIS	62
5.5 SUMMARY	64
CHAPTER 6: VIRTUAL SIMULATOR AND HAPTIC EVALUATION	65
6.1 DYNAMIC BACKHOE SIMULATOR.....	66
6.2 SIMULATOR DYNAMICS	68
6.3 FORCE FEEDBACK EVALUATION.....	70
6.4.1 PERFORMANCE METRICES	73
6.4.4 TASK DESCRIPTION	74
6.4.5 PROCEDURE	75
6.5 RESULTS	76
6.5.1 SAND LOADING EXPERIMENTS	76
6.5.2 ROCK LOADING EXPERIMENTS	78
6.7 SUMMARY	83
CHAPTER 7: CONCLUSION AND FUTURE WORK	85
7.1 CONCLUSION.....	85
7.1 CONTRIBUTIONS	86
7.2 FUTURE WORK.....	87
REFERENCES	90
APPENDIX A	107
A.1 DYNAMIC MODELLING OF ELECTROHYDRAULIC SYSTEM	107
A.1.1 HYDRAULIC CYLINDER MODEL	107
A.1.2 SERVO-VALVE MODEL	108
APPENDIX B	110

APPENDIX C	117
JOURNAL PUBLICATIONS	121

LIST OF ABBREVIATIONS

AERB	:	Atomic Energy Regulatory Board
CTC	:	Computed torque controller
CAD	:	Computer Aided Design
DH	:	Denavit Hartenberg
DOB	:	Disturbance Observer
DOF	:	Degree of Freedom
EHS	:	Electrohydraulic systems
EOM	:	Equations of motion
FB	:	Feedback Controllers
FC	:	Feedforward Controllers
FEE	:	Fundamental Earthmoving Equations
FFB	:	Force Feedback
GPU	:	Graphical Processing Unit
HFJ	:	Haptic Feedback Joystick
HIL	:	Hardware in loop
HMI	:	Human Machine Interface
NdFeB	:	Neodymium magnet
NFJ	:	Non Force-feedback Joysticks
RMS	:	Root mean square
SD	:	Standard Deviation
SMA	:	Shape Memory Alloy
VE	:	Virtual Environment
VR	:	Virtual Reality

LIST OF SYMBOLS

O_i	:	origin of i^{th} coordinate system
a_i	:	length of link i
θ_i	:	Joint Angles
d_i	:	Joint Twist in link i
α_i	:	Joint offset of link i
A_i^{i-1}	:	homogenous transformation of frame $\{i\}$ with respect to frame $\{i-1\}$
P_i	:	position coordinates in the i^{th} coordinate frame
c_i	:	$\cos\theta_i$
s_i	:	$\sin\theta_i$
l_{ij}	:	distance between points i and j
J	:	Jacobian Matrix
F_l	:	Bucket forces
τ_a	:	Loading torque
τ_i	:	torque on joint i
$\theta_i, \dot{\theta}_i, \ddot{\theta}_i$:	angular displacement, velocity and acceleration of joint i
$M(\theta)$:	Pseudo inertia matrix
$H(\theta, \dot{\theta})$:	Coriolis and centrifugal forces
$G(\theta)$:	Gravity matrix
p_i	:	load-pressures of the hydraulic cylinder
A_i	:	Area of the cylinder
Q_i	:	Load flow to cylinder
V_{ij}	:	Total volume of the cylinder chamber
β_e	:	Bulk modulus
C_{tl}	:	Leakage coefficient
m	:	Load mass on piston
b	:	Coefficient of viscous damping
k	:	Spring constant

p_s	:	Supply pressure
p_t	:	Tank pressure
p_r	:	Return pressure
θ_{dg}	:	digging angle
θ_b	:	angle between bucket bottom and X4 axis
F_r	:	Soil reaction force
F_n	:	normal components of reaction force
F_t	:	tangential components of reaction force
C_d	:	Discharge coefficient
w	:	Area Gradient
ρ	:	Discharge coefficient
x_v	:	spool position
K_s	:	servo valve gain constant
u	:	control voltage
K_p	:	proportional gain
K_d	:	derivative gain
K_0	:	observer gain
h_t	:	sensor threshold value
F_r	:	range of force value

LIST OF FIGURES

Fig 1.1. Mini backhoe loader	2
Fig 1.2. Mini excavator overturn	3
Fig 1.3. Loading chart and visual warning device in excavators	3
Fig 2.1. Haptic interface	13
Fig 2.2. Haptic backhoe test-bed.	13
Fig 2.3. Excavator simulator platform aided with a haptic interface.	20
Fig 2.4. Delta3D platform based dynamic excavator simulator	21
Fig 3.1. Coordinate frame arrangement along with joint angle representation of the robotic backhoe.	24
Fig 3.2. Bucket orientation	28
Fig 3.3. Excavator coordinate frames	29
Fig 4.1. Control system proposed for the hybrid control of the robotic backhoe	38
Fig 4.2. Design of the proposed disturbance observer.	40
Fig 4.3. Soil-bucket interaction during digging	41
Fig 4.4. Desired digging trajectory for the robotic backhoe	43
Fig 4.5.(a),(b),(c): Time profile: Position tracking time profile for the boom, stick, bucket joints in one dig cycle of operation.	44
Fig 4.6.(a), (b), (c): Time profile: Position error time profile of the boom, stick and bucket joint in a digging cycle of the robotic backhoe.	45
Fig 4.7.(a), (b), (c): Joint disturbance tracking time profile of the boom, stick and bucket joint of the robotic backhoe.	46
Fig 4.8 (a),(b),(c): Disturbance error time profile of boom, stick and bucket joint in the soil-contact task of a robotic backhoe.	47
Fig 4.9. Co-simulation experiment of robotic backhoe in MATLAB/ Adams platform. The top image shows the model developed in Simulink. The bottom image shows the digging operation during co-simulation by the robotic backhoe.	49
Fig 4.10.(a), (b), (c): Loading torque estimation time profile of the boom, stick and bucket joint in the co-simulation experiment.	50
Fig 4.11.(a), (b),(c): Position tracking of boom, stick and bucket joint of the robotic backhoe in the co-simulation experiment.	51
Fig 5.1. The proposed design of the initial prototype.	54
Fig 5.2. SAE Pattern for Motion Control	57
Fig 5.3. The haptic link design:(a) Shaft link front view showing the hall sensor-magnet arrangement(b)Shaft link rear view.	58
Fig 5.4. The dimension of haptic link with sensor arrangement. The force would be applied from the joystick through the uncut side of the link which would change the sensor-magnet alignment.	59
Fig 5.5. The schematic design of the Haptic joystick	59

Fig 5.6. User torque detection to activate variable stiffness feedback	60
Fig 5.7. Flowchart presenting the variable stiffness actuation in haptic joystick	61
Fig 5.8. Variation in joystick current with different digging forces	62
Fig 5.9. The variation in joystick torque and angle with loading	63
Fig 5.10. Final prototypes of the haptic joysticks	64
Fig 6.1. Correlation between various elements in the haptic framework.	66
Fig 6.2. Simulator environments made for sand loading	67
Fig 6.3. Rock loading environments made in VR simulator	68
Fig 6.4. Different operator perspective for the rock loading operation.	68
Fig 6.5. The modified soil tool model.	70
Fig 6.6. Block diagram representing system architecture.	71
Fig 6.7. Commanded joint angle positions and the responses from the simulator.	72
Fig 6.8. Digging forces at the bucket tip and loading torques estimation at the joints.	73
Fig 6.9. Human subject experiments with the developed haptic joystick.	76
Fig 6.10. Avg. amount of material in bucket. Error bars show standard deviation.	77
Fig 6.11. Collision experiments with the two interfaces.	78
Fig 6.12. Box plot showing the piles dropped outside the bin	79
Fig 6.13. Box plot showing the mean of the excess force applied during the trials	80
Fig 6.14. Box plot showing the mean volume of load in bucket during the trials.	81
Fig 6.15 Subjective rating comparison for the interfaces.	82
Fig A.1 The configuration of EHS.	82

LIST OF TABLES

Table 2.1. Interactive hand controllers explored in excavator applications	15
Table 3.1. The DH parameter representation of the robotic backhoe	24
Table 4.1 Parameters of the robotic backhoe used in study.	42
Table 4.2. RMS Error: Position and Disturbance tracking.	52
Table 5.1. Specification of Hall sensor and Neodymium magnet	58

CHAPTER 1: INTRODUCTION

A haptic interface is a robotic device that uses force reflection to enable user interaction with a virtual or remote environment. The interfaces enable basically a force (or touch) feedback that allows realistic sensations to the user from computer simulations. The haptic cues or the touch stimulus can influence user's judgements, behaviour and attitudes [1][2] and can raise the learning outcomes and motor skills in users. The objective of the thesis is the development of a novel haptic framework that addresses operational safety in mini excavator/backhoe.

1.1 MINI EXCAVATION MACHINERIES

The small earth moving machineries like mini excavators and small backhoes are widely used for construction and agricultural activities due to small size, versatility and reduced costs. These machineries are lighter and compact and normally weigh typically less than seven metric tons [3]. With the great mobility and versatility they are also used in digging, landscaping and other utility works. However, safety hazards are associated with the operation of these mini excavators are quite high. The hazards not only lead to human casualties but also has a negative commercial effect on the excavator industry.

Safety challenges

According to Atomic Energy Regulatory Board (AERB) India, excavation is classified as one of the most hazardous construction operation [4]. The highest number of accidents occurred in Indian agricultural fields is also reported from farm machineries (31%)[5]. The work injuries and fatalities for excavation work is 112% higher compared to general construction. In Great Britain 20% of all death in workplace transport occurred due to machine overturns [6][7]. In 2014 from the data of US Bureau of Labor Statistic 18% of the fatal injuries in construction

industry is caused from ‘contacts from objects and equipments’ [7]. A mini backhoe manipulator is shown in Fig 1.1.



Fig 1.1. Mini backhoe loader

Safety hazards in excavators is mostly caused the machines loosing stability leading to machine overturn as shown in Fig.1.2. The stability is a function of machine's centre of gravity. Rapid change in centre of gravity may arise due to improper, uneven or overloading. As for smaller machineries, the situation is aggravated with their narrow width and varying centre of gravity and dynamic forces while performing the work[3]. The machine operation directly depends on operator commands to interact with the unstructured environments. There are many cases where the operator's misjudgment or misperception about the system limitations led to accidents. The rate of mini excavator/backhoe overturn are high and presents high safety and health risk to person, property and machine[8].

The operator uses visual feedback and senses the machine vibration for direct control. However, blind spot leads to visibility issues and has been one of the leading reasons behind accidents. Blind spot restricts the operator view and are mostly the result of equipment configuration which is inevitable [9].



Fig 1.2. Mini excavator overturn [3]

Many of the excavators are currently provided with visual indicators (overload warning device) or loading chart as shown in Fig 1.3. The overload warning devices on the excavator is not a rated capacity indicator.

LIFT POINT HEIGHT		RATED LIFT CAPACITY OVER BLADE, BLADE DOWN - kg (lb)			RATED LIFT CAPACITY OVER BLADE, BLADE UP - kg (lb)			RATED LIFT CAPACITY OVER SIDE, BLADE UP - kg (lb)		
		LIFT RADIUS - mm (in)	LIFT @ MAXIMUM RADIUS - kg (lb) @ mm (in)	LIFT @ MAXIMUM RADIUS - kg (lb) @ mm (in)	LIFT RADIUS - mm (in)	LIFT @ MAXIMUM RADIUS - kg (lb) @ mm (in)	LIFT @ MAXIMUM RADIUS - kg (lb) @ mm (in)	LIFT RADIUS - mm (in)	LIFT @ MAXIMUM RADIUS - kg (lb) @ mm (in)	LIFT @ MAXIMUM RADIUS - kg (lb) @ mm (in)
4300 (157.5)		902 (1767)	967 (1911) @ 4315 (165.9)	796 (1688)	929 (1828) @ 4315 (165.9)	839 (1855)	918 (2024) @ 4315 (165.9)			
3000 (118.1)		815 (1798)	918 (2024) @ 4947 (194.8)	782 (1724)	748 (1644) @ 4947 (194.8)	861 (1898)	633 (1395) @ 4947 (194.8)			
2000 (78.7)		1214 (2670)	973 (2146)	1167 (2572)	979 (2159)	725 (1599)	666 (1467) @ 5246 (206.5)	1248 (2750)	1048 (2311)	608 (1340)
1000 (39.4)		1885 (4155)	1315 (2898)	1078 (2376)	1029 (2288) @ 5246 (206.5)	1790 (3947)	1941 (4296)	635 (1409) @ 5246 (206.5)	1370 (3020)	865 (1906)
Ground		2288 (4999)	1530 (3372)	1169 (2578)	1106 (2437) @ 5149 (202.7)	1615 (3560)	1009 (2225)	693 (1527)	655 (1445) @ 5149 (202.7)	1307 (2881)
-1000 (-39.4)		3012 (6639)	2372 (5230)	1559 (3459)	1209 (2663) @ 4738 (186.5)	2909 (6433)	1557 (3432)	989 (2180)	737 (1635) @ 4738 (186.5)	2532 (5581)

* Rated Hydraulic Lift Capacity



Fig 1.3. Loading chart [11] and visual warning device [12] in excavators

They are calibrated in cross carriage (cross carriage) and when machine operates in line with the tracks alarm gets turned on before the maximum rated radius for the load being picked up [10]. This may lead to operator frustration. Also, the lift charts are valid for machine operation on level ground.

1.2 MOTIVATION

Operators play a key role in guarding the machine safety. Operator performance decides the productivity and overall machine utilization. However, the machine control is complex and often requires the operator to be an expert to be aware of machine limitation. There are several practical challenges in the operation of excavators. Operator commands the machine directly using hand controllers. Conventionally manual levers and pedals were used and later got evolved to electronic control with joysticks. Joysticks interfaces are easier to use, less fatiguing and ergonomically pleasing to operators compared to levers and pedals.

However, the joysticks cannot provide feedbacks related to machine interaction unlike levers and pedals that are directly connected to machine through mechanical connection. When bucket force rises, the operator can detect a rise in lever resistance. The feedback can alert an expert operator to react quickly preventing damage. Electronic controls in joysticks decouple the machinery from operator, and this inhibits the feedback. The operator's lack of skills arising from poor judgement of bucket forces may lead to manipulator instability and accidents.

To prevent damage the operator requires high skill and intense concentration. The operators normally take a several years to become proficient. Typically, the operational tasks last for several hours and operators are vulnerable to errors and misunderstandings. This brings new possibilities for improving the design of user interfaces with infusion of haptic feedback. A sense of bucket forces and loading limit feedback to operator through intuitive interfaces can enhance safety. The task dependent characteristics of interfaces can provide an intuitive feedback that can mitigate operator errors.

The objective of the thesis is to develop a novel haptic platform implemented through joysticks that can alleviate the learning and minimize operator errors. The

study covers the interface design, associated control law development and the development of software environments for experimental validation.

1.3 THESIS SCOPE AND PROPOSED APPROACHES

The research objective of implementing haptic framework for an achieving a better operator efficiency can be divided in to three parts; design of the hardware, developing the control laws and implementing in virtual environment for validation. Though various technologies have been demonstrated for backhoe control, for years the industry follows bimanual operation with mostly joysticks. The proposed interface combines haptic feedback to the conventional design of joysticks for preserving ergonomics and learning.

Design of the Haptic Joystick

The operator perception can significantly impact the performance. Therefore, haptic illusion is generated from the loading forces arising from payload variations. Force reflection along with motion control is proposed to enhance the overall safety. Generally, in force feedback (FFB) joysticks the cost depends on the actuation technology and the mechanical parts imparting haptics are high. An important design criterion to be maintained is that the failure of the haptic element should not compromise the control aspect of the joystick interface. The joysticks should have a safe design and reliable actuation. In the proposed interface, the kinesthetic feedback is applied to joystick axis through four custom made links. The feedback force is modulated through combination of actuators and sensors. The braking torque is generated in specific direction of joystick motion.

Development of the Control System

The haptic control law should estimate the loading torque regardless of the nature of the bucket interaction with the working environment. The uncertainties and disturbances arising from the interacting environment is dynamic and hence cannot be measured accurately. The torque/force sensors are costly and there are practical limitations to attaching the sensors to the tool tip. The direct loading force measurements is often difficult, and this affects the fidelity of device.

The requirements in this study suggest a control system that do not depend on direct measurement of interaction forces and yet tracks the loading torques effectively. A certain control system is adopted as a solution and the proposed model is validated with extensive simulations and collaborative simulation experiments. The model considered do not include actuator dynamics to reduce complexity.

Validation of Haptic Framework

A virtual reality (VR) backhoe simulator is developed as test bed for the validation of the haptic joysticks and the control law. The overloading is determined through including physics of the reaction from ground induced due to loading. The excavation forces are predicted using the fundamental modelling equations. Also, real time interactivity is maintained using the high quality of visual representation of terrain. Extensive experiments are carried out to validate the haptic joystick performance on simulator platform. The objective is to identify if the methodology adopted contributed to a better intuition and a quality of performance both of which are very likely to contribute to reduced dependence on one's skill.

1.4 PRINCIPLE CONTRIBUTIONS

The principle contribution of this research work is the development new haptic joysticks that can carry out an intuitive interaction between a robotic backhoe and an operator and improve safety perception. The research aims in providing a novel haptic modality in the joysticks for the operators, especially novices, to lower the dependency on one's skill. The key contributions include:

- Presentation of a formal and systematic method of obtaining mathematical model, both kinematic and dynamic of excavator in digging.
- Development of a hybrid control system that can be used to estimate the effect of bucket forces. The derivation and stability analysis of a disturbance observer for estimating the joint disturbance without the need of large feedback gains. The observer is based on joint velocity, this can be used widely in other robotic manipulators.

- Design of a new haptic rendering mechanism actuated through variable stiffness based on lading torque and necessary algorithm the activation of haptic modality.
- Development of virtual simulator environment and detailed evaluation of the haptic interface in transferring in-situ perception. The dynamic simulator represents excavation operation with effective calculation methodology.

1.5 THESIS OVERVIEW

A short overview of the chapters following this introduction is presented below.

- **Chapter 2:** The chapter discusses background reviews of haptics interfaces explored for excavator control. The advantages and limitations of the mechanisms are studied to understand how the particular interfaces contributed towards fidelity of the systems. The chapter also examines various FFB approaches in control laws with haptic interfaces. A brief review about various virtual test beds used for haptic interfaces in excavator control is also presented.
- **Chapter 3:** The mathematical modelling of a backhoe mechanism is presented in the chapter. Relevant equations are developed using the theory of robotics kinematics and dynamics. Denavit-Hartenberg (DH) guidelines and geometrical approaches are used for deriving the kinematic model. The dynamic model of the backhoe is derived using well known Lagrangian equations of motion. This model serves as an effective means to compute joint torques and also to develop control strategies. An insight into the modelling of hydraulic system in excavators are presented as well.
- **Chapter 4:** The significance of loading torques in the system is addressed and presents the development of an observer based hybrid control system. The stability of the observer is proved with Lyapunov stability criterion. The proposed observer estimates loading torques from digging force and can be used in the compensation of loading disturbance for motion control approaches. Extensive simulation and co-simulation results are presented as validation.

- **Chapter 5:** The chapter explains the design and development of the haptic joysticks . The first part presents the previous approach adopted, its limitation and brief review on actuation technologies in haptic joysticks. The second part deals with the physical design and algorithm rendering haptic feedback.
- **Chapter 6:** The technical and user evaluation of the haptic joysticks and control laws with human subject experiments is described. The evaluation is performed on loading environments developed on dynamic virtual simulator. Different performance matrices are evaluated, and results are presented. The objective of the experiments is to determine whether the proposed framework reduces the operator errors and affects the perception of safety.
- **Chapter 7:** The final chapter summaries a general conclusion and recommendations for future works.

CHAPTER 2: LITERATURE REVIEW

This chapter gives an overview of the previous studies that are categorised in to three main areas, first it gives an overview of the various haptic interfaces that have been used in excavation. This discusses both commercial and academic research based hand controllers that have been used to explore haptics in excavation. Second, the various techniques used to render FFB in the haptic devices are discussed. Finally, the various testbeds used for the evaluation of the haptic control of excavator/backhoes is discussed.

2.1 OVERVIEW

The term haptics originated from the Greek verb “haptesthai” meaning ‘of or relating to the sense of touch’[13]. It deals with sensing and manipulation of environment through touch. As far as the mechanism of ‘touch’ goes it can be made by man, machines or combination of both. The technology brings a bidirectional flow of energy and information between the user and environments. This is referred to as ‘active touch’. The sense of touch is recreated through force, motion or vibrations where the user can feel a remote or a virtual object indirectly [14]. This requires a bi-directional flow of information between the user and environment. The devices with haptic feedback are highly prevalent in several fields like surgery[15], automobiles [16], education, defense and tele-robotics [17] [18] and space exploration.

Human haptics is made of cognitive, motor-sensory and mechanical components. It relates to contact manipulation and human-sensory perception. Two types of information are relayed through human haptics: tactile and kinesthetic. The former is the acquiring of information by sensors connected to user’s body and the latter is the acquiring of information by sensors in joints. Upon touching an object the skin receives the interaction forces. The interaction forces convey the perception of the physical world. As a result brain cells activates the muscle which causes the movement. Human haptics thus makes a

closed loop between the physical world and the humans with aspects related to touch.

Machine haptics deals is about devices that exchange information with humans with physical contact. Generic force through actuators would be measured by sensors. Computer haptics includes algorithms that are involved in generation and rendering of touch of virtual objects and environments. In computer haptics, the information from virtual environment (VE) to user is relayed through haptics and visual rendering. Detecting point of contact and the force of interaction between VE and user is relayed through haptic rendering. Visual rendering uses mathematical modelling techniques to compute real time behaviour of VE graphics .

The crucial element in a haptic device is the actuator. The actuators apply forces for the replicate sensation of touch. Based on electrical stimulation, the actuator produces a mechanical motion. Earlier rendering of haptic feedback was implemented through electro-magnetic technology. The electro-magnetic motors provided strong feedback sensations and operate at resonance. However, the method could produce only fewer sensations. The responses from the device were limited as the vibratory sensations were relayed from the entire device rather than from an individual part. In the next generation, 'micro chips' were used and haptic rendering was localized and was specified to a location. The actuators however worked on electro-magnetic principle. Here in this attempt, range of response was increased than the first attempt and the response time was brought down to 5-15 milli sec from 35-60 milli sec. The next stage of haptic rendering used the concept of 'reverse electro-vibration' and implemented fully customizable touch specific response. In this concept a sensation is created with a weak current from haptic device on the user's fingertip. The technique uses the interaction of oscillating electric field around the fingertip skin. The current trend utilizes most advanced concepts and utilizes pressure sensitivity where the response is proportional to the amount of force applied.

2.2 HAPTIC INTERFACES IN EXCAVATION

Haptic interfaces have widely been explored in excavation and other earth moving machineries. Mostly haptic interfaces have been used in overcoming the complexity of operation in excavator backhoes as the machine controls are difficult to master. The benefits of intuitive control have led researches to explore tele/remote operation with excavators. Haptic devices gives the ability to perform tasks with the machinery without actually exposing the operators to the dangers of operating environment. Interfaces with haptic feedback can simultaneously exchange information between operator and the machinery[19]. The transparency in haptic devices increases the operator understanding of realism of virtual or remote environment. Transparency relates how precisely the interface displays the forces from virtual or remote environment. Considering the complexities in the operation of excavators/backhoes the operators could definitely benefit from force reflection. Over the years haptic researches explored in context to various excavator applications and their potential benefits are summarized below.

Some of the earlier attempts of FFB in excavation was first implemented by Starzewski and Skibniewski in 1989[20]. They developed a prototype of master slave FFB manipulator that would enable the joint-level FFB when the end tool applies force on an object. This new tool were provided as an additional feature that would enhance the flexibility in the machines.

A patent on FFB mechanism based on the load being applied was received by Caterpillar Inc[21]. Here the actuator applies force to the control lever proportional to the load being applied thereby providing the feel to the operator. Considering the toxicity of waste, the nuclear industry have also explored the FFB excavators for uncovering and removal of waste [22]. Most of the works carried out in nuclear industry were using tele-operated excavators in different levels of force feedback.

Haptics in excavator was experimented by Lawrence et al using a 6-DOF magnetically levitated (maglev) joystick and demonstrated that FFB helps in

the application of controlled forces[23]. The tasks were completed faster when the force information was relayed back to the operators. Even novices operated the machine more readily than with standard controls. Parker et al presented the implementation of magnetically levitating joystick as the ‘force reflecting master’ on a heavy duty hydraulic machinery[24]. The experiments showed the stiffness feedback to be much more effective than rate control for direct force feedback. Hadank et al proposed an intuitive control interface for excavator control[25]. Two joysticks were proposed as control interfaces where right joystick controlled the horizontal, vertical and bucket movements. Left joystick controlled the swing movement with one axis. The object of the study was to address the stress and fatigue in operators.

Danko et al proposed a control system that can correct the position error in the end-effector movements along the preselected trajectories[26]. The context used two joysticks for speed and direction control and cutting angle along pre-selected trajectories. However diverse working environments pose limitation in the working of control system. A 6DOF FFB device in tele-operated excavators were proposed by Salcudien et al The master device controlled the excavator position and was capable of providing joint level force feedback in rate mode[27]. However, in order to maintain stability the sensed end-effector forces were controlled. To improve transparency in tele-operated excavator an impedance based control scheme was proposed by tafazoli et al [28].

Researchers from the Universidad Politecnica de Madrid developed certain methods for the teleoperation of a backhoe excavator using bilateral control methods with FFB, as shown in Fig 2.1[29]. The objective was to provide the operator an easy way to operate.

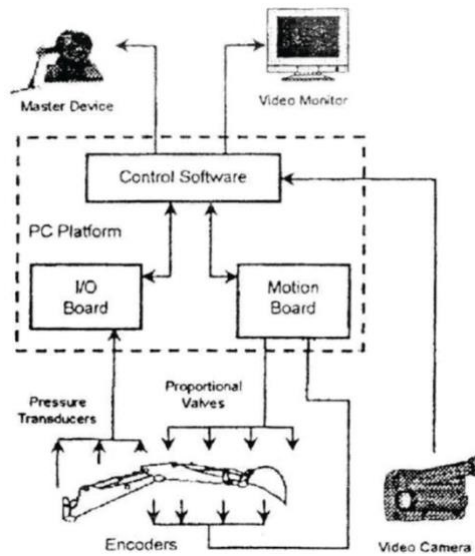


Fig 2.1. Haptic interface[29]

Commercial haptic devices have been explored in backhoe applications. One of the popular haptic devices explored with excavator applications is PHANTOM. The haptic device is capable of a six degree of freedom (DOF) positional-sensing and three DOF FFB. Much of the notable work has been conducted at Georgia Tech using PHANTOM device. In 2002, Frankel et al developed a haptic test rig for studies using a small backhoe as shown in Fig 2.2 [30].



Fig 2.2. Haptic backhoe test-bed [30].

The study was intended for programming controller and haptic interface for a robotic backhoe.


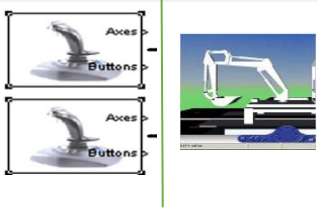


Kontz et al explored haptic algorithms in small sized backhoes to maximize the operator performances [31]. Load cell, load pins and position sensors were mounted on to the backhoe. Various measures like digging productivity, detection and force on buried objects were analysed using human factor tests. A Geomagic PHANToM Premium haptic device was compared against conventional interface by Elton et al. to compare the operator performance [32]. Though experiments revealed performance improvement however identified certain problems with the PHANToM device for excavator control. Lack of comfort in operation and sensitivity for small motions were identified as some of the issues.

Kim et al proposed a more intuitive means of controlling an excavator by attaching the sensors to operator's arm [33]. The sensor signals are transmitted as operating commands and excavator arm moves in alignment to the operator's arm. However, this method needs recalibration depending on the body sizes of the operators. Also, the method may cause fatigue when the operation has to be performed for a long time. Dongnam et al developed a newly designed haptic-interface using pressure transmitters for excavator control [34]. The system uses pressure transmitter to estimate the related forces in the system. The 4 DOF device uses inverse kinematics equations to calculate the position of boom and stick and lets the user control the excavator interacting with the end part of the interface.

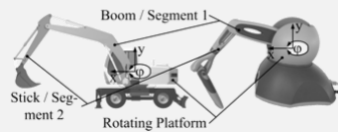
A master-slave operation of a mini excavator with grapple and sensory perception was carried out by Yamada et al [35]. The test rig consisted of a FFB joystick as the master and the mini excavator as the slave. The FFB joysticks were used to operate the grapple. Yusof et al, conducted studies on operator sensitivities to different modalities of visual, audio and force feedback in construction robots [36]. By observing the FFB graphically and audio signals combined with reaction torques from joysticks increased the operator performances. The results showed that operators could distinguish between the force variations and improve safety perception as well [36][37]. Table 2.1 summarizes some of hand controllers explored in excavator applications

The combination of Hardware in loop (HIL) simulation and haptic joysticks for the control of virtual excavator simulator was explored by Nam et al[38] . The haptic joysticks employed were based on Magnetorheological (MR) fluid. To reflect the non-linearities and dynamics of the excavators, hydraulic system hardware were incorporated with simulation software. The results showed the concept to be close to reality addressing nonlinearities.

Table 2.1. Interactive hand controllers explored in excavator applications

Hand Controllers	Image	Features
<p>Novint Falcon</p>	 <p>[39]</p>	<ul style="list-style-type: none"> • 3DOF ,translational mechanism • Feedback force upto 8.9N • Need to use 2 HI to feel the movement of remote end effector • Improved performance with the HI compared to joystick and glove interface.
<p>Intuitive User Interface</p>	 <p>[40]</p>	<ul style="list-style-type: none"> • Independent control of horizontal and vertical motion • Natural and intuitive operation • Inexpensive and less complex • No FFB
<p>PHANToM Premium 1.0A</p>	 <p>[41]</p>	<ul style="list-style-type: none"> • Implements coordinated control • 6 DOF device with 3 DOF spherical wrist • Programable force feedback • Resembles real operation
<p>Novel Design for Haptic Devices</p>	 <p>[34]</p>	<ul style="list-style-type: none"> • Cost effective, simple and light weight • Requires only one hand operation for the main links except swing • Grater operator comfort as human arm can rest on device

**SensAble
PHANToM
OMNI**



[42]

- HI geometry resembles to the hydraulic arm
- Used in bilateral position control
- Gives haptic feedback of the position of boom hyd cylinder.

Yoon and Manurung proposed an interesting approach of intuitive control with two electronic joysticks using cylindrical robotic concepts[40]. They used a joystick mapping method which allowed independent bucket control. Each joystick could perform independent vertical and horizontal motions. The user studies demonstrated reduced task completion time with increased accuracy. The excavators volume of motion in three dimension can be reduced to two dimension as the swing motion of the cab is operated less with the other three motions in activities like digging. This idea has led to the development of certain intuitive devices.

Hayn et al split the total excavator control using two separate devices; a rotatory knob for the cabin rotation and another operating element capable of controlling the bucket tilting and translation of tool centre[43]. Also, an interface kinematically similar to excavator arm was designed by Winck et al to enhance operational capabilities in excavators[44]. The swing motion was controlled separately using a separate joystick. The experiments were conducted by mounting the device in two configurations; horizontal and vertical both of which showed benefits in operation.

Morosi et al proposed a control logic for the control of excavators for reducing cognitive effort in operators[45]. The control scheme was demonstrated with Haptic Master as main interface to provide FFB and a rotary knob to ensure cab control. The experiments were performed compared to a conventional joystick configuration. The results verified a significant increase in the intuitiveness especially related to bucket rotation compared to conventional joysticks.

2.2 FORCE FEEDBACK

Haptic interfaces render FFB from virtual/remote environments which enhances a sensation of reality in the user. In case of virtual environment haptic devices enable user interaction through force/torque transmission. With the visual feedback from virtual environment errors are evaluated with respect to the desired values. There are two basic methods that are used widely in the design of haptic interfaces: admittance and impedance control.

In admittance control, the force exerted by the user on the device is measured and based on the target system, a motion output is produced. The manipulator would include force sensors which measure force input and generate a motion output. The haptic devices employing admittance control can be employed with transmission mechanisms like gears. The devices can generate high stiffness; however, losses in the transmission mechanism is to be considered.

In impedance control the motion input from user is measured and force from the target system is fed back. Position sensor in the device senses motion and generates a force input. The commercial haptic devices like Phantom, Falcon and Omega are impedance type devices. The haptic devices with impedance control need to be back drivable.

Various researches have proposed impedance and admittance control in haptic control of excavators. Using admittance controlled haptic device Haptic Master, a control logic to reduce cognitive effort of the operator is demonstrated [45], [46]. An impedance and admittance type haptic controller was implemented by Carignan et al., to investigate the quality of haptic feedback in VR operations [47].

DiMaio et al employed an impedance control model in a simulator with a haptic device[48]. The purpose was to analyse the training performance in operators and evaluate control strategies. Toreres-Rodiquez et al proposed an excavator training with a force position control algorithm and haptic interfaces [49] . The research study by Wen et al, demonstrated haptic device dynamics induce

significant errors in open loop force control [50]. The experiments were demonstrated with a haptic device interaction with virtual environment.

An adaptive impedance based control system to enhance operator performance was proposed by Suzuki et al [51]. The control system tunes the impedance of the virtual model based on operator characteristics. For impedance haptic devices when workspace is similar to or greater than the human arm, the inertia the operator feels is more. The method of reducing inertia felt by users is proposed by Juan Gil [52]. The method was demonstrated on a LHifAM haptic-device. In haptic based tele operation impedance and admittance based force control techniques were proposed [53][54][55]. The studies were aimed at enhancing reflection in tele operation. A 6 DOF admittance based haptic display, Cobotic Hand Controller was demonstrated by Eric L. Faulring [56]. An impedance based force control for a 6 DOF parallel haptic device was presented by Vu et al [57]. The experiments showed the compensation of dynamic force due to the haptic device in tele operation. Various studies have also included the modelling of human hand in control systems as it could induce disturbances. The idea was to increase transparency of operation [58][59].

The forces at the bucket tip can be measured directly to enhance force tracking. The studies have shown force tracking performance based on direct measurement from sensor equipped on tool shows superior force tracking compared to FFB based on position difference [60]. However, due to technical limitations direct contact force measurement is difficult. Also, it's difficult to attach the sensors to the tip of tool. An alternate method is to use dynamic observers that can estimate the external contact forces, or the joint torques.

Force/torque observer based on neural networks was proposed by Smith et al, [61]. The results showed human hand and environmental contact forces could be estimated with an accuracy of 98.3%. Gupta et al demonstrated disturbance observer (DOB) based impedance control for contact force estimation in a 1 DOF haptic device [62]. A DOB based contact force estimation using an acceleration based controller was proposed by Kastura et al [63]. An algorithm for force estimation was proposed by Daly et al for multi DOF robotic

manipulators during time delay [64]. A contact force estimator was proposed by Garcia et al as the end effector forces are difficult to measure [65]. Another force estimation method for contact force using manipulator inverse dynamics was proposed by Tadano and Kawashima [66].

2.4 SIMULATOR TEST BED

The performance of haptic devices can be evaluated through user evaluations through human subject testing[67][68]. VR based platforms are popular test beds for evaluating haptic devices. These simulators are capable of emulating the haptic rendering and are used to enhance psychomotor performance in various applications[69][70]. Through vibrations or resistance of the actuators the haptic interfaces generates an illusion of touch upon interacting with virtual objects[71][72]. The VR simulators are popular choice among many especially in training due to safety and economic reasons. A virtual backhoe simulator is designed to evaluate the proposed device. The VR platforms helps to simulate various control algorithms in different test environments and assess the actuation in haptic devices.

Over the years the VR platforms have evolved with various fidelities and highly realistic models for environment and excavator machines to train the novices and also to evaluate various control algorithms [73]. The platform provides the operator an opportunity to learn from the mistakes and correct them without any waste of resources. The skills acquired can be retained with practice and can be transferred to real life operations [74].

Simulator training to enhance operator skills are very common in fields of surgery [75] and driving [76]. However, earth moving simulator platforms are different from other field simulators due to the level of complexity required in the operational tasks. These operational tasks also demand cognitive skills and motor abilities in operators [77].

To test and evaluate control strategies simulator based on impedance model of excavator-arm was developed by DiMaio et al [78]. The test environment included the soil-tool interaction model, 6-DOF haptic device and graphical

environment. Torres et al developed an excavator simulator platform aided with a haptic interface for training purpose [49]. The simulator is developed with the nonlinear dynamic model of an industrial excavator and the graphics environment was built in Java 30 as shown in Fig 2.3. The purpose was providing information to the operator regarding bucket-soil interaction forces. Another graphics simulator for operator training in excavators was presented by Wang et al [79]. The simulator was developed using a game engine with a good level of visual fidelity.

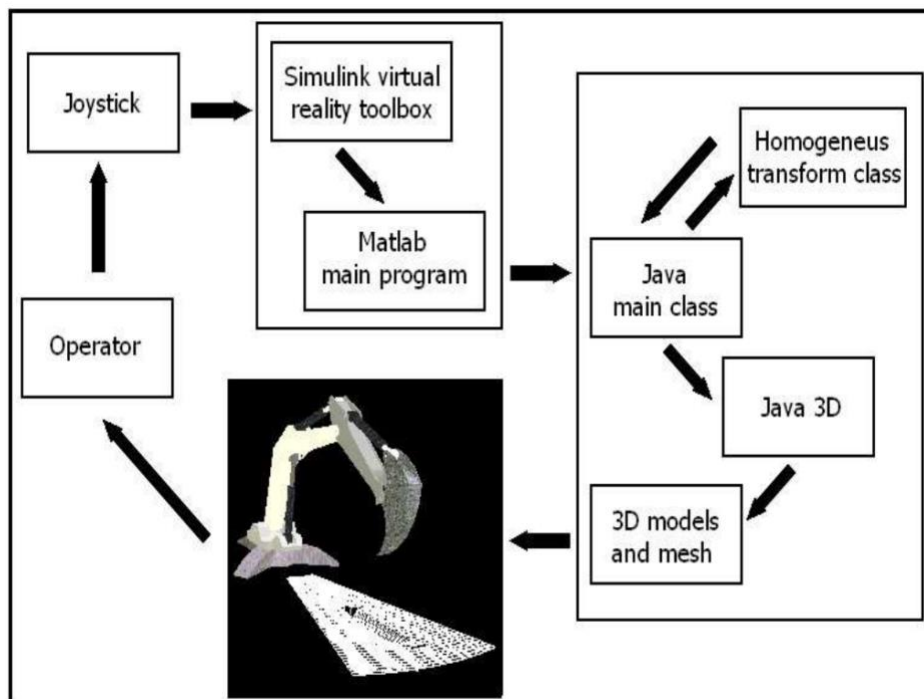


Fig 2.3. Excavator simulator platform aided with a haptic interface [43].

Holz et al presented a study where, physical models form terramechanics and soil mechanics are combinedly used to model a rover in excavation task that demonstrated the impact in trajectory with rover ground interaction [80]. A combination of the simulation softwares, Matlab/Simulink and MSC Adams were combined to develop a excavator arm model by Makkonen et al [81]. The model had 4 DOF with 2 DOF accessory at the end of arm. Towarek et al presented work based on 3D excavator interaction with deformable soil base

[82]. Low cost VR excavator simulators with an improved dynamic model supported with multibody system dynamics were developed by González et al. and Dopico et al [83]. The developed 3D excavator simulator had 17 DOF and was made of 14 rigid bodies. It could to simulate different kinds of maneuver including dangerous environments .

A virtual excavator combining the hydraulic and dynamic model was developed by Le et al. Simulation results verified the performance of the combined system model . However, no soil bucket interaction model was implemented. Based on a Delta3D a dynamic excavator simulator was developed by Nam et al to evaluate the control algorithms and for training operators [73] as shown in Fig 2.4. The excavation forces were predicted with modified Fundamental Earthmoving Equations (FEE) and the visual appearance of operating regions were enhanced with Graphical Processing Unit (GPU) based method. Another study using particle simulations and GPU based method was performed by Schmidt et al. Models based on Particle simulation can visually reproduce digging models [84].



Fig 2.4. Delta3D platform based dynamic excavator simulator

A 3D VE for conducting force feedback experiments in OpenGL and Visual C++ for a novel haptic device is modelled by Kim et al. Though the FFB algorithm was implemented with position and rate control, no soil-bucket interaction model was included for the simulation [33]. A test environment for autonomous excavator, THOR, Terraforming Heavy Outdoor Robot was developed using SimVis3D by Schmidt et al [85]. Choi et al., used a virtual

environment as an experimental platform to assess situational awareness in forklift operations[86]. The simulator environment helped to identify the factors influencing the operator awareness while performing various tasks. A combination of haptic feedback and construction simulator has been used to give error feedback and defect-management to workers [87][88]. Also the studies pertaining to combinations of audio-visual modalities from simulators combined with haptic sensations shows that users learn through multiple channels, build better mental models and enhance knowledge retention [89].

2.5 SUMMARY

The review of background works related to haptic interfaces in excavation leads to the following conclusions: Haptics enabled user interfaces can enhance operator skills and enhance interactivity especially learners. Though with great potential, the commercial haptic interfaces have not been deployed fully as control interfaces in mini excavator/backhoes. The cost, ergonomics, and complexity of controllers are some of the challenges that limit the implementation of commercial haptic controllers. This brings new possibilities for improving the design of excavator interfaces with the infusion of haptic feedback. Intuitive feedback of bucket forces and loading limits can enhance operator awareness and prevent overloading leading to accidents. Haptic joysticks could be used to render the high-fidelity kinesthetic feedback to enhance situational awareness in novice operators. The task-dependent characteristics of haptic joysticks can provide intuitive feedback that can mitigate operator errors.

The force rendering provided using variable stiffness actuation would be an efficient way to present an awareness of the loading environment to the operator. This can improve the perception of loading forces and system limitations especially in test beds using virtual simulators.

CHAPTER 3: MODELLING OF ROBOTIC BACKHOE

Several factors affect a successful loading operation using backhoe/excavators. Along with the loading point, even the dynamics of the medium where the loading is performed varies, sometimes within each cycle of operation and hence the force exerted by or acting on the bucket. In such diverse conditions, to perform the tasks like controlling the bucket trajectory or to estimate the loading torques, mathematical model is necessary. The objective of the chapter is to present the kinematic and dynamic relations that can be used control the motion of the backhoe in any given environment. The kinematic equations presented are developed from fundamental theories of robotic manipulators. The jacobian transformation is used to relate the bucket forces to joint torques. The equations developed in the chapter are used to devise control law that assists in haptic force estimation.

3.1 BACKHOE KINEMATICS

Previously various works have demonstrated the modelling of backhoe and excavators using robotic concepts [90], [91],[92] . The kinematic relations are significant as it allows to map the operator commands in task space to joints-space of the backhoe. The backhoe attachment is a manipulator like mechanism and consists of five links that are connected to each other by revolute joints. It can be considered as a 4 DOF rigid link mechanism with the swing axis normal to the ground and the other three axes namely boom, stick (also called as arm) and bucket parallel to the ground. To define the bucket pose, initially a world coordinate system is defined. A fixed-rectangular righthand Cartesian coordinate system, $X_0Y_0Z_0O_0$ with the centre O_0 is arbitrary chosen at the ground level. This is followed by the assignment of local reference frames to all the joints.

3.1.1 FORWARD KINEMATICS

The component frames along with joint angles are assigned as per Denavit-Hartenberg (DH) conventions[93]. Fig.3.1 gives the coordinate frame arrangements along with the joint angle representation of the robotic backhoe.

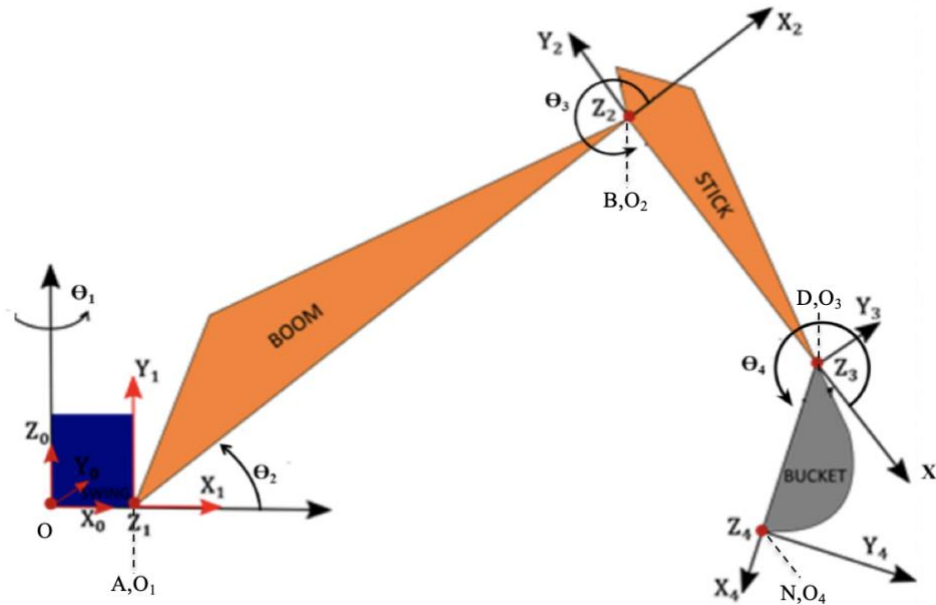


Fig 3.1. Coordinate frame arrangement along with joint angle representation of the robotic backhoe.

The kinematic relations are used to relate joint variables to the bucket position and orientation. The parameters of the backhoe based on DH representation are given in Table 3.1.

Table 3.1. The DH parameter representation of the robotic backhoe

Joint #	Link Length a_i	Joint Angles θ_i	Joint Twist d_i	Joint offset α_i
1	a_1	θ_1	0	90°
2	a_2	θ_2	0	0
3	a_3	θ_3	0	0
4	a_4	θ_4	0	0

DH parameters help to establish the homogeneous transformation matrices from the joint and link parameters. The homogenous transformation matrix A_i^{i-1} can be used to describe the position and orientation of frame $\{i\}$ w.r.t $\{i-1\}$ (where $i = 1,2,3,4$). The general form as,

$$A_i^{i-1} = \begin{bmatrix} \cos\theta_i & -\cos\alpha_i \sin\theta_i & \sin\alpha_i \sin\theta_i & a_i \cos\theta_i \\ \sin\theta_i & -\cos\alpha_i \cos\theta_i & -\sin\alpha_i \cos\theta_i & a_i \sin\theta_i \\ 0 & \sin\alpha_i & \cos\alpha_i & d_i \\ 0 & 0 & 0 & 1 \end{bmatrix} \quad (3.1)$$

The transformation matrix of the end frame (bucket tip) with respect to the base frame, can be obtained by multiplying individual homogeneous transformation matrices as

$$A_0^4 = A_0^1 A_1^2 A_2^3 A_3^4 \quad (3.2)$$

where, the individual frame transformation matrix can be given as,

$$A_0^1 = \begin{bmatrix} c_1 & 0 & s_1 & a_1 c_1 \\ s_1 & 0 & -c_1 & a_1 s_1 \\ 0 & 1 & 0 & 0 \\ 0 & 0 & 0 & 1 \end{bmatrix} \quad (3.3)$$

$$A_1^2 = \begin{bmatrix} c_2 & -s_2 & 0 & a_2 c_2 \\ s_2 & c_2 & 0 & a_2 s_2 \\ 0 & 0 & 1 & 0 \\ 0 & 0 & 0 & 1 \end{bmatrix} \quad (3.4)$$

$$A_2^3 = \begin{bmatrix} c_3 & -s_3 & 0 & a_3 c_3 \\ s_3 & c_3 & 0 & a_3 s_3 \\ 0 & 0 & 1 & 0 \\ 0 & 0 & 0 & 1 \end{bmatrix} \quad (3.5)$$

$$A_3^4 = \begin{bmatrix} c_4 & -s_4 & 0 & a_4 c_4 \\ s_4 & c_4 & 0 & a_4 s_4 \\ 0 & 0 & 1 & 0 \\ 0 & 0 & 0 & 1 \end{bmatrix} \quad (3.6)$$

where $c_i = \cos\theta_i$ and $s_i = \sin\theta_i$. Specifically, from equation 3.2, A_0^4 can be represented as,

$$A_0^4 = \begin{bmatrix} c_1 c_{234} & -c_1 c_{234} & s_1 & c_1(a_1 + a_2 c_2 + a_3 c_{23} + a_4 c_{234}) \\ -s_1 c_{234} & -s_1 s_{234} & -c_1 & s_1(a_1 + a_2 c_2 + a_3 c_{23} + a_4 c_{234}) \\ s_{234} & c_{234} & 0 & a_2 s_2 + a_3 s_{23} + a_4 s_{234} \\ 0 & 0 & 0 & 1 \end{bmatrix} \quad (3.7)$$

In equation 3.7, $c_{234} = \cos(\theta_2 + \theta_3 + \theta_4)$ and $s_{234} = \sin(\theta_2 + \theta_3 + \theta_4)$. The vector p_i^N represents the coordinates of point N in the i^{th} coordinate frame. The 3x1 position vector of the bucket tip w.r.t to the base frame can be expressed as, $p_0^N =$

$$\begin{bmatrix} c_1(a_1 + a_2 c_2 + a_3 c_{23} + a_4 c_{234}) & s_1(a_1 + a_2 c_2 + a_3 c_{23} + a_4 c_{234}) & a_2 s_2 + a_3 s_{23} + a_4 s_{234} \end{bmatrix}^T \quad (3.8)$$

The knowledge of joint angles $\theta_1, \theta_2, \theta_3, \theta_4$ helps to determine the position and orientation of the point D which lies on the edge of the bucket.

3.1.2 INVERSE KINEMATICS

Inverse kinematics helps to compute the joint angles from the coordinates of bucket tip position. To solve for the joint angles, the vectors are re-arranged to express in first coordinate frame, $X_1 Y_1 Z_1 O_1$. To express p_0^D in the first coordinate frame, p_1^D is used and is expressed as,

$$p_1^D = A_1^0 p_0^D = A_1^2 A_2^3 p_3^D = A_1^3 p_3^D \quad (3.9)$$

Substituting values for A_1^3 and p_3^D , the p_1^D is obtained as,

$$p_1^D = \begin{bmatrix} c_1 & s_1 & 0 & -a_1 \\ 0 & 0 & 1 & 0 \\ s_1 & -c_1 & 0 & 0 \\ 0 & 0 & 0 & 1 \end{bmatrix} \begin{pmatrix} p_{0x}^D \\ p_{0y}^D \\ p_{0z}^D \\ 1 \end{pmatrix} = \begin{bmatrix} c_1 p_{0x}^D + s_1 p_{0y}^D - a_1 \\ p_{0z}^D \\ s_1 p_{0x}^D - c_1 p_{0y}^D \\ 1 \end{bmatrix} \quad (3.10)$$

By rewriting equation 3.9 as,

$$(A_1^2)^{-1}p_1^D = A_2^3p_3^D \quad (3.11)$$

Solving for equation 3.11,

$$\begin{bmatrix} (c_1p_{0x}^D + s_1p_{0y}^D - a_1)c_2 + p_{0z}^Ds_2 - a_2 \\ -(c_1p_{0x}^D + s_1p_{0y}^D - a_1)s_2 + p_{0z}^Dc_2 - a_2 \\ s_1p_{0x}^D - c_1p_{0y}^D \\ 1 \end{bmatrix} = \begin{bmatrix} a_3c_3 \\ a_3s_3 \\ 0 \\ 1 \end{bmatrix} \quad (3.12)$$

From equation 3.12, the joint angles are calculated as,

$$\theta_1 = \tan^{-1}\left(\frac{p_{0y}^D}{p_{0x}^D}\right) \quad (3.13)$$

$$\theta_2 = \tan^{-1}\left(\frac{p_{0z}^D}{p_{0x}^D}\right) + \tan^{-1}\left(\frac{\{4a_2^2[(p_{0z}^D)^2 + d^2] - [(p_{0z}^D)^2 + d^2 + a_2^2 - a_3^2]^2\}^{1/2}}{(p_{0z}^D)^2 + d^2 + a_2^2 - a_3^2}\right) \quad (3.14)$$

where $d = c_1p_{0x}^D + s_1p_{0y}^D - a_1$. The third joint angle θ_3 can be solved as,

$$\theta_3 = \tan^{-1}\left(\frac{c_2p_{0z}^D - s_2d}{s_2p_{0z}^D + c_2d - a_2}\right) \quad (3.15)$$

The joint angles, θ_1 , θ_2 and θ_4 are obtained w.r.t to p_0^D (from O_3). Fig. 3.2 shows a plane containing the front edge of bucket and the point N and is defined by the bottom of the bucket. Then joint angle θ_4 can be determined w.r.t to the orientation of the bucket. It can be determined as,

$$\theta_4 = \theta_b + \theta_{dg} + (2\pi - \theta_2 - \theta_3) \quad (3.16)$$

where, θ_b is the angle between the plane with the bottom of bucket and the x_4 axis. θ_{dg} is the angle the which the foregoing-plane makes with the horizontal plane.

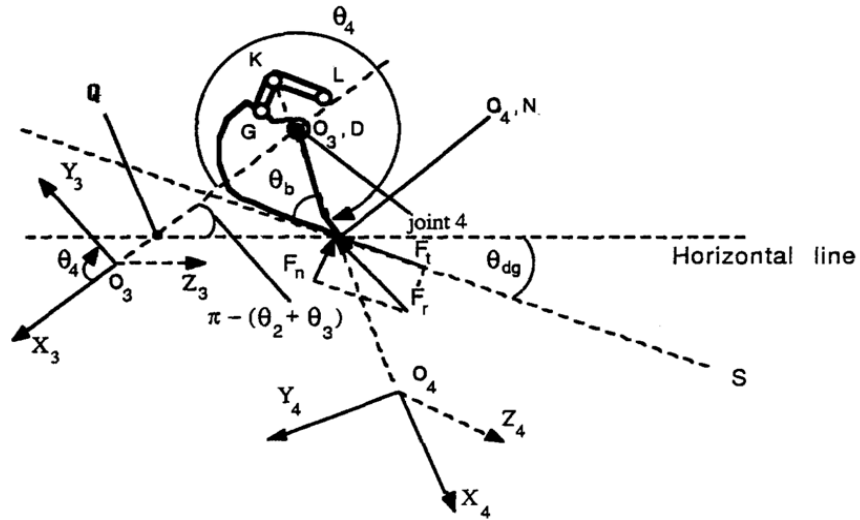


Fig 3.2. Bucket orientation [90]

3.1.3 RELATION BETWEEN JOINT SPACE VARIABLES TO CYLINDER SPACE VARIABLES

The hydraulic rams act as the actuators in the excavator/backhoe machinery. Therefore, to completely define the kinematic model, the variables in task space (bucket position and orientation) should be converted to joint space which in turn should be converted to cylinder space (actuator-space) in inverse kinematics and vice versa in forward kinematics. It is important to understand how the joint angles and the length of piston rods in these hydraulic actuators are related to each other and how this relation affects the pose and configuration of the mechanism.

Joint 1 which rotates the base is actuated with a swing motor. The joint variable θ_1 gives the vertical plane in base co-ordinate system where the backhoe/excavator operation occurs. The positions of the other three joints are actuated by hydraulic cylinders are determined. l_{IJ} is used to denote the length of the piston-rod in the hydraulic cylinder as shown in Fig.3.3 where the subscripts I and J are the start and end points for the segment.

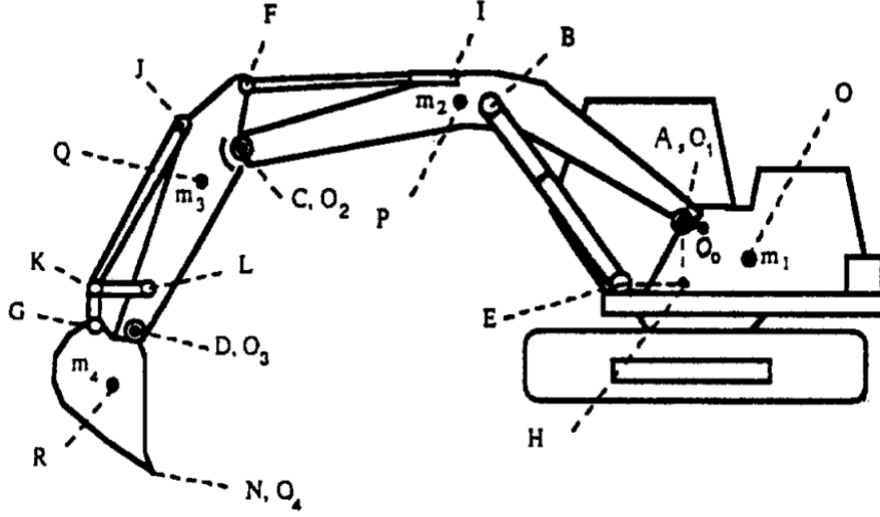


Fig 3.3. Excavator coordinate frames [90]

The boom joint (joint 2) is connected to the piston rod of actuator 2. The joint angle θ_2 is related to the length of the piston, l_{BE} as,

$$l_{BE}^2 = [l_{AB} \sin(\theta_2 + \beta) + l_{AH}]^2 + [l_{AB} \cos(\theta_2 + \beta) - l_{HE}]^2 \quad (3.17)$$

where, the length of line segments l_{AH} , l_{AB} and l_{HE} remains constant for given backhoe/excavator mechanism. Also, β is a constant angle and is considered between line segment BA and AC. The stick joint (joint 3) is connected to the piston-rod in hydraulic actuator 3. The length of actuator l_{FI} can be related to joint variable θ_3 by cos theorem for ΔFIC as,

$$l_{FI}^2 = l_{FC}^2 + l_{CI}^2 - 2l_{FC}l_{CI} \cos(3\pi - \theta_3 - \gamma_1 - \gamma_2) \quad (3.18)$$

The equation 3.18 is developed by considering $\angle ACI = \gamma_1$ and $\angle FCD = \gamma_2$ and are constants determined from the machine structure. The lengths l_{FC} and l_{CI} are also constants irrespective of backhoe/excavator configuration.

The joint angle θ_4 is related to the length of actuator 4 from ΔJKL using cos theorem. By considering $\angle JLD = \nu_1$, a constant for a given backhoe/excavator and $\angle KLD$ as ε_1 . The equation can be expressed as,

$$l_{JK}^2 = l_{JL}^2 + l_{KL}^2 - 2l_{JL}l_{KL} \cos(\nu_1 - \varepsilon_1) \quad (3.19)$$

where ε_1 in equation 3.19 can be determined by,

$$\varepsilon_1 = \nu_1 - \tan^{-1} \left[\frac{\sqrt{4l_{jL}^2 l_{kL}^2 - (l_{jL}^2 + l_{kL}^2 - l_{jK}^2)^4}}{(l_{jL}^2 + l_{kL}^2 - l_{jK}^2)^2} \right] \quad (3.20)$$

ε_1 and θ_4 can be related by the equation 3.21 as,

$$\varepsilon_1 + \varepsilon_2 = 2\pi - [2\pi - (\theta_4 - \pi) - \nu_2 - \nu_3] - \varepsilon_3 \quad (3.21)$$

where, $\nu_2 = \angle CDL$, $\nu_3 = \angle GDN$, $\varepsilon_2 = \angle KGD$ and $\varepsilon_3 = \angle LKG$. ν_2 and ν_3 are constant for a given backhoe/excavator structure. An encoder attached on the shaft of the bucket joint can be used to determine ε_3 . In equation 3.21, ε_2 can be calculated by applying cos theorem to ΔKLD and ΔKDG as,

$$l_{KG}^2 + l_{GD}^2 - 2l_{KG}l_{GD} \cos(\varepsilon_2) = l_{KL}^2 + l_{LD}^2 - 2l_{KL}l_{LD} \cos(\varepsilon_1) \quad (3.22).$$

Similar to determining the length of piston rod extension or retraction from joint angles, the reverse calculation can be implemented in case of forward kinematics. The length of piston rods can be related to the joint angles to control bucket-pose and orientation. Determination of the actuator length l_{BE} is can be used to calculate the values for the boom joint angle θ_2 as,

$$\theta_2 = -\beta - \tan^{-1} \left(\frac{l_{AH}}{l_{HE}} \right) + \tan^{-1} \left\{ \frac{l_{AB}^2 + l_{AH}^2 + l_{HE}^2 - l_{BE}^2}{\sqrt{(4l_{AB}^2 (l_{AH}^2 + l_{HE}^2) - h_1^4)}} \right\} \quad (3.23)$$

If the piston length l_{FI} can be determined. Then the joint angle for arm θ_3 , can be calculated as,

$$\theta_3 = 3\pi - \gamma_1 - \gamma_2 - \tan^{-1} \left[\frac{\sqrt{(4l_{FC}^2 l_{CI}^2 - (l_{FC}^2 + l_{CI}^2 - l_{FI}^2)^4)}}{l_{FC}^2 + l_{CI}^2 - l_{FI}^2} \right] \quad (3.24)$$

The joint angle θ_4 can be calculated as,

$$\theta_4 = \pi - \nu_2 - \nu_3 + \varepsilon_1 + \varepsilon_2 + \varepsilon_3 \quad (3.25)$$

3.2 BUCKET FORCE TO LOADING TORQUE

The loading operation with backhoes/excavators consists of a number of steps to transfer material from the ground (or heap) to an unloading point. The process is quite complex and the tool (bucket) needs to interact with a heterogenous medium that has a dynamic nature. While digging bucket exerts a force on the medium and this contact leads to different interactive forces (digging force) and moments at the soil-tool interface. With each cycle of operation, these forces vary and hence the loading torque acting on the machinery. In any loading operation understanding the digging forces is important as it actuates all the, boom, arm and bucket mechanisms (swing joint is held stationery during digging). The bucket forces can be related to the joint torques using Jacobian matrix [94], [95],

$$\tau_{digging} = J^T F_l \quad (3.26)$$

where $\tau_{digging}$ is the represents the loading torque vectors acting on the joints and F_l is the generalized force vector acting on the bucket. F_l consists of reaction forces and moment vector acting from medium to bucket. It can be resolved in x, and z direction and can be considered to be acting at origin O₄. The bucket-soil interaction is difficult to be modelled accurately as the medium is unpredictable. Various studies have modelled the bucket-soil interaction and the two models taken for the project are explained in chapter 4 and chapter 6. The study do not consider the effects of internal forces and friction and hence assume that the end point forces are balanced with the net joint torques.

To jacobian matrix is developed by the expression,

$$J(\theta) = \frac{dp_0^N}{d\theta_i} \quad (3.27)$$

where p_0^N is the translational vector of homogeneous transformation matrix A_0^4 which is nothing but the fourth column of matrix A_0^4 in equation 3.7 and $i=1,2,3,4$. The Jacobian matrix gives a correlation between the joint velocities, $\dot{\theta}$ to end-effector velocity (bucket velocity, V). $J(\theta)$ can be defined for each

separate link of the backhoe mechanism [96]. The relationship between the bucket velocity to the joint velocities can be given by,

$$V = J(\theta)\dot{\theta} \quad (3.28)$$

The matrix $J(\theta)$ can be expressed as,

$$J(\theta) = \begin{bmatrix} -s_1 a_{14} & c_1(-a_4 s_{234} - a_3 s_{23} - a_2 s_2) & c_1(-a_4 s_{234} - a_3 s_{23}) & -c_1 a_4 s_{234} \\ c_1 a_{14} & s_1(-a_4 s_{234} - a_3 s_{23} - a_2 s_2) & s_1(-a_4 s_{234} - a_3 s_{23}) & -s_1 a_4 s_{234} \\ 0 & a_4 c_{234} + a_3 c_{23} + a_2 c_2 & a_4 c_{234} + a_3 c_{23} & a_4 c_{234} \\ 0 & 1 & 1 & 1 \end{bmatrix} \quad (3.29)$$

where, $a_{14} = a_4 c_{234} + a_3 c_{23} + a_2 c_2 + a_1$.

3.3 BACKHOE DYNAMICS

During the operation, it is necessary to understand the correlation between the torques applied to the joints of the system and the position and orientation of the bucket along with necessary joint variables. This relation is developed from the dynamics equations of the system [97][30]. For the dynamic modelling of backhoe, Lagrangian approach based on the kinetic and potential energy of the system is used [98]. The Lagrangian function is defined as,

$$L = K - P \quad (3.30)$$

where K and P are the total kinetic and total potential energy of all links of the system respectively. For the system, the equations of motion (EOM) can be written as,

$$\frac{d}{dt} \left(\frac{\partial L}{\partial \dot{\theta}_i} \right) - \frac{\partial L}{\partial \theta_i} = \tau_i \quad (3.31)$$

The joint torque, τ_i equation can also be expressed as,

$$\frac{d}{dt} \left(\frac{\partial K}{\partial \dot{\theta}_i} \right) - \frac{\partial K}{\partial \theta_i} - \frac{\partial P}{\partial \theta_i} = \tau_i \quad (3.32)$$

where K is a function of both joint angles, θ_i and joint velocity $\dot{\theta}_i$ and U is a function of joint angles θ_i . The total dynamics of the machine in the Lagrange formulation can be written as,

$$M(\theta)\ddot{\theta} + H(\theta, \dot{\theta})\dot{\theta} + G(\theta) + \tau_d = \tau \quad (3.33)$$

where $M(\theta) \in R^{4 \times 4}$ is the inertia matrix which is a positive-definite symmetric matrix $H(\theta, \dot{\theta}) \in R^{4 \times 4}$ represents the coriolis and centrifugal forces, $G(\theta) \in R^4$ is the gravity matrix of the reduced system. The joint torque vector τ , is expressed for torque for link $i - 1$, acting on link i acting along z_{i-1} and $\tau_d = [\tau_{d1}, \tau_{d2}, \tau_{d3}, \tau_{d4}]$ represents the loading torque vectors acting on the joints during digging. In the equation 3.33, τ_d is used to include the loading forces acting during soil-bucket interaction and can be computed using the equation 3.26. The dynamic equations obtained for backhoe manipulator are presented in Appendix B. Also, equation 3.33 can be solved for $\ddot{\theta}$ and can be integrated to obtain joint variables θ and $\dot{\theta}$ and hence can be used to compute the bucket position and orientation.

Also, the modelling of robotic backhoe is incomplete without actuator dynamics. Therefore, an insight in to modelling aspects of electrohydraulic actuators present is presented in Appendix A.

3.5 SUMMARY

The main contribution of the chapter is the kinematic and dynamic equations required for the mathematical modelling of robotic backhoe. First, the kinematic relations that relate the joint angles to bucket pose are presented. The relation between the joint angles to the cylinder length are then presented to bring out a detailed insight into the configuration of the backhoe mechanism. The mapping of digging forces to loading torque are derived with Jacobian transformations. Later, to understand the computation of torques acting on the backhoe mechanism, dynamics equations are developed with Lagrange formulations.

These equations are necessary to develop control algorithms for the machinery.
Such insights help to get a clear understanding of the system behaviour.

CHAPTER 4: CONTROL OF ROBOTIC BACKHOE

Automation in excavation is a widely researched topic for over three decades. Significant contributions have been made in areas like trajectory planning for bucket motion [104][105], modelling of hydraulic actuators and bucket [102][95], analysis of interaction forces [94] and computer vision to estimate the loaded materials [106] to automate the loading cycles. The complexity of operation led the researches to concentrate on breaking down the challenges in excavation and separately addressing them.

Operator assistance functions are vital in this approach and plays a major role in enhancing machine performance. The main objective of the research is to develop a haptic platform that can reflect the loading forces acting in the machinery in various environments. This chapter focuses on the development of a control system that can accurately estimate the loading torque and the digging forces without any sensors. The results for the simulation study performed to validate the control system are presented. The validation study of the control system on a virtual prototype of the robotic backhoe in Adams - MATLAB platform.

4.1. LOADING TORQUE ESTIMATION

During the process of excavation, the bucket must penetrate into the material (medium) in either digging, scooping or cutting motion. The penetration is successful once the bucket force exceeds the resistive force from the medium. One of the major complexities in loading process is attributed to the heterogenous nature of the medium and its stochastic behaviour. As there exist many parallels between a robotic manipulator and a backhoe, a robotic modelling approach can help to determine a relationship between the bucket forces while excavating and the joints. However, the digging force experienced at the bucket tip while loading is non-uniform and varies within the cycle and from cycle to cycle of operation. High force transients during loading may

sometimes drive the actuators to its maximum capacity, that happens more likely when the medium is non-heterogeneous (mixture of soils and fragmented rocks). Also, with the large resistive loads, the body of the machinery can deform [107]. Another issue associated with excessive resistive force at the bucket tip is wheel slip. It is common among learners and damages tires of the machinery. According to the study by Anderson, wheel slip largely contributes to the machine maintenance cost, in earthmoving machineries [108][109]. Also, it is of huge risk to operators especially novices and occurs from loss of friction in icy surfaces as well.

Conventionally, the operator judges the digging forces acting on the bucket based on engine sound, vibration, manipulator stall and on what he sees. The operator controls the backhoe motion with this judgement skills and controls the machinery. It takes years of practice for an operator to gain the necessary expertise to effectively maneuver the manipulator (backhoe). Therefore, developing a control system that can estimate loading torque acting in the machinery would greatly assist the operator and thereby result in a force reflective operation. Also, this would be of great significance in tele or remote operations as the operator is isolated from the machinery.

The varying nature of the ground resistance forces makes the development of a feedback controller (FB) extremely difficult. The feedback regulation in FB is based on error between the output measured and the setpoints. Therefore, in presence of strong disturbances these feedback controllers are not fast enough and cannot suppresses the disturbances directly [110]. Feedforward controllers (FC) in other hand are direct and active control methods for disturbance suppression. However, FC requires the disturbances to be measured[111]. The complexity of bucket-soil interaction process makes it difficult to be modelled. Though, there exists various models for prediction of soil-bucket interaction forces, they are not accurate. Even the models based on detailed soil-mechanic models has a prediction error of 20% [112] [113]. Moreover, with the heterogenous and dynamic nature of medium even the industrial sensors do not

give an accurate load measurement. This limits the application of disturbance rejection solely through FC insufficient.

4.2 DESIGN OF THE CONTROL SYSTEM

To alleviate the limitations of the traditional control methods in estimating loading torque, a disturbance observer-assisted control technique has been developed [98]. DOB are considered to be very effective in disturbance estimation and is widely applied in robotic manipulators to ensure robust tracking of disturbances [13][14][15]. In absence of uncertain disturbances, FB controllers provide good disturbance attenuation. Therefore, a combination of DOB and a non-linear FB controller has been explored to estimate the loading disturbances and ensure tracking. Here, the DOB acts as a patch to the base line controller and improves the robustness of the FB controller. Also, DOB does not a force/torque sensor to estimate disturbances.

In the study, a DOB based technique is used to estimate loading torque acting on the system. The disturbance observer is added as an addition to existing controller (baseline controller), that normally maintains accurate tracking performance and good stability but shows performance degradation in presence of uncertainties. In this work, the well-established Computed torque controller (CTC) is chosen as the baseline controller. The disturbance compensation provided by DOB improves the robustness and disturbance attenuation of the baseline controller and ensures reliability.

For the robotic backhoe, the following nonlinear control law is proposed,

$$\tau = \hat{M} (\ddot{q}_d + K_p e + K_d \dot{e}_d) + \hat{N} (q, \dot{q}) - \hat{\tau}_{dis} \quad (4.1)$$

where $\hat{M} (q)$ and $\hat{\tau}_{dis}$ denote the estimates of $M(q)$ and τ_{dis} and $\hat{N} (q, \dot{q})$ represents the estimates of $\hat{H}(q, \dot{q})\dot{q}$ and $\hat{G}(q)$. The observer is applied to all the joints to estimate the loading torque acting at each joint during digging. The $\hat{\tau}_{dis}$ is an estimate of the loading torque vector, $\tau_{digging}$ which is obtained from equation 3.26. The system block diagram of the overall system is shown

in Fig. 4.1. The desired trajectory to be tracked is denoted by y_d . In the system, the loading torque acting in the joints is estimated by the observer and provides a compensation to counteract the effect of the disturbance torque (loading torque).

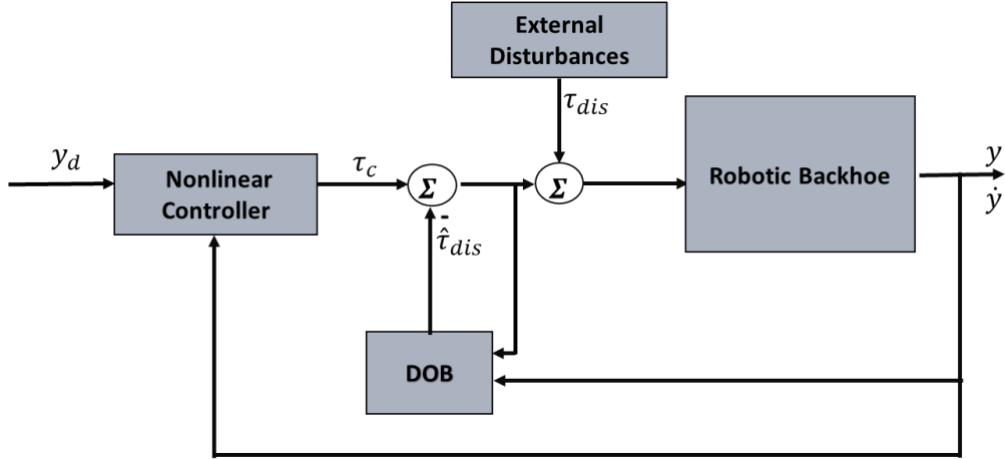


Fig 4.1. Control system proposed for the hybrid control of the robotic backhoe

In many of the robotic systems, the non-linear DOB are proposed w.r.t to joint acceleration measurements [117]. The work related to the development for a DOB based on acceleration measurements for a spatial serial robot, is published in Meera.et al[118]. However, unavailability of accurate accelerometers poses a big problem. Here the estimate of the loading torque estimate, (which is taken as the disturbance acting in the joints) $\hat{\tau}_{dis}$ is proposed as a function of joint velocity i.e. $\hat{\tau}_{dis}=f(\dot{q})$. $\hat{\tau}_{dis}$, can be expressed as:

$$\hat{\tau}_{dis} = K_0 \hat{M}(q) \dot{q} + \eta, \quad (4.2)$$

where η is an arbitrary vector. Choosing $\dot{\eta}$ as,

$$\dot{\eta} = -K_0 (\tau - \hat{N}(q, \dot{q}) + \hat{\tau}_{dis}) \quad (4.3)$$

where K_0 is a positive gain matrix. The adaption laws for the disturbance estimate vector is chosen as,

$$\dot{\hat{\tau}}_{dis} = -K_0 \tilde{\tau}_{dis} \quad (4.4)$$

The observer error vector is,

$$\tilde{\tau}_{dis} = \tau_{dis} - \hat{\tau}_{dis} \quad (4.5)$$

Remark 1: The disturbance τ_{dis} is bounded such that there exists a vector $\tau_L > 0$ such that $0 \leq |\tau_{dis}| \leq \tau_L$

Remark 2: Rate of change of disturbances and system uncertainties are negligible when compared to the slowly varying disturbance. Therefore $\dot{\tau}_{dis} \approx 0$. From equation 4.4 and equation 4.5

$$\dot{\hat{\tau}}_{dis} = -K_0(\tau_{dis} - \hat{\tau}_{dis}) \quad (4.6)$$

The closed-loop stability and error convergence for the proposed observer is considered with Lyapunov's direct method as,

$$V = \frac{1}{2}(\tau_{dis} - \hat{\tau}_{dis})^2 \quad (4.7)$$

From above equation 4.5 and equation 4.6 and taking the time derivative of equation 4.7, the following equation is obtained

$$\dot{V} = (\tau_{dis} - \hat{\tau}_{dis})(\dot{\tau}_{dis} - \dot{\hat{\tau}}_{dis}) \quad (4.8)$$

then the update law from equation 4.6 ensures that

$$\dot{V} = (\tau_{dis} - \hat{\tau}_{dis})(-K_0(\tau_{dis} - \hat{\tau}_{dis})) \leq 0 \quad (4.9)$$

\dot{V} is negative semi definite for $\tilde{\tau}_{dis} \in R^n$. As \dot{V} is negative definite it confirms the stability of the proposed controller. Fig. 4.2 shows the design of the DOB proposed for the tracking control. The difference between the control torque

τ_{dis} and the estimated disturbance torque, $\hat{\tau}_{dis}$ is the actual torque which drives the system in the given trajectory compensating the disturbances.

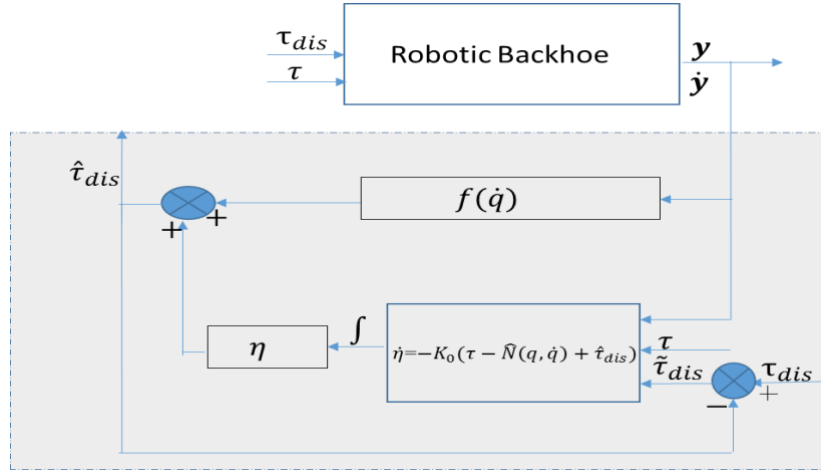


Fig 4.2. Design of the proposed disturbance observer.

4.3 SOIL TOOL INTERACTION MODEL

Several modelling approaches had been adopted for predicting the nature of the loading force acting on the bucket, during soil-tool interaction. For the study, the soil-tool modelling approach has been taken from Koivo et al.,[119][94]. The work is mostly stated in empirical terms and gives a generalized force exerted by the bucket or the end effector. For the study performed on a pre-planned trajectory with varying soil resistance, the model addresses the estimation of contact forces required to overcome the soil shear strength. The model is typical for excavators and the comparatively less computational complexity made the model a good fit to be chosen for the study. Fig. 4.3 shows the bucket interaction with the soil during digging.

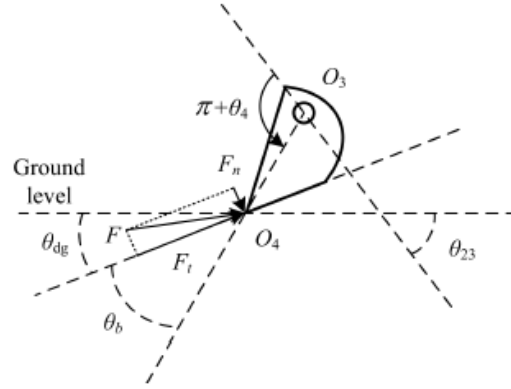


Fig 4.3. Soil-bucket interaction during digging [94]

In this approach, the loading torque is given as,

$$\tau_{dis} = \begin{bmatrix} \tau_b \\ a_2 [F_t \sin(\theta_2 - \theta_{dg}) - F_n \cos(\theta_2 - \theta_{dg})] \\ a_3 [F_t \sin(\theta_{23} - \theta_{dg}) - F_n \cos(\theta_{23} - \theta_{dg})] \\ a_4 (-F_t \sin\theta_b + F_n \cos\theta_b) \end{bmatrix} \quad (4.10)$$

where, F_t and F_n denotes the tangential and normal components of the reaction force in the soil bucket interaction. τ_b is not considered in the study as θ_1 remains constant during digging operation. The reaction force F_r , is defined parallel to the direction of digging. F_t and F_n are calculated as,

$$\left. \begin{aligned} F_t &= F_r \cos(\theta_{dg} - \beta) \\ F_n &= -F_r \sin(\theta_{dg} - \beta), \end{aligned} \right\} \quad (4.11)$$

where β is a dimensionless coefficient and the value is held constant at as 0.1. The reaction force F_r , is calculated as,

$$F_r = k_p [k_s b h + \mu N + \varepsilon \left(1 + \frac{v_s}{v_b}\right) v_d] \quad (4.12)$$

where k_p and k_s are the specific resistance to cutting. ε and μ denotes the coefficient of resistance during bucket filling and the coefficient of friction of

bucket and ground respectively. N denotes the pressure force exerted by bucket on soil. v_s , v_b and v_d are the volume of prism of soil, volume of bucket respectively and amount of the soil inside the bucket.

4.3 SIMULATION STUDY AND RESULTS

To validate the performance of control scheme simulation study was performed using MATLAB/Simulink 2014a package. The parameters of the robotic backhoe used for the study are given in table 4.1. The study validates the control system performance of the proposed control system for a cycle of digging operation. The reference trajectory the system has to follow is developed from the workspace of the robotic backhoe and is defined in cartesian space as shown in Fig. 4.4. As digging happens in the vertical plane, the swing motion stays constant and the dynamic model is reduced to a 3-DOF model with boom, stick, and bucket motions and the swing joint dynamics are neglected.

Table 4.1 Parameters of the robotic backhoe used in study.

Parameters	Value	Parameters	Value
Mass of boom, m2	33.43 kg	Soil density	1.3kg/m ³ ,
Mass of stick, m3	10.1 kg	Width of soil cut	60 cm
Mass of bucket, m4	2.45 kg	Thickness of soil cut	40 cm
Link length boom, a1	1.42 m	Pressure force of the bucket with soil, N	1 kg m/s ²
Link length stick, a2	0.699 m	coefficient of friction, μ	0.1
Link length bucket a3	0.55 m	Volume of bucket	1.66 m ³
Moment of inertia, boom	9.80 kgm ²	Acc" due to gravity, g	9.81 N/kg

Moment of inertia, bucket	2.432 kgm ²	coefficient of resistance €	55,000 kg/(m ² /s ²)
Moment of inertia, stick	6.21 kgm ²	Penetration angle	30 deg

The simulation study is performed with the comparison of the baseline controller and the combination of proposed control system (combination of DOB and CTC) to estimate the loading torque for the given dig cycle. As the bucket hits the ground, the system encounters the ground reaction torque in the opposite direction. The gain values used for the simulation are $K_p=100I$, $K_d=20I$ and $K_0=2I$.

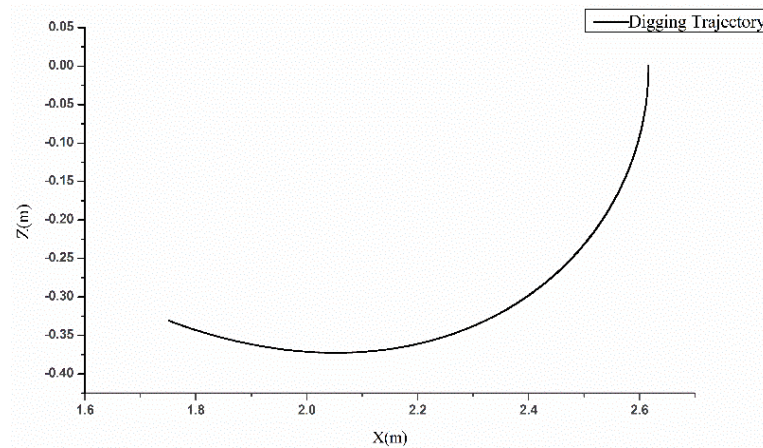


Fig 4.4. Desired digging trajectory for the robotic backhoe

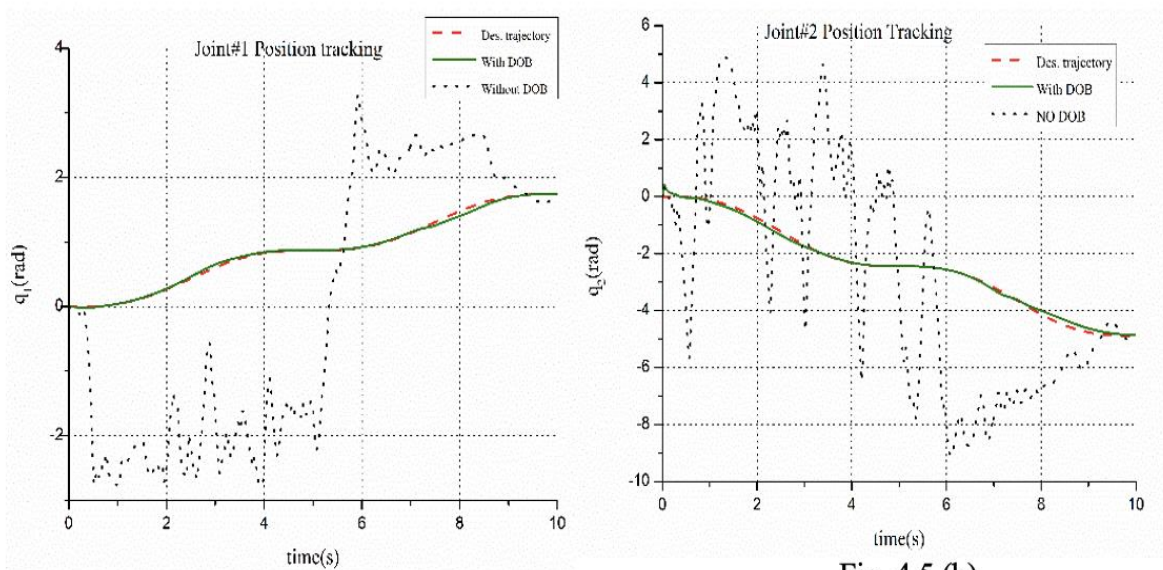


Fig. 4.5 (a)

Fig. 4.5 (b)

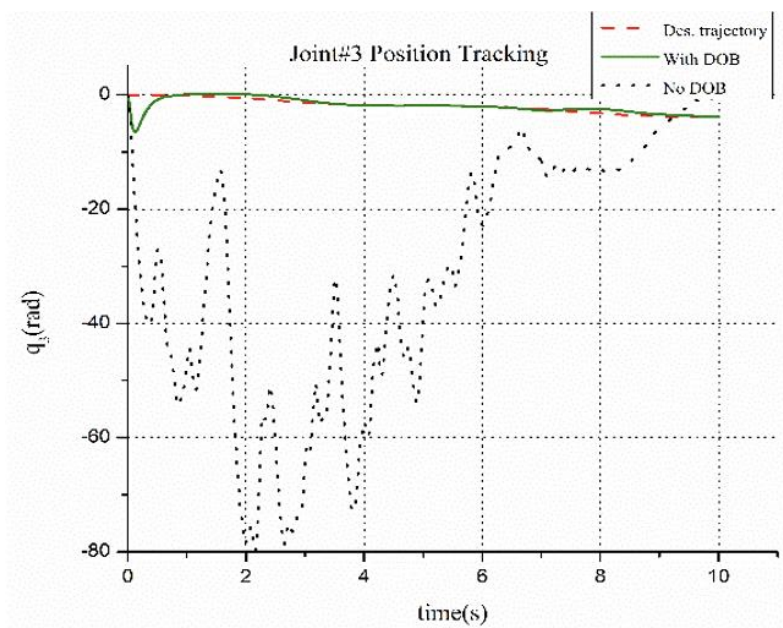


Fig. 4.5 (c)

Fig 4.5.(a),(b),(c): Time profile: Position tracking time profile for the boom, stick, bucket joints in one dig cycle of operation.

The joint trajectory tracking for the three joints, boom (joint#1), stick(joint#2) and bucket(joint#3) with the desired trajectory with DOB and without DOB is presented in Fig 4.5. Fig. 4.6 shows the position tracking error which is the

difference between the actual joint trajectory and desired joint trajectory in following the given digging profile.

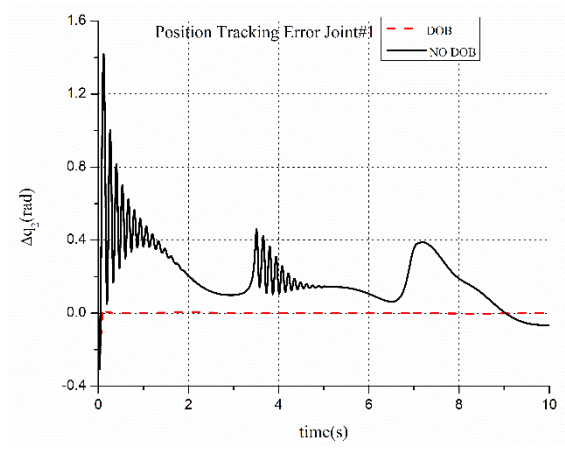


Fig.4.6(a)

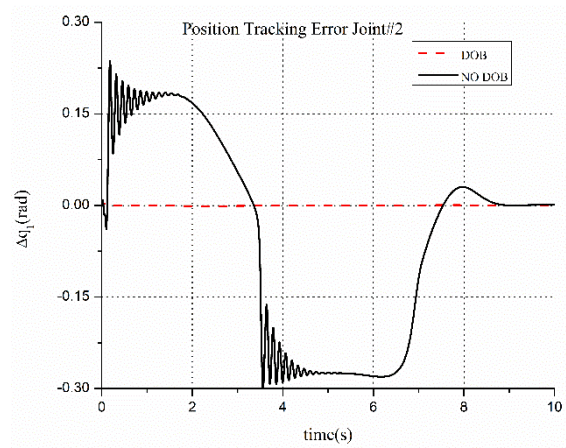


Fig.4.6(b)

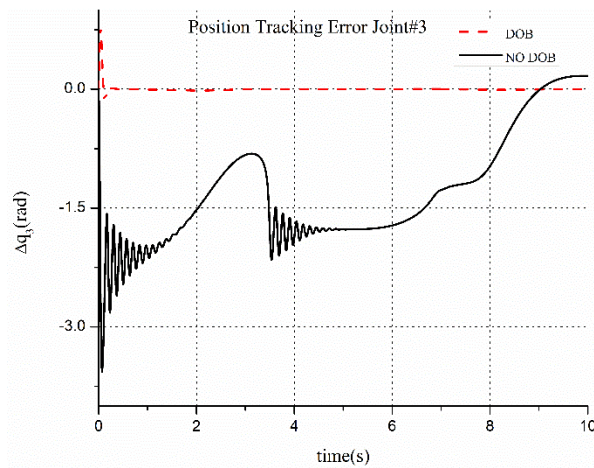


Fig.4.6(c)

Fig 4.6.(a), (b), (c): Time profile: Position error time profile of the boom, stick and bucket joint in a digging cycle of the robotic backhoe.

Fig. 4.7 shows the loading torque estimation in the three joints: boom, stick and bucket.

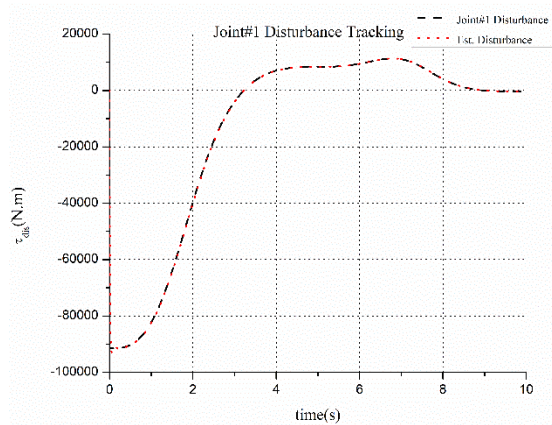


Fig. 4.7(a)

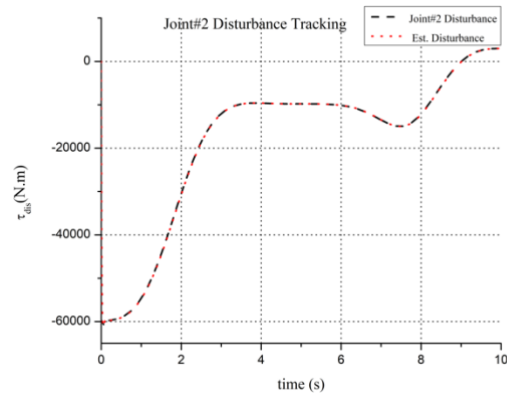


Fig. 4.7(b)

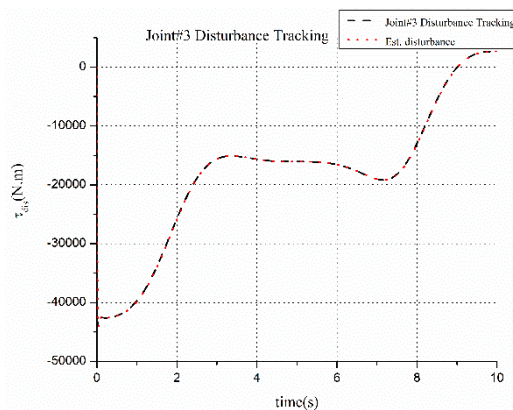


Fig. 4.7(c)

Fig 4.7.(a), (b), (c): Joint disturbance tracking time profile of the boom, stick and bucket joint of the robotic backhoe.

The error in the estimation of loading torque in the three joints is shown in the Fig. 4.8. From the above analysis, it is clear that the joint-trajectory tracking in the robotic backhoe was improved with the DOB assisted control system. Also, the control system is effective in estimating loading torque acting in the joints. The high values of the tracking errors in the initial stage is due to the presence of non-zero initial errors, mechanical inaccuracies.

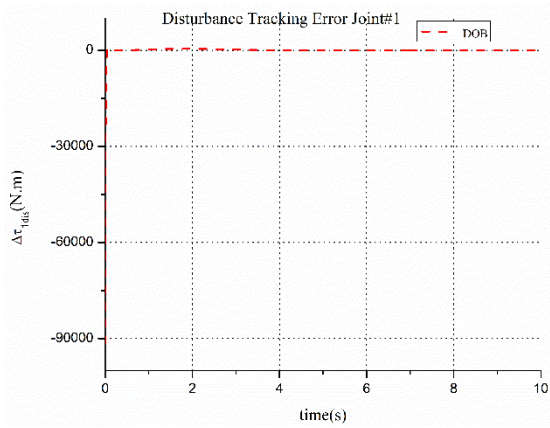


Fig.4.8(a)

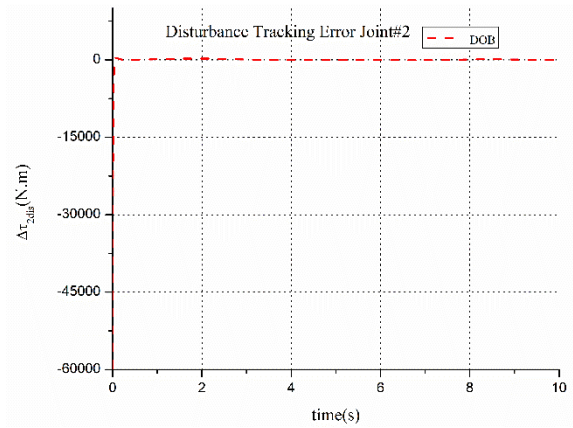


Fig.4.8(b)

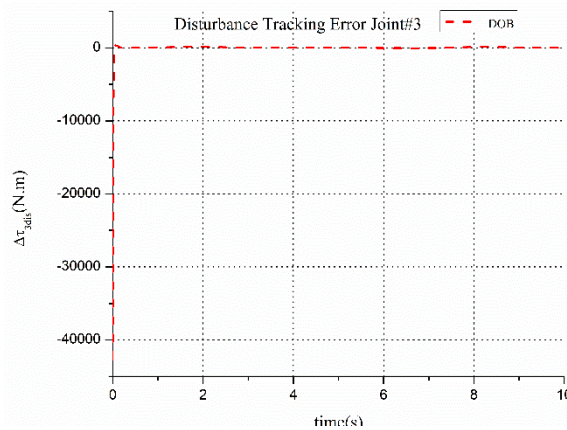


Fig.4.8(c)

Fig 4.8 (a),(b),(c): Disturbance error time profile of boom, stick and bucket joint in the soil-contact task of a robotic backhoe.

4.4 CO-SIMULATION ANALYSIS AND RESULTS

Collaborative simulation (co-simulation) is a technique used to examine various system aspects with the help of specialized software packages. It is a very powerful tool to solve multi physics problem, provides a visual output of the system performance in real time. Co-simulation helps to validate the system performance on virtual prototype of the machinery[120][121]. Various dynamic parameters like force, velocity, position, friction and torque generated can be evaluated easily in the co-simulation platform, thereby reducing the dependency

on dynamic system model derived for the robotic backhoe. Also, the technique gives the flexibility to validate the control system without an actual prototype of the system hardware. In the research, to validate the control system performance for loading torque estimation, a co-simulation analysis is performed on Adams /MATLAB platform. The list of coordinates for the bucket tip to achieve a specific dig cycle is given in MATLAB/Simulink to control the joint motions of the robotic backhoe. These values are used to develop the digging trajectory for further processing in Adams /MATLAB environment.

For co-simulation, initially a scaled down model of the robotic backhoe in a digging environment was developed in SOLIDWORKS software. The inertial parameters for the dynamic model were obtained from the computer aided design (CAD) model. The cycle of operation considered was to dig on a coarse sand environment and load the bucket. The soil bed for digging was made with small boxes of varying dimensions and density. The particle number was limited to 75000 to reduce the calculation burden on the computer. The model was later invoked in Adams environment and necessary markers, inputs and output variables were assigned as per the requirements. State variables were used to define the input and output variables. The input variables created were torque and were assigned to the joint motions. Output variables created were position, velocity and digging force during the soil-bucket interaction and were calculated with markers placed.

The feature Adams/Control Plant Export is used to create a controls_plant.m file that can be invoked MATLAB to establish the Co-simulation environment. The ideal trajectory for the motion of robotic backhoe is specified in cartesian x, y, z coordinates. The coordinates for the bucket motion was collected with a dynamic analysis of the system in Adams environment. The cartesian coordinates information, inverse kinematics and the control system equations were numerically solved in MATLAB. These equations calculate the torque required to control each joint of robotic backhoe. The control torques calculated to carry out the operation in the environment is the input to the adams_sub

block. The `adams_sub` block forms the medium with the necessary functions to communicate between Adams /Simulink environment as shown in Fig 4.9. The actual joint positions, joint velocities and the digging force calculated is given as input to the control system developed in Simulink to estimate the loading torque during the process.

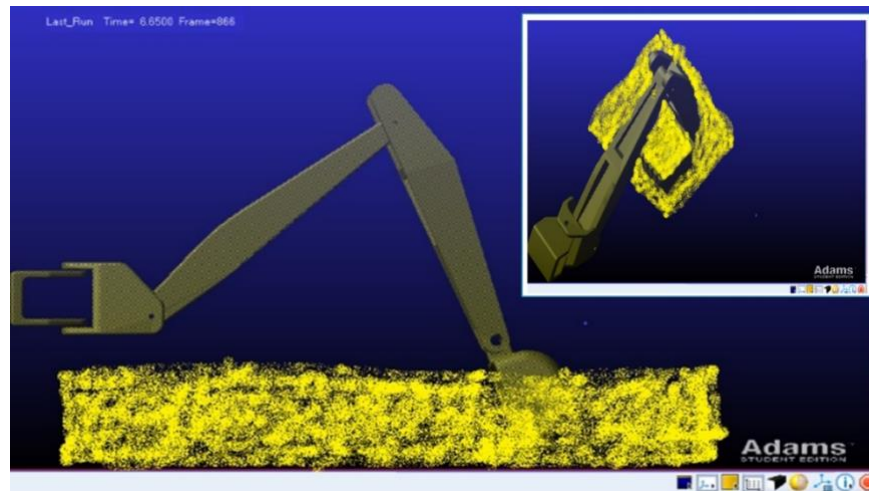
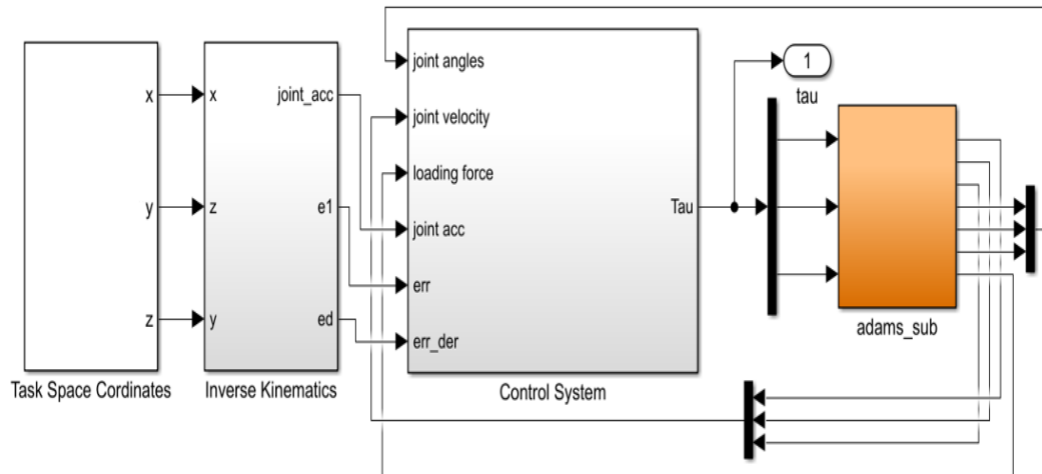


Fig 4.9. Co-simulation experiment of robotic backhoe in MATLAB/ Adams platform. The top image shows the model developed in Simulink. The bottom image shows the digging operation during co-simulation by the robotic backhoe.

The range of motion for the joints of the robotic backhoe is derived from inverse kinematics equation. Joint motions and the control scheme are applied to individual joints to archive the desired trajectory in MATLAB/ Adams co-simulation. The digging force calculation begins once the bucket touches the

sand bed and is evoked in Adams environment. This force is converted to loading torque of robotic backhoe in MATLAB/Simulink. In the experiments only digging operation is considered and hence the swing motion is held constant. The gains for the operation were manually tuned until the motion controller with observer gave desired performance. The selected gain values gave the least root mean square (RMS) error for simulation and co-simulation experiments. The chosen gains for the operation were $K_p=2I$; $K_d=.5I$; $K_0=5I$.

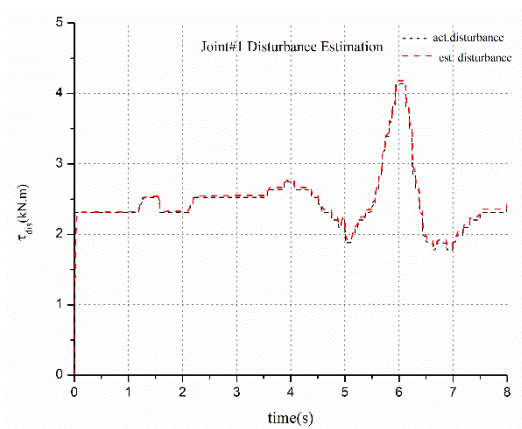


Fig.4.10(a)

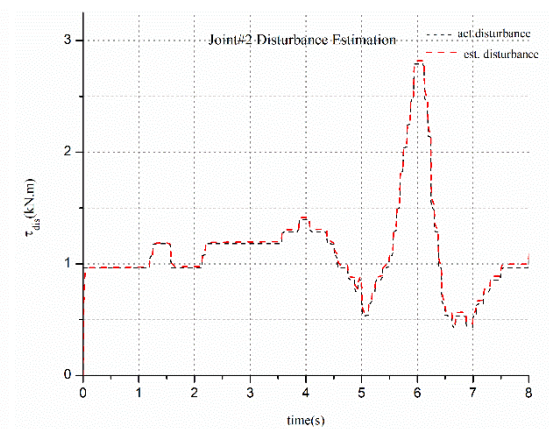


Fig.4.10(b)

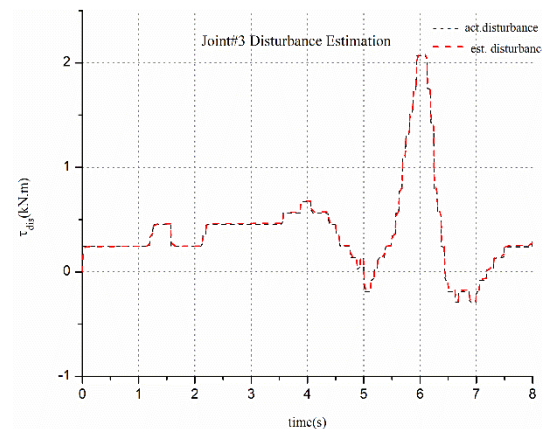


Fig.4.10(c)

Fig 4.10.(a), (b), (c): Loading torque estimation time profile of the boom, stick and bucket joint in the co-simulation experiment.

The real time values for the joint angles and the loading torques are compared with ideal values. Comparison of estimated loading torque values with desired values are shown in Fig 4.10. The real-time joint trajectories and the ideal joint trajectory comparison plots for the three joints are shown in Fig. 4.11.

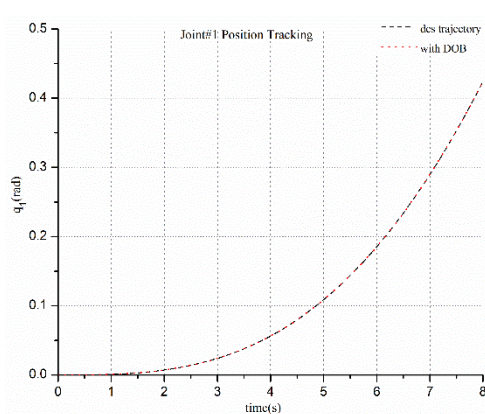


Fig.4.11(a)

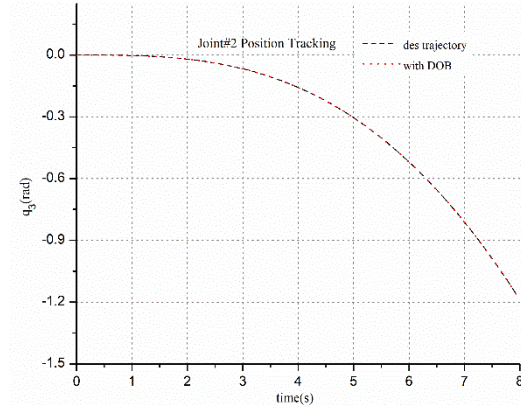


Fig.4.11(b)

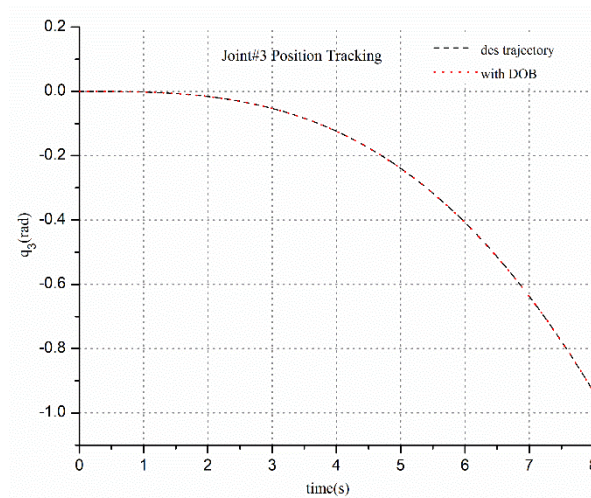


Fig.4.11(c)

Fig 4.11.(a), (b),(c): Position tracking of boom, stick and bucket joint of the robotic backhoe in the co-simulation experiment.

The results of the co-simulation experiment showed that performance of the control system is consistent with the desired results, both in estimation of joint trajectory and loading torque. The results verify the efficiency of the proposed

control system in estimating the loading torque in operation of robotic backhoe in the context of loading. The RMS error value for the position and disturbance tracking is given as,

$$Err_{q_{rms}} = \sqrt{\sum_{i=1}^n \frac{(q_d - q_i)^2}{n}} \quad (4.13)$$

$$Err_{\tau_{dis_rms}} = \sqrt{\sum_{i=1}^n \frac{(\tau_d - \tau_i)^2}{n}} \quad (4.14)$$

Table 4.2 gives the RMS value of the tracking error computed for the robotic backhoe in co-simulation analysis.

Table 4.2. RMS Error: Position and Disturbance tracking.

RMS Error	Joint#1	Joint#2	Joint#3
Trajectory Tracking (rad)	0.1426	0.3424	0.2343
Disturbance Tracking (N)	1.319	1.412	1.012

4.5 SUMMARY

In this chapter, the development and validation of a control system in estimating the loading torque acting on the backhoe is presented. The challenges in the development of control system for loading torque estimation is discussed. A DOB is developed, and its stability analysis is performed. The proposed observer is added to a motion controller, Computed Torque controller. For a given dig cycle, simulations are performed to validate the performance of the control system. Furthermore, co-simulation experiments performed with the virtual prototype of the robotic backhoe in a sand loading task presents results w.r.t tracking the loading torques and joint trajectories. The results obtained demonstrates the feasibility of the control system that can be used in developing haptic feedback for an intuitive operation.

CHAPTER 5: INTUITIVE JOYSTICK INTERFACE

Haptic interfaces can provide intuitive feedback that could mitigate operator errors. Excavator operators are often inexperienced and engage in unsafe practices. Bucket forces and loading limit are the major factors that could help the operator to comprehend the safety perception [98]. A haptic interface rendering kinesthetic feedback based on digging forces could help to raise environmental awareness in operators. In this chapter we have presented the design and development of an intuitive haptic interface that helps in acquiring necessary perceptual skills for excavator operations. The previous approaches adopted in the research is briefed. The unimanual haptic devices used in excavation and also the actuation technologies used for haptic joysticks are detailed. Also, the analysis of stiffness actuation method that enable haptic feedback is presented.

5.1 INITIAL DESIGN

Of the proposed methodologies initial approach was to develop a 4-DOF kinematically similar haptic device where the kinesthetic feedback is activated through clutch mechanism. The device proposed looks similar to the links of backhoe mechanism and operator can hold device handle to control the machinery. The device is vertically mount with encoders used for joint rotation measurement and haptic feedback rendered analogous to loading conditions. The bearings would be mounted between the joints and would be driven by a clutch inside one another based on the loading torque.

The stiffening of the joints would help the user to identify the digging force acting on the bucket. On maximum loading, the clutch mechanism would lock the bearings jamming the mechanism inducing maximum braking torque. The user would be unable to move the device as a result of the lock and would require releasing the bucket load to unlock the device. The variable stiffness would help the operator understand the loading limit of the machinery.

The links of the proposed device was made from nylon sheets with ball bearings fitted inside the joints. The joints were connected using a spring mounted rod. However, design suffered many limitations and was not found suitable after the initial phase evaluation. The chosen material was heavy, and device was heavy to handle and mount. The handle could not be held still and always had a tendency to fold due to excess weight. This would be a problem when the operator leaves the handle, the backhoe links would move (even in steady state). Though the design was intuitive, ergonomically the device operation was fatiguing as the operators need to hold the arms elevated. Fig 5.1 shows the proposed design and the initial stage of development of the prototype.

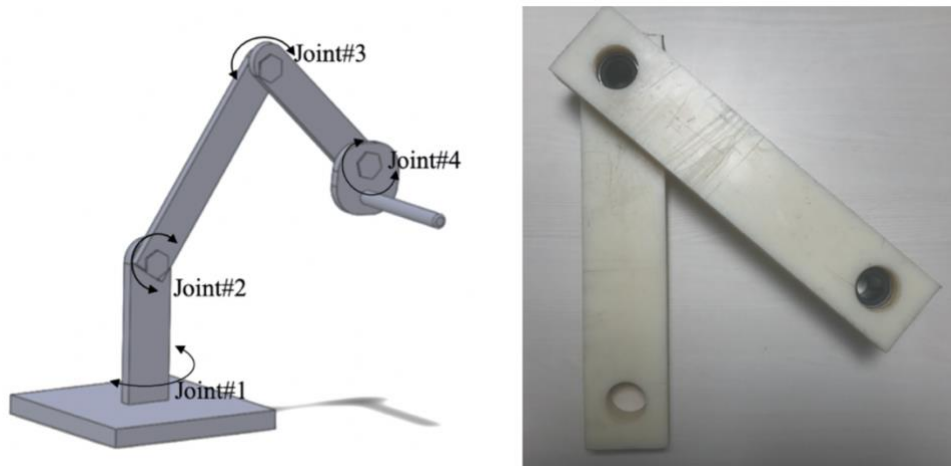


Fig 5.1. The proposed design of the initial prototype.

The hand controller used in excavators have remained the same since years where the operators use both the hands to change the controls. Majority of the previous works in haptic-excavator applications have focused on single hand interaction in VR despite the nature of bimanual interaction that occurs in excavator applications. The excavation industry is resistant to new technologies and considering the significance of interactions with both hands, the local feedback rendered in single hand may be not beneficial to be implemented in real operations. Generally, in bimanual operations could help to complete tasks faster and also increase tasks accuracy[122][123][124].

Haptic joystick is proposed as a solution to render the proprioceptive feedback to bring situational awareness in operators. The digging force is estimated with loading torque acting in the joints and feedback force rendered based on the loading torque. The similarity in configuration to conventional joystick allows the operators to acquire the required hand motions without any confusion. These features provide a more natural and realistic feeling and enhances the operator perception of risk and safety. The design is simple, cost effective and can alleviate the learning and minimize risks.

5.2 HAPTIC INTERFACES IN EXCAVATION

Several haptic interfaces are investigated in context to excavators in virtual environments. The haptic devices have shown to improve operator's task performance with force feedback. The feedback in the interfaces is usually in the form of torque, force and vibrotactile responses. Through haptic rendering machine responses are recreated and relayed back which allows the operator to immerse in the working environment [75].

Various commercial haptic devices are investigated for excavator operations in VR. Phantom devices are the most commonly explored in excavator applications[31], [41]. Though experiments revealed performance improvement however identified certain problems with the device application. However, the interface was less comfortable, and the operators had to hold the arms elevated for long time [44]. Dongnam et al. developed a newly designed haptic-interface using pressure transmitters for excavator control [34]. Morosi et al. proposed the excavator control using a Haptic Master (main interface to provide FFB) for reducing cognitive effort in operators [45]. The devices significantly increased the intuitiveness in operation, however their applications are limited due to cost of implementation, safety and complex controllers. Recently immersive technologies like HTC VIVE[125] and Oculus Rift [126], are demonstrated in context to excavation through VR systems. However, the haptic abilities of the systems are mostly limited to vibrotactile sensations.

Variable stiffness actuation based on digging forces would be an efficient way to present an dynamic digging forces to the operator. Mechanisms with variable stiffness are demonstrated in various haptic robotic applications to deal with the compliance [127] [128]. The common actuation methods to include approach in haptic joysticks the rheological fluids brake (magneto and electro) [38] [129], shape-memory alloy (SMA)[130] , jamming, particle brakes with DC motors [131]. In haptic joysticks, mostly actuation is in the form of kinesthetic feedback on the shaft. The researches use individual or a combination of actuation mechanisms to generate the restoring torque and the required reaction torque to oppose the users movement.

However, SMA and particle brakes require longer actuation periods. The rheological fluids have shorter reaction time but are prone to sedimentation over time. Interfaces with particle jamming techniques promise high stiffness gains but when unjammed reduce the flexibility and also the weight mechanism increases with volume of matter required. However, the excavation industry is resistant to new technologies and therefore there exists several practical challenges in the implementation of commercial haptic controllers.

Existing actuation techniques to implement variable stiffness in haptic joysticks could achieve good stiffness control along with high braking torque. However the technologies are infeasible due to cost (in actuation methods), size and power constraints. Therefore, a new electro mechanical actuation method is investigated for the development of haptic joysticks. The haptic links can dynamically alter the stiffness perceived in the user's hands based on the effect of digging force on each joint. At maximum loading they can restrain the user motion by high resistive torque in specific direction of motion.

5.3 HAPTIC JOYSTICK

The development of the proposed joystick is divided in to two sections: design of the prototype and the electromechanical actuation technique.

5.3.1 DESIGN AND CONSTRUCTION

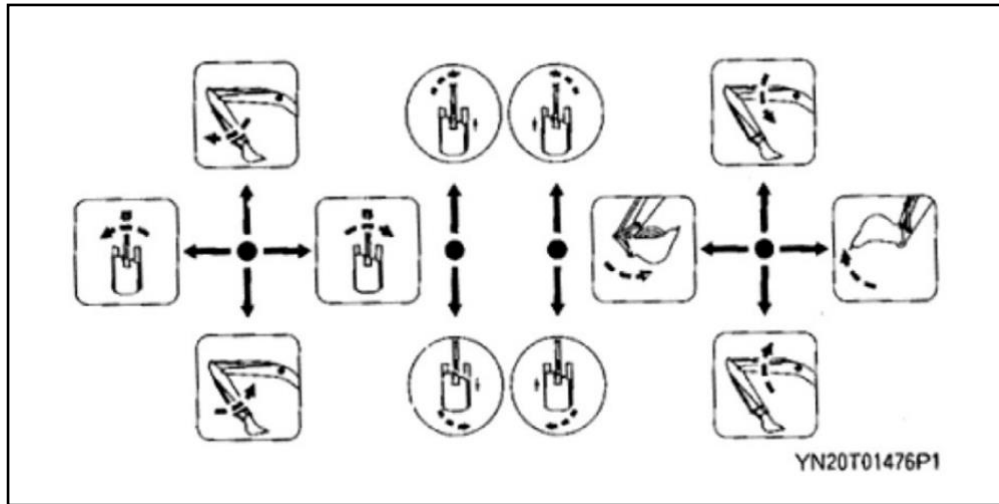


Fig 5.2. SAE Pattern for Motion Control [132][133]

For joystick motion control, the control standard adopted is SAE standard, where the dipper and swing are operated by the left joystick and the boom and bucket by the right joystick as shown in Fig 5.2 [132] [133]. The main design consideration in the implementation of the interface was motion flexibility on free motion, stiffness with constrained motion (loading), power consumption, stiffness resolution, speed of actuation and weight. Two commercially available joysticks were modified to implement the prototype (Extreme 3D Pro Joystick, Logitech). The joystick direction of motion is detected with two rotatory encoders attached to base.

The haptic effect was displayed through two main mechanisms: a haptic link rendering FFB to the shaft of joystick and a servo motor to where the haptic link is attached. Four haptic links (each of thickness 1cm, cut from PVC sun board) were assembled on four sides of joystick shaft to render FFB in both motion of joystick axis. The servo actuator (11 kg-cm torque, 180° rotation in 2.1 milli sec) drives the haptic link mounted to its shaft. The other end of the haptic links was attached to U groove pulley bearings to reduce friction. The actuation of variable stiffness is implemented with a particular arrangement of hall sensor and magnet set. For the prototype, ultra-small rare earth permanent magnet, (4mm

x 2mm, NdFeB magnets) were used and mounted to the links through tiny slits. The ratiometric linear hall sensor, (model: MH481) was mounted fixed to each link using fully threaded M4X6mm screws.

Table 5.1. Specification of Hall sensor and Neodymium magnet

Hall Sensor, MH481		NdFeB magnets	
Operating voltage	3.5 V to 6.5 V	Performance Grade	N35 Ni
Output Voltage	2.3V to 2.7 V	Diameter	4mm
Output type	Linear, Sourcing	Thickness	2mm
Magnetic Flux Density	No limit	Tolerance	±0.1mm
Response Time	3 μs	Density	7.5 g/cc
Sensitivity	1.2 to 2.1 mV/G	Compression Strength	780 N/mm ²

The output voltage of the IC varies in proportion to the magnetic field strength. The links design is presented in Fig. 5.3. The hall sensor was mounted such that the sensor appears above the magnet.

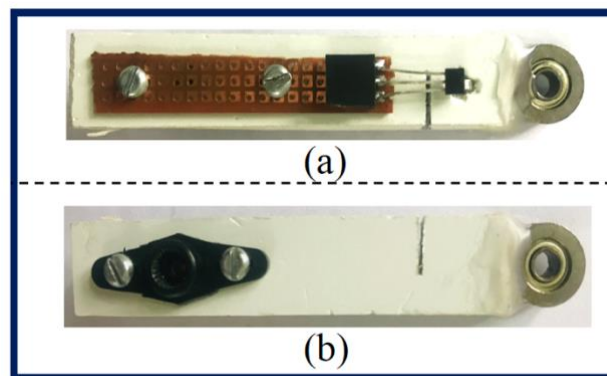


Fig 5.3. The haptic link design:(a) Shaft link front view showing the hall sensor-magnet arrangement(b)Shaft link rear view.

To deflect the hall sensor-magnet alignment, a small slit (width 2mm and depth 10mm) was made in the link. The hall-effect IC can sense the presence of any ferrous materials. Within the air gap, a Hall element is used to sense the magnetic flux density. The output voltage of the sensor varies in proportion to the magnetic field strength.

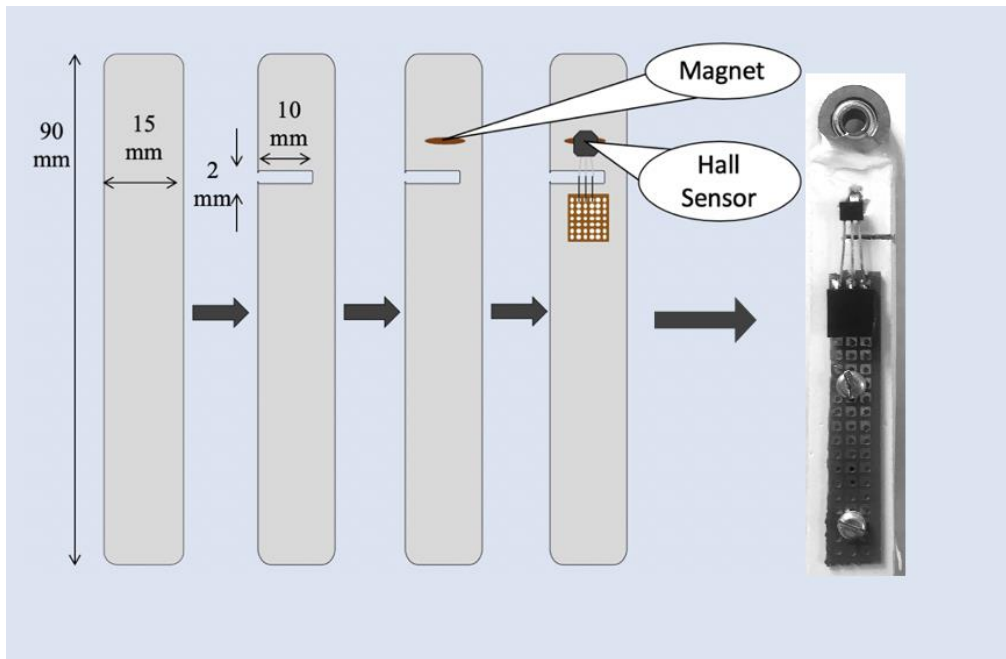


Fig 5.4. The dimension of haptic link with sensor arrangement. The force would be applied from the joystick through the uncut side of the link which would change the sensor-magnet alignment.

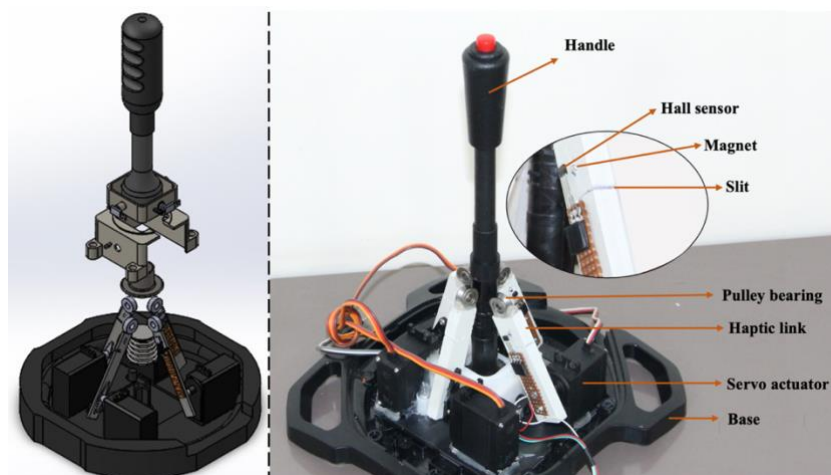


Fig 5.5. The schematic design of the Haptic joystick

The dimensions of haptic link and the sensor arrangement are presented in Fig 5.4. The slit opening could be deflected with force applied from the uncut side of link which would change the sensor-magnet alignment. The schematic design of the haptic joystick prototype developed is shown in Fig 5.5.

5.3.2 VARIABLE STIFFNESS ACTUATION

The haptic rendering is implemented by an electro-mechanical actuation technique of configuring servo as a ‘virtual spring’. The variable stiffness of the spring is rendered as haptic feedback in the joystick. The servo characteristics are transferred through fixtures ‘haptic links’ to the operator. In the design of haptic joystick, the hall sensors are configured as a motion sensor.

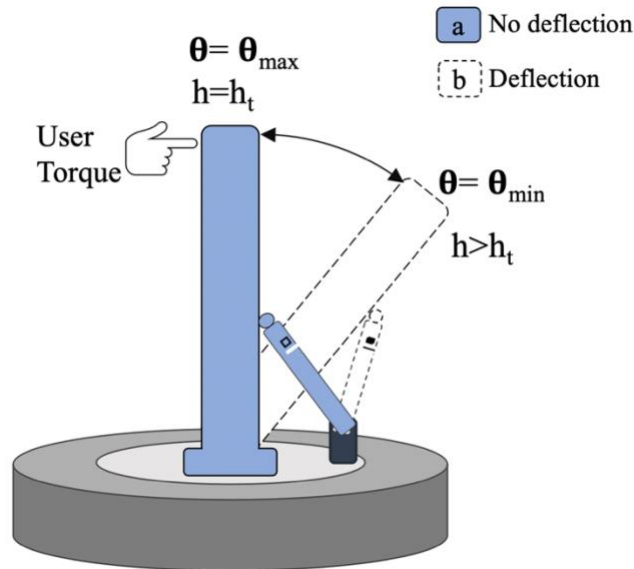


Fig 5.6. User torque detection to activate variable stiffness feedback

The sensor output signals are compared to pre-defined threshold values to detect the displacement of joystick-shaft from datum. When sensor reading exceeds threshold value i.e. $h > h_t$ the haptic effect is activated as per the bucket force. The spring constant sets the stiffness in the haptic link proportional to loading torque, τ . The spring constant can be characterized as a function of load, loading torque and sensor threshold value and can be modelled with the following expression as,

$$k = F_r \tau + h_t$$

The system input is the loading torque τ and the output is the spring stiffness k . F_r is the range of load, (the difference between the maximum and minimum loads defined in simulator). The point (b) where it crosses Y axis is the sensor threshold value h_t . The expression introduces a variation in the range between k and h_t according to load conditions. Once k is generated the controller calculates required servo angle θ as,

$$\theta = \text{map} \left(\underbrace{\text{value}}_h, \underbrace{\text{fromLow, fromHigh}}_{h_t, k}, \underbrace{\text{toLow, toHigh}}_{\theta_{min}, \theta_{max}} \right); h > h_t$$

The expression re-maps the sensor value h from range (h_t to k) to a new range (minimum, θ_{min} to maximum, θ_{max}). θ_{min} and θ_{max} are the maximum and minimum angles of servo rotation as shown in Fig 5.6. The new value is assigned to θ , which determines the servo position.

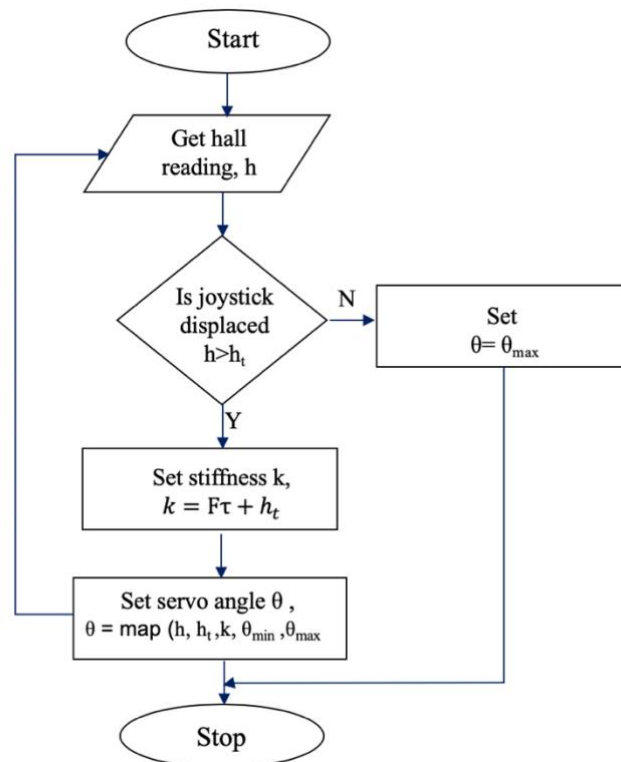


Fig 5.7. Flowchart presenting the variable stiffness actuation in haptic joystick

An increase in digging force, loading torque and spring constant, increases the data points in the lower range of mapping. As a result, the servo becomes stiffer

and the haptic link restrains the operator torque. The stiffness in the servo actuator constraints the joystick motion replicating the loading force to the user as in real time. The flowchart presenting the variable stiffness actuation in haptic joystick is presented in Fig 5.7.

5.4 ANALYSIS

The variation in joystick current measured for different digging forces by applying constant 1Nm torque in joystick is presented in Fig 5.8. The input actuator current drawn is proportional to the variable stiffness in haptic links and the reactive torque in joysticks. Based on the bucket force, the haptic links constraints the range of motion in joysticks. The input actuator current was measured using a current sensor and the values generally ranged from 100-900mA for the prototype. It was found that at maximum loading the haptic-links push the joystick with maximum stiffness by holding at stall-torque. It can be seen that joystick motion is limited with an increase in bucket contact forces.

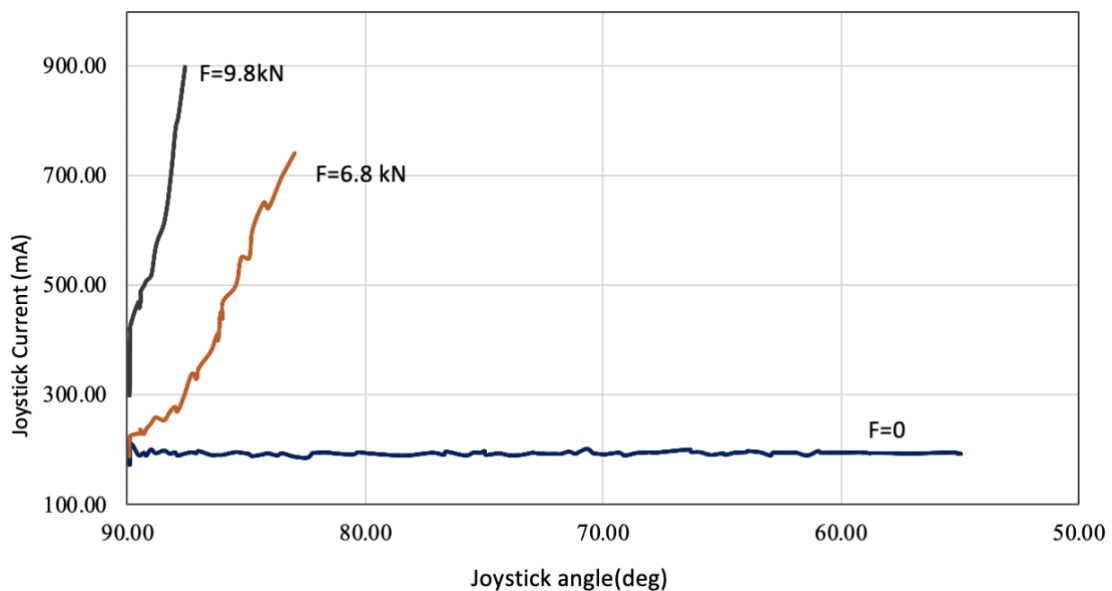


Fig 5.8. Variation in joystick current with different digging forces

The reactive torque output and joystick angle measurements for a digging operation(bucket joint) is shown in Fig.5.9. The reactive torque remains low due to relatively low loading torque in the initial stage. As the digging is initiated in the simulator, the reactive torque in the joystick increases analogously providing variable stiffness to the joystick motion in the particular DOF.

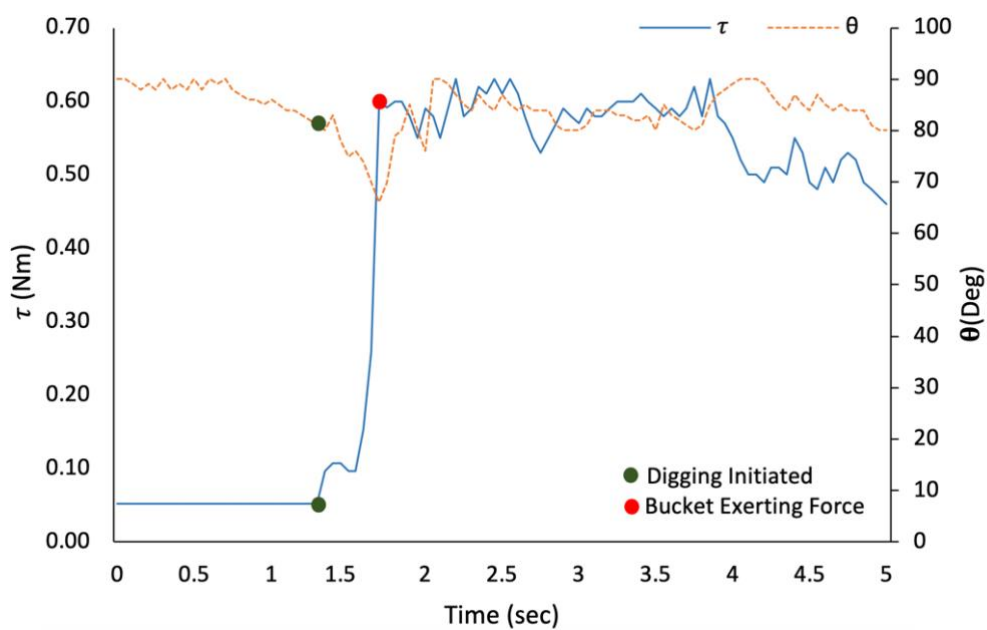


Fig 5.9. The variation in joystick torque and angle with loading

The final prototypes of the haptic joysticks developed are shown in Fig 5.10



Fig 5.10. Final prototypes of the haptic joysticks

5.5 SUMMARY

In this chapter, the development of an intuitive haptic joystick is discussed. The haptic joysticks developed are economic, has similar configuration to conventional joysticks and therefore can easily master the hand motion required to operate the machinery. The haptic feedback is based on the loading torque acting on the machinery while performing different operations and helps the operator to handle the machinery with better judgement of safety and efficiency. The haptic joysticks developed render a natural stiffness as in real excavator operation. Haptic feedback is implemented using servos and a set of hall sensor and magnet. The links are attached to small pulley which reduces the friction to the motion of the stick. Though proposed device is developed for excavator, use of the device can be extended to other hydraulic machinery training purpose as well owing to the excellent kinaesthetic-feedback and the simplicity in system geometry.

CHAPTER 6: VIRTUAL SIMULATOR AND HAPTIC EVALUATION

The virtual environments bring out the behavioural tendencies and perception of individuals and therefore simulator environments are used as evaluation platform for haptic devices. The simulations in VR can be characterized as a computer generated virtual immersive environments that allows users interaction with reality [134]. Also, virtual simulators can render various kinaesthetic and tactile sensations allowing them to be an ideal test bed for haptic controllers [135][136][137][138]. The implementation of haptic feedback with VR environments can enhance the realism and user presence [139].

VR simulators are widely used within safety and training aspects in construction for risk assessment [140], and hazard recognition [141]and also decision making [142]. The simulators offer many benefits; it ensures an environment for repeated operations and helps to assess the operator performance saving fuel, money and resources. Also, the operators can be exposed to high risks environment without compromising the safety. Skills learnt from simulator experience can be retained and applied in real life. The cutaneous sensation together with audio-visual information is shown to improve memory capacity [143].

A virtual backhoe simulator is made as a testbed for the force feedback and user evaluation of haptic platform. The dynamic simulator provides an exact imitation of set-ups for assessing the proposed haptic framework. It ensures a fair and reliable test environment for evaluation of operator skills. In the VR haptic framework, different steps are followed to perform the excavation task in the virtual environment. The user is the human layer, haptic joysticks are the hardware layer and virtual environment is the software layer. The operator interacts with the haptic joysticks that are coupled to the simulator environment through haptic rendering. All the elements are linked through interaction

techniques which allow the operator to control the virtual backhoe. The Fig.6.1 represents correlation and the transfer of data between various elements in a haptic framework.

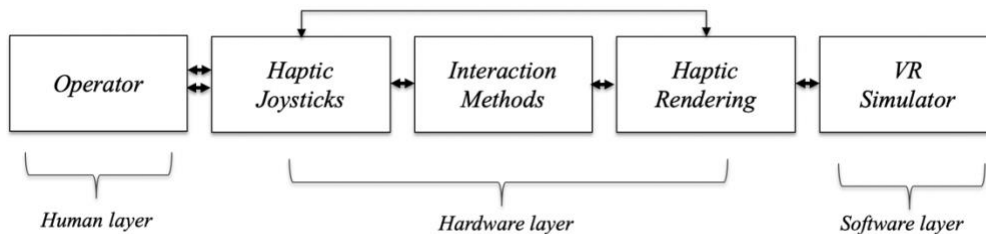


Fig 6.1. Correlation between various elements in the haptic framework.

6.1 DYNAMIC BACKHOE SIMULATOR

For the study, the interactive 3D simulator was developed using feature-rich game engine platform UNITY. The platform supports rigid-body dynamics, supporting the application of forces and collision. The built-in physics engine and shaders, the manipulation effects and the appearance of the models were made more realistic. UNITY 3D encapsulates physics to approximate the universal forces and allows the dynamic interaction of objects. Several built in functions like Colliders, Rigidbody, PhysicsMaterials and other features like Terraineditor were used to define the objects and interaction with the environment. Modelling of soil-bucket interaction, collisions and other aspects were carried out using Scripting function. This enabled the computation of contact forces, coordinates of bucket tip, digging depth etc. The joints of the machinery were defined as fixed and hinge joints to enable the application of torques and range of motion was constrained with joint limiter. These built in modalities assure the collision, penetration, friction and other features to be enabled in the platform.

The simulator environment is made with backhoe arm, rocks, sand blocks, and trees. The virtual backhoe consisted of a boom, stick and bucket mechanism with a rotating swing link. The rigid bodies like rocks can move under the application of forces, even collide with each other. The operators were to sit in

front of the screen, control the machinery with the joysticks. With digging, the operation realism is enhanced with change in the elevation and texture of the dug pits. The signals were sent and transmitted through the serial port communication to the simulator PC.

Two test scenes were developed in the simulator for evaluation: sand loading and rock loading. The simulator screen also shows the information like depth of dig, warning indicator' and time for loading information. Fig.6.2 shows the sand loading environment made in the simulator. The soil particles in the simulator were simulated with large number of small brown boxes and were placed as a heap in the ground. Though simulated soil had to be optimized to reduce computational burden of the computer, the physics and attributes of friction, penetration and bounce were maintained.

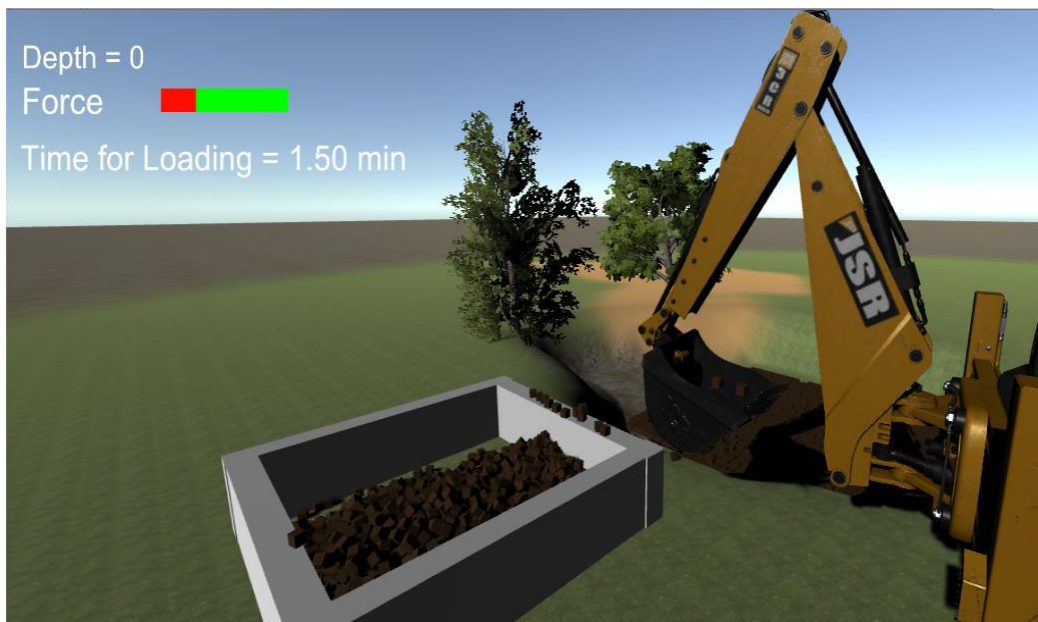


Fig 6.2. Simulator environments made for sand loading

The level of difficulty and judgement were increased with rock loading scene. The environment consisted of rocks of varying sizes and mobility. Some of the rocks were fixed to ground. Fig.6.3 shows the rock loading environment made in the simulator.

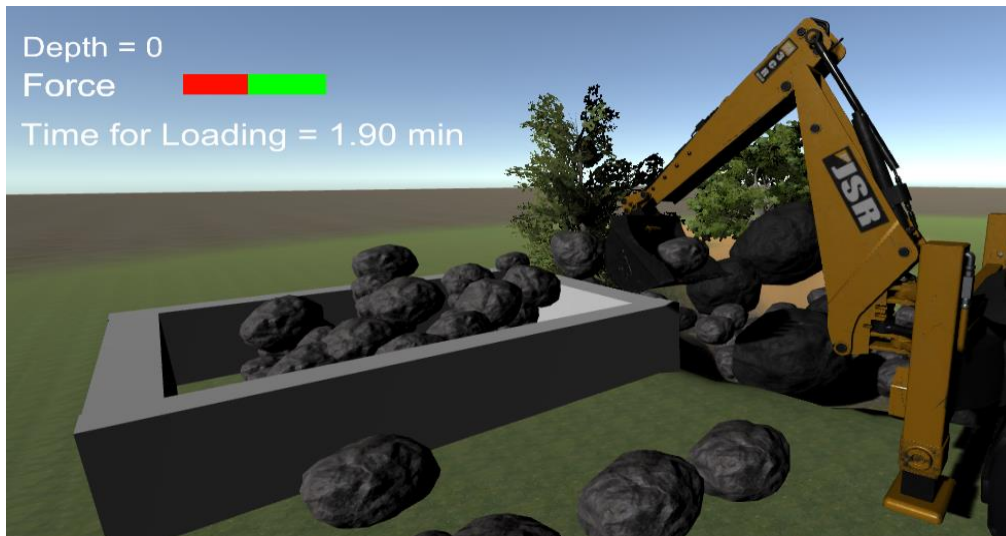


Fig 6.3. Rock loading environments made in VR simulator

The simulator provides the capability to change the operator perspective and adjust the operator view. Fig 6.4 shows different operator perspective for the rock loading operation.

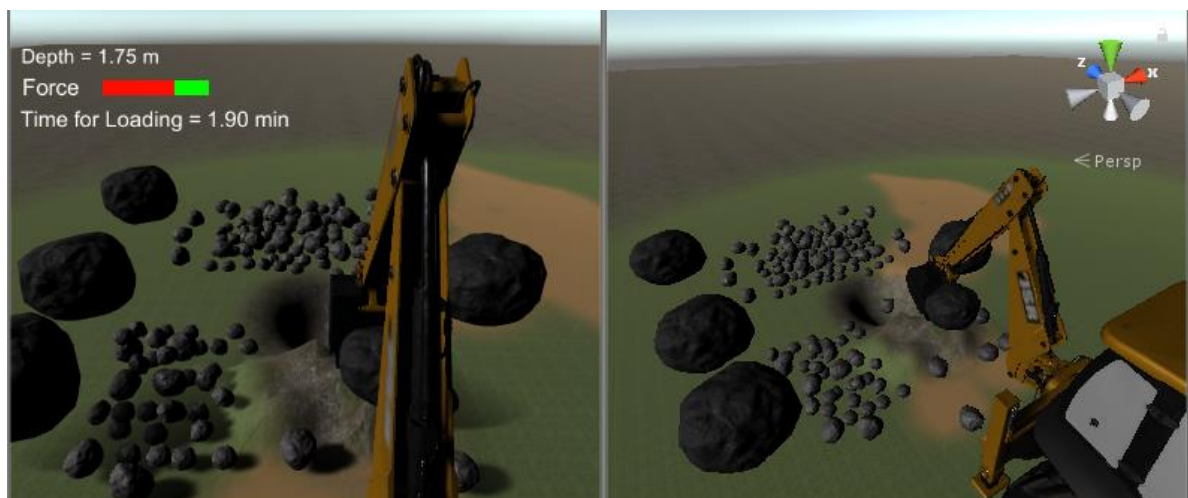


Fig 6.4. Different operator perspective for the rock loading operation.

6.2 SIMULATOR DYNAMICS

The loading torques are computed as a result of the resistive forces arising from bucket-ground interaction. The forces required to overcome the shear-strength of the soil are computed as the resistive forces. In the process of earthmoving, the interacting ground should be brought to complete failure state. Therefore, in

the simulator environment principle of soil mechanics and modified Fundamental Earthmoving Equation are followed to model the bucket-contact forces [144][145]. The soil-bucket contact forces F_l are shown in Fig. 6.5 and computed as,

$$F_l = d^2 w \gamma g N_\gamma + c w d N_c + V_s \gamma g N_q \quad (6.1)$$

where, d is the depth of tool below soil, γ is the soil-density, c is the soil cohesion, w is the tool-width, q is the surcharge-pressure acting vertically on soil, and N_γ, N_c , and N_q are factors which depend on both soil frictional strength, tool geometry and soil-tool strength properties.

$$\begin{aligned} N_\gamma &= \frac{(\cot\beta - \tan\alpha)(\cos\alpha + \sin\alpha \cot(\beta + \phi))}{2(\cos(\rho + \delta) + \sin(\rho + \delta) \cot(\beta + \phi))} \\ N_c &= \frac{1 + \cot\beta \cot(\beta + \phi)}{\cos(\rho + \delta) + \sin(\rho + \delta) \cot(\beta + \phi)} \\ N_q &= \frac{\cos\alpha + \sin\alpha \cot(\beta + \phi)}{\cos(\rho + \delta) + \sin(\rho + \delta) \cot(\beta + \phi)} \end{aligned} \quad (6.2)$$

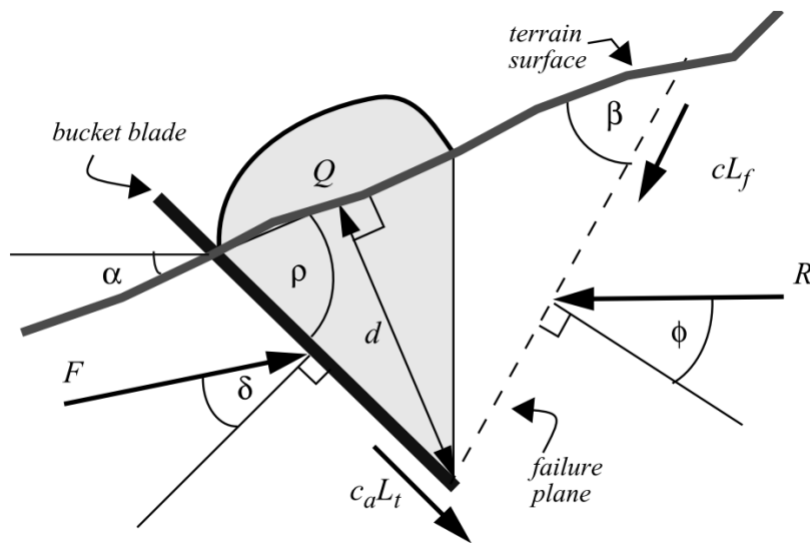


Fig 6.5. The modified soil tool model[113].

The digging forces computed can be used to model the braking torque in the haptic joystick by means of loading torque. The bucket interaction with ground initiates the calculation of contact forces as well as the bucket depth below the soil (which is calculated only for the span of digging).

6.3 FORCE FEEDBACK EVALUATION

The soil tool model computes the digging force exerted at the bucket tip from the ground. The effect of digging force is calculated through loading torque at the boom, stick and bucket joints and fed back to the operator. The direct estimation of loading torques enables transparency and hence better performance. The digging force would be uneven and can have high frequency transients. The application of the nonlinear observer is proposed to enhance the fidelity required to display the bucket forces during haptic interactions. The block diagram representation of system architecture is shown in Fig.6.6.

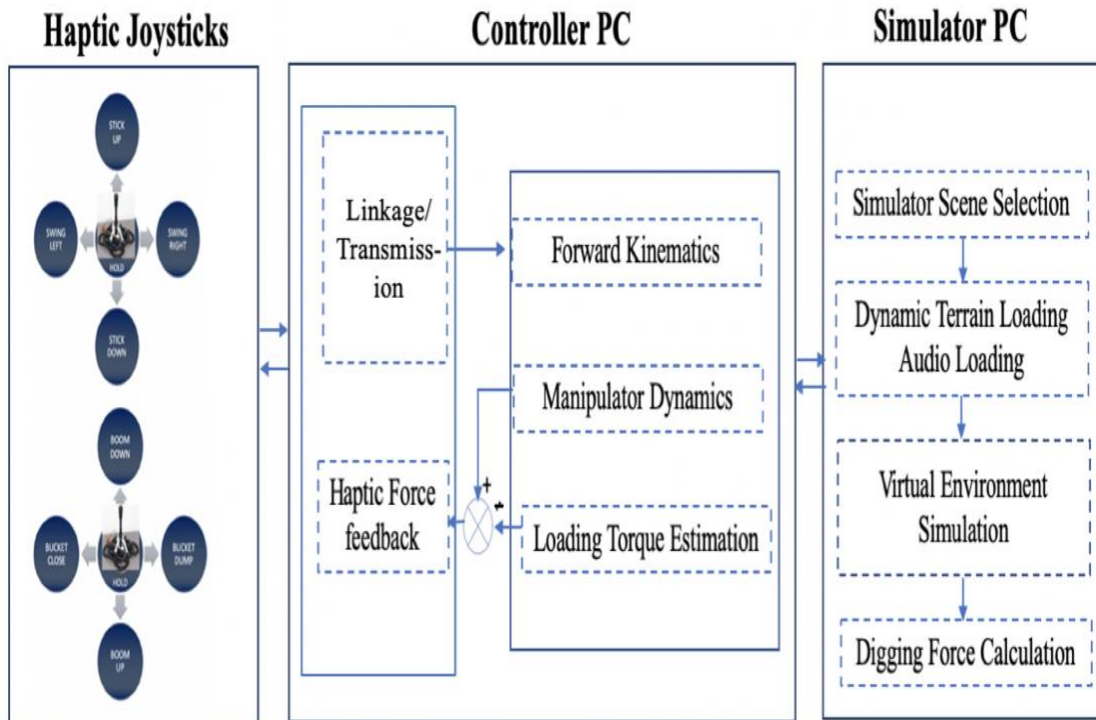


Fig 6.6. Block diagram representing system architecture.

Two desktop computers were used: 24-in, Intel i7-8700, 3.2GHz processors with AMD Radeon R7 200 series graphic card and 16 GB RAM. The haptic joysticks were interfaced to Computer#1 and Computer#2 ran simulator graphics and the digging force calculations. The loading torque is computed from Simulink-Arduino model implemented in Computer#1. In the simulator the joints of backhoe are controlled through torque provided from the controller PC. The digging force and the joint information are obtained from the simulator PC.

In free motion, the output torque, is only due to $\tau_{actuators}$ (equation 3.33). The bucket- soil interaction is computed with the bucket tip co-ordinates using forward kinematic equations (equation 3.8). As bucket interacts with soil (or the medium), $\tau_{digging}$ is computed with manipulator jacobian (equation 3.26). To render operator feedback, the output torque is analogously scaled down to the range of 0-0.9 Nm. The signals were sent and transmitted through the serial

port communication. The motion accuracy is maintained through a control signal proportional to position error between the desired and actual joint motion given (equation). The comparison between the commanded joint position and the simulator joint position in free motion is shown in Fig 6.7.

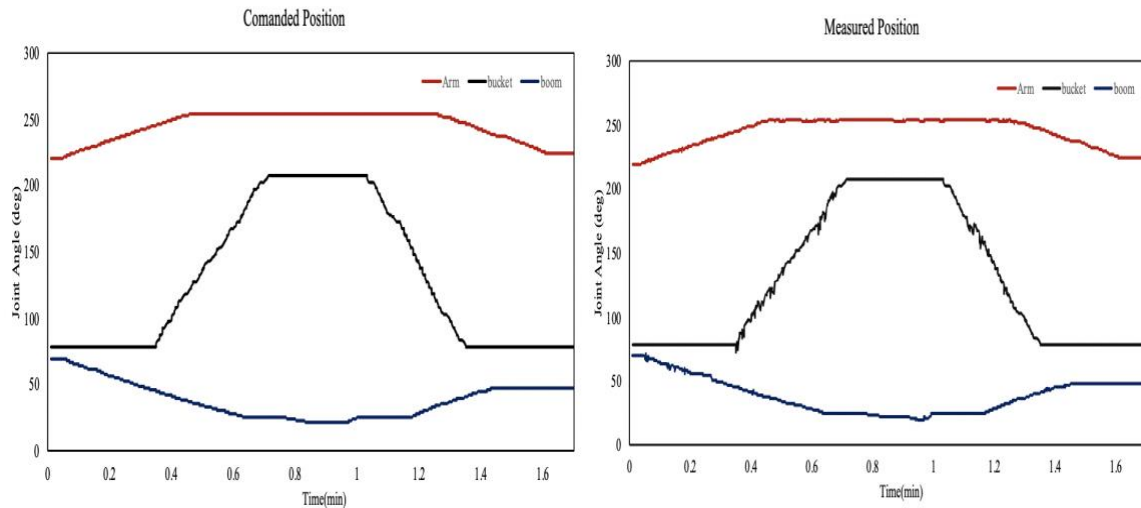


Fig 6.7. Comanded joint angle positions and the responses from the simulator.

Fig 6.8 shows the digging force computed at the bucket tip and the resultant loading torques estimated at the joints. The maximum loading torque as for the particular motion is estimated at the boom joint. The results shown are for a cycle of digging motion (scooping) of sand from the bed, where it can be seen that the controller is accurately estimating the predicted loading torques at the joints.

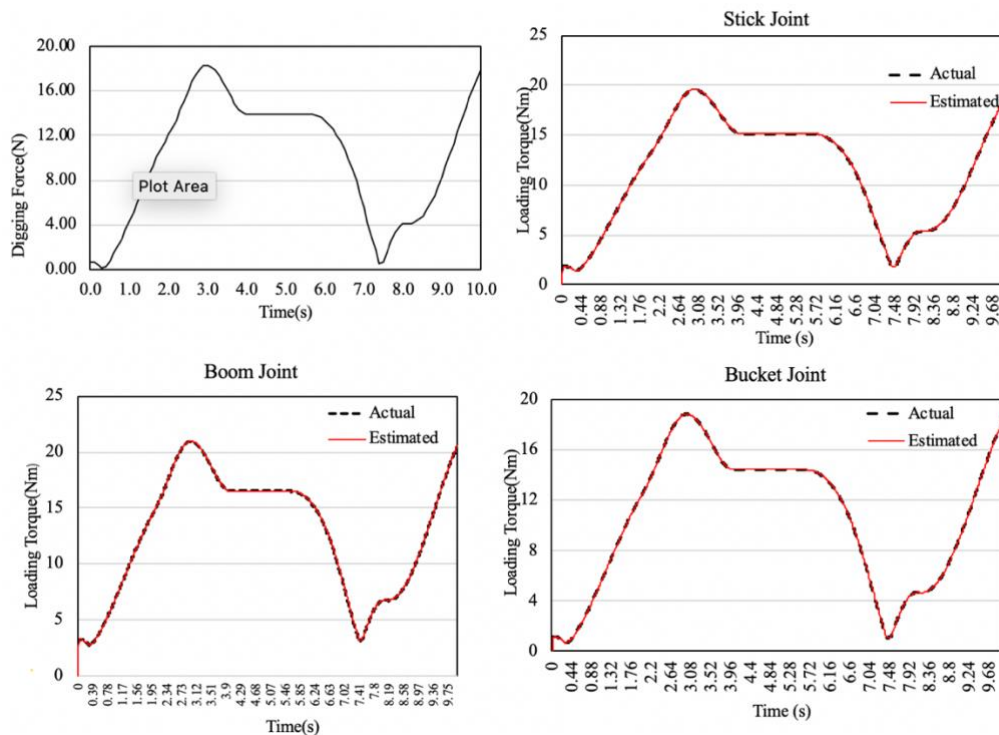


Fig 6.8. Digging forces at the bucket tip and loading torques estimation at the joints.

6.4 USER EVALUATION

To assess the effectiveness of loading force with the developed interface on operator performance the following methodologies are adopted:

6.4.1 PERFORMANCE METRICS

A random within subject design methodology was used to assess the performance of the developed device in operator training. We investigated device performance in two different simulator environments; sand loading and rock loading. The objective assessment of the excavator operation with the haptic interface was carried out with the simulations in simulator environments. The following key performance matrices were measured:

- a. Volume of soil removed: The average amount of material removed from the digging trench

- b. Number of collisions: Average number of times that the bucket collided with the walls of the bin
- c. Smoothness of bucket motion: The number of times the materials dropped from the bucket.
- d. Force applied: The number of times the applied force reached the maximum limit while performing the operation

The volume of the material removed can indicate productivity, collisions and the force pattern can indicate the care taken by trainee. Any sudden movement or rotation of the bucket would make the material drop from the bucket [146], [147].

6.4.2 APPARATUS

The equipments for the study consisted, a gaming joystick (Non Force-feedback Joysticks, NFJ) and the haptic joysticks (Haptic Feedback Joysticks, HFJ) interfaced alternatively to Computer#1 which ran the control system for haptics simulation. The simulator graphics and the excavator dynamic simulation were installed on #Computer2. The participants controlled the virtual excavator from the operator perspective inside the machine cabin.

6.4.3 PARTICIPANTS

Twenty participants from the University of Petroleum and Energy Studies community (5 women and 15 men) age between 19 and 32 years (mean = 24.6, standard deviation, (S.D) = 4.30) were recruited for the study. Nine participants had used a VR simulators one to two times, but none had previous experience with excavators. One participant had used a similar force-feedback haptic device on a virtual reality simulator as part of coursework. According to the self-reports, all participants had normal touch sensitivity.

6.4.4 TASK DESCRIPTION

The task involved the two scenarios in independent virtual scenes; excavation of sand and rocks. The operator had to choose the particular scene to go to the

loading environment. The objective in the scenes were to perform a Move: Dig: Move: Dump cycle. The subjects were to move the excavator, dig up the material located in the worksite, move the dug-up load back and dump them in the bin placed at a fixed location. The level of difficulty and judgement were increased with rock loading by varying sizes and mobility of the rocks. Some of the rocks were fixed to ground with their location were unknown to the subjects. The rocks were placed at vantage locations and to dig and dump the subject should apply the necessary combination of boom, arm and bucket motion with the joystick.

6.4.5 PROCEDURE

The experiments started with the briefing about purpose of study, basic parts and controls of excavator simulator. Participants were also explained about the ‘warning indicator’, a measure of bucket force, in the top of the monitor display. Two interaction methods are adopted to verify the proposed design. First method utilized a gaming joystick control with only visual feedback from the simulator, (NFJ). Second method utilized simulator display with haptic joystick (HFJ). The participants were asked to use the two sets of joystick controls to maneuver the excavator to fill the bin. The operators were given 15 minutes warmup session to get them familiarize with the hand controllers and the simulator loading environment.

Each participant got a three-minute session (with the interfaces individually) to complete the task. Entire experiment was divided into four sessions and each subject performed two sessions per day with an average interval of 2 hours between the sessions. The test procedures continued for a period of four weeks and the data from the tests were recorded.

The operators were asked to fill a pre-test questionnaire before the experiments. The main idea was to collect the knowledge of users about haptic interfaces. During the trials the operator performance was obtained, and the subjective measures of experience were gathered using post-questionnaire (0 to 5). Finally, the comments were taken for further improvement and modification. The pre

and post questionnaire used for the study is given in Appendix C. Fig 6.9 shows the experiments of haptic joysticks carried out with human subject.



Fig 6.9. Human subject experiments with the developed haptic joystick.

6.5 RESULTS

The section presents the results for human subject experiments conducted for the two loading environments separately.

6.5.1 SAND LOADING EXPERIMENTS

Average volume of material in bucket and average number of collisions against the walls of the bin were compared in sand loading environment. The volume of the material in bucket can indicate operator efficiency in terms of how many loading repetitions were required to complete the task. The bucket capacity was limited to 1.35 m³. Collisions with the walls of bin can indicate the care taken by the participant. Bucket loading is an inconsistent task and without this skill the equipment may get worn and even damaged.

The amount of soil removed has significantly increased over the trial runs with both the joysticks. This may be the result of the participants getting familiar with the excavator control and operation. With NFJ, the bucket fill improved by 42% over the course of trials. However, with FFB joystick an improvement of 52.6% was observed in bucket fill. Fig 6.10. shows the results of the experiment with the two interfaces.

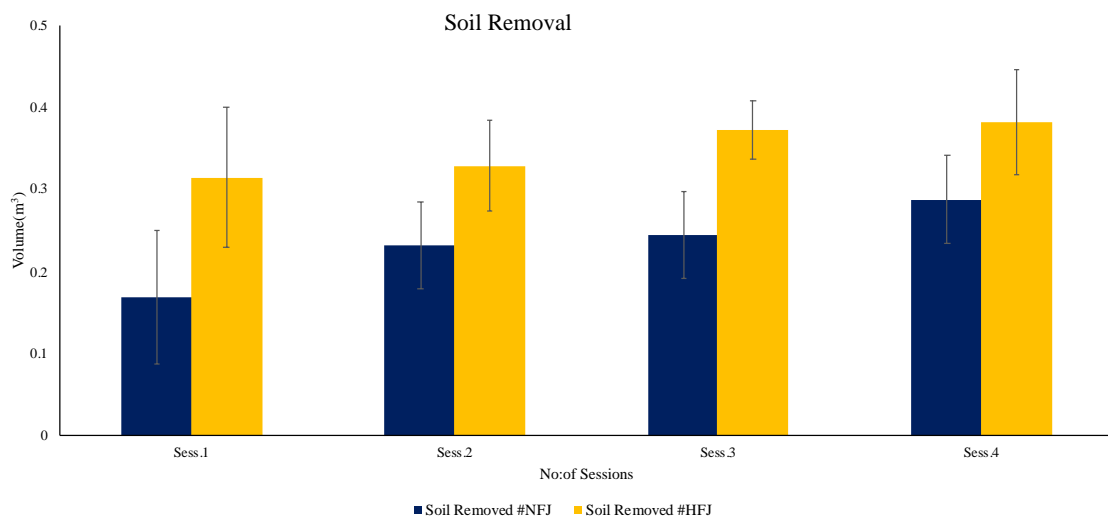


Fig 6.10. Avg. amount of material in bucket. Error bars show standard deviation.

The collisions with walls of the bin occurred mostly while the operators were trying to drop the pile. The average times the operators have hit the bin walls have significantly reduced to 70.9% with the haptic joysticks while with NFJ, it was 43.9%. The errors in task significantly dropped with the haptic joystick. Fig 6.11 shows the results of the collision experiment with the two interfaces.

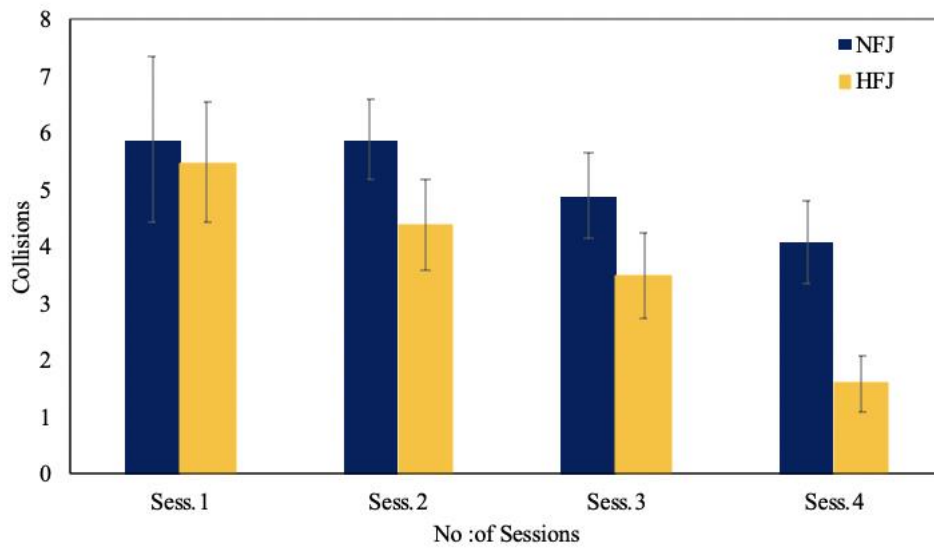


Fig 6.11. Collision experiments with the two interfaces.

6.5.2 ROCK LOADING EXPERIMENTS

The haptic joysticks showed a significant impact in the operator performance with sand loading and therefore level of difficulty was significantly raised with the rock loading. In the real excavator audio cues are significant to operators. Therefore, a third combination of engine sounds with haptic joysticks were experimented in the operation. The engine sounds were played with speakers and synced with the machine simulation. The experiments with rock loading compared smoothness of bucket operation, force application and average load in bucket to understand effect of proposed interfaced. The objective was to assess if the combination would upgrade the operator performance with haptic joysticks and enhance learning.

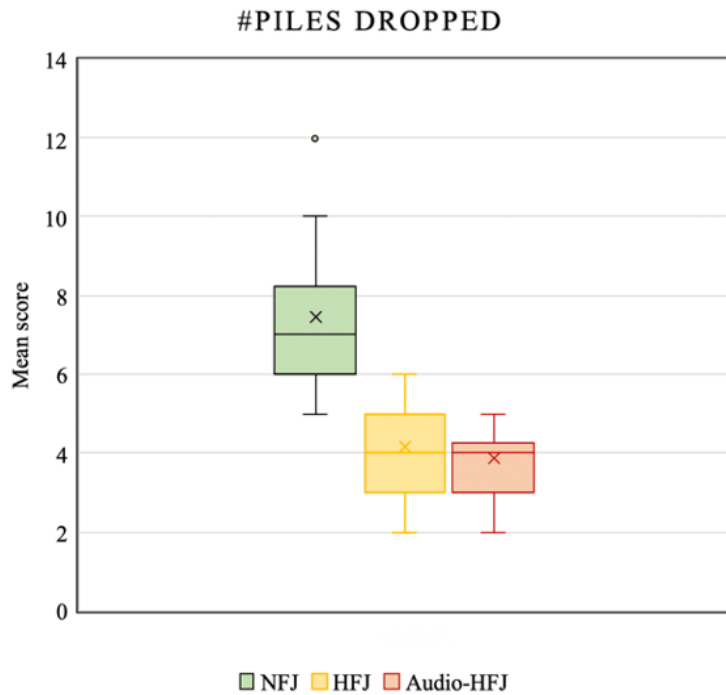


Fig 6.12. Box plot showing the piles dropped outside the bin

During loading, bucket handling should be smooth, if not the materials would drop from the bucket. Smoothness of motion is possible only with efficient coordination between boom, stick and bucket. For this reason, the average number of drops outside the bin were measured to analyze the operational skill in smoothness in bucket handling. The results of the experiments are presented in Fig 6.12 and it showed a significant decrease of drops outside the bin with FFB (HFJ: mean=4.15, S.D=1.13) than with no feedback, (NFJ: mean=7.45,S.D=2.11). Also, the particular combination of engine sounds and HFJ also showed a slight improvement in operator performance (audio-HFJ: mean=3.95, S.D=0.93). A one-way ANOVA test with confidence interval of $\alpha=0.05$ was conducted to analyze the experiment results in three combinations. The test results show that there is a statistically significant difference in the smoothness of bucket operation for the haptic joystick and audio-HFJ over NFJ. The test results show that there is a statistically significant difference in the smoothness of bucket operation for the different interface combinations (F2,57

=3.15884272, $p= 7.48507E-11$). A post-hoc Tukey test was carried out to compare the mean score of piles dropped for different interface combinations. The results showed a statistically significant difference between the mean of NFJ and the means of HFJ and audio-HFJ. However, the means of HFJ and audio-HFJ were not significantly different.

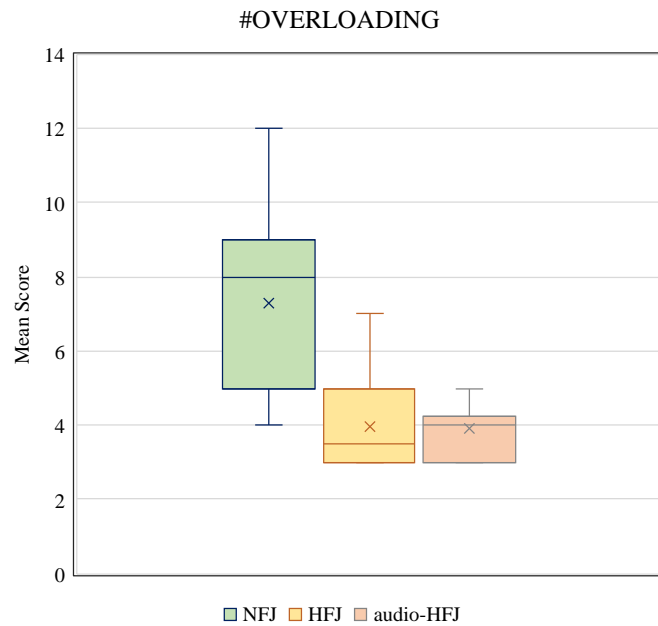


Fig 6.13. Box plot showing the mean of the excess force applied during the trials

Force patterns could be easily analyzed within a VR platform and help to evaluate the operator skill [148]. The focus in preventing overloading indicates the operator's perception of digging forces. Excess throttle may lead to wheel slip and may even damage the machinery [108]. The digging forces calculated at the tip of the bucket is compared against the rated standard (safe limit) to determine overloading. The safe limit is set at 8.9kN according to standards of SAE [31]. Also as a visual aid, the warning indicator on the simulator screen turned red from green with overloading. The average times the applied force exceeded the safe limit was observed to measure the skill and the results are presented in Fig.6.13. ANOVA test showed statistically significant difference for the three modes: NFJ (mean=7.45,S.D=2.11), HFJ(mean=4.15,S.D=1.136) and audio-HFJ(mean=3.85,S.D=0.93). A post hoc Tukey test showed that the

mean value of NFJ showed statistically significant difference than HFJ and audio-HFJ ($F(2,57) = 3.158842719$, $p = 7.485E-11$). The operator performance with HFJ and audio-HFJ were similar and post hoc Tukey's test showed no statistically significant difference between the two.

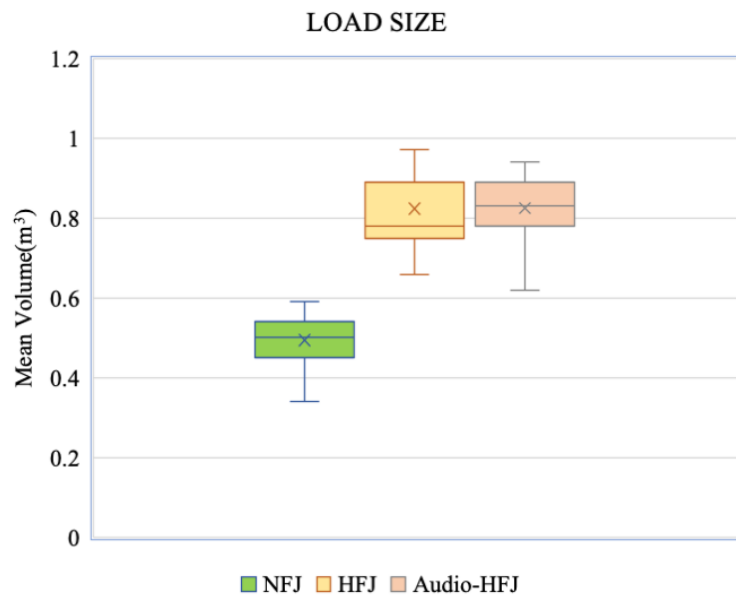


Fig 6.14. Box plot showing the mean volume of load in bucket during the trials.

In the third experiment, average volume of load in bucket were analysed. The results are presented in Fig 6.14. The results show the performance of operators improved by 40.10% with HFJ compared to NFJ. The ANOVA test showed statistically significant difference for the three-modes. A post hoc Tukey test showed statistically significant difference for the average volume of load for NFJ and HFJ ($F(2,54) = 3.158842719$, $p = 1.82167E-10$).

6.6 OPERATOR OBSERVATIONS

Based on the post questionnaire feedbacks, the operators were asked to rate the interfaces from 1 to 5 (5 being the best). The assessment was based on four criteria: the ease of operation, perception of risk, reliability in operations and their personal preference (which interface was most preferred) for training operations. The results of the survey are presented in is Fig 6.15.

The hand controllers used in excavators has maintained a conventional design over many years and the objective of the study was to develop an innovative force reflective interface while maintaining the ergonomics. The experiments confirmed an enhanced perception of digging forces with fewer errors and safety. Though the subjects admitted the excavator control as mentally demanding, the performance improved with practice.

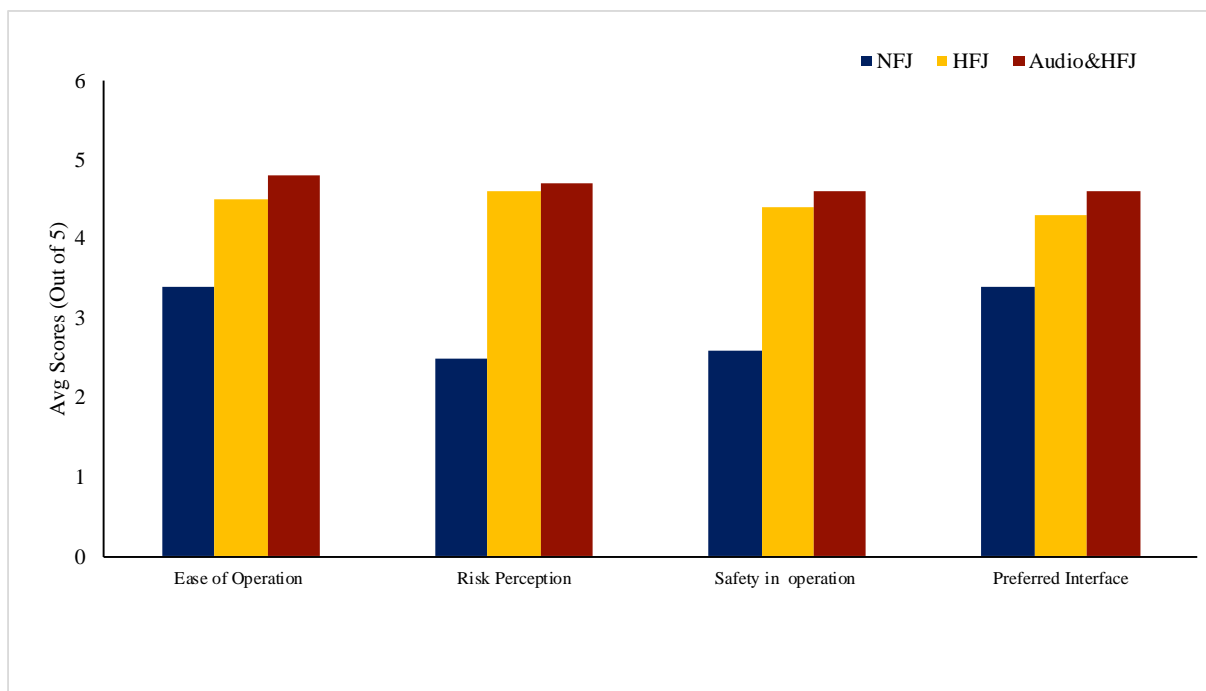


Fig 6.15 Subjective rating comparison for the interfaces.

However, the error rate significantly fell with the haptic joystick. The operators found FFB joysticks helpful especially in experiments pertaining to force patterns and collision. The subject could perceive the force and weight of the objects. With normal joysticks, the operators have shown more of a reckless operation. The auditory cues when combined with haptics were well received as it enhanced the realism in interaction. The test results showed that the subject performance was better compared to NFJ and visual feedback. With haptic assistance, the subject has paid more attention to the audio cues which caused a cognitive response specially when encountered with immobile rocks. Though

the warning indicator was provided as a guidance for loading force on simulator screen, only few operators found on the force bar to be useful. Some of them complained while they concentrated on the warning indicator, it took up more time to complete the task.

The proposed haptic joysticks are ergonomically pleasing compared to many commercial haptic interfaces explored for excavator control. The operator need not hold their arms elevated for the operation and therefore relieves hand fatigue. Training with the configuration helps the operators to return easily to real machine control without any confusion. Also, workspace relatability of the joysticks to the excavator eliminated the haptic walls and other constraints to limit workspace. The proposed device is much simpler and can be commanded like the real hand controller used in excavator.

After the experiments, the operators have suggested some improvements in design in the post survey. Some operators have reported the problem of slipping of shaft links when the handle was moved too quick during the operation. Two of the operators reported that the sensor arrangement had to be recalibrated while performing rock loading. This was the result of extensive use and improper handling of the joystick which resulted in misalignment of the sensors. The joysticks developed were only a prototype and were not ready to handle such extend of reckless operation. The operators appreciated on the feeling of a varying stiffness w.r.t to load. They were of the opinion that they could “feel” the weight and force of materials with the FFB joysticks. Many of them appreciated effect of engine sound with simulation. Mostly, the operators found training with new joysticks satisfactory and left a positive response.

6.7 SUMMARY

The chapter presents the technical and user analysis of the haptic joysticks in the VR platform. The digging force reflection is based on an observer-based control and the haptic feedback is analogous to loading torque acting on the machinery. The experiment results suggest that force reflection enhances

transparency of operation and helps the operator to handle the machinery with better judgement of safety and efficiency. Also, a greater impact is shown specially in operations pertaining to smoothness in bucket motion, collision and excessive force. The results of the proposed device are promising, and it is expected that such device will benefit the novices in improving the operating experiences significantly.

CHAPTER 7: CONCLUSION AND FUTURE WORK

The chapter draws the conclusion and summarises the entire work presented in the thesis. The details of thesis contribution and the future work of the research are discussed.

7.1 CONCLUSION

Under various loading conditions the operators of mini excavators and backhoes face several challenges in preventing machine overturn caused due to instability. The current joystick interface lacks the facility to provide informative feedbacks and hence the chances of operator misjudgements regarding bucket forces and weight of load are high, which is one major reason for machine accident. The main objective of the work reported in thesis is the development of a suitable haptic framework for mini backhoe control that can reduce the operator error and alleviate learning.

An insight in to the previously demonstrated haptic hand controllers for excavator control and the various force feedback methodologies adopted is presented through a detailed survey. As a virtual backhoe simulator is proposed as testbed for the evaluation of haptic interface, the various virtual simulator test beds for excavator training and control is also reviewed.

With high resemblance to manipulators, considering a planar manipulator structure and using robotic concepts the kinematic and dynamic modelling of backhoe is presented. The forward and inverse kinematic modelling is performed using the DH guidelines and the geometrical relationships. The dynamic equations for the backhoe have been developed using Lagrangian dynamics.

A hybrid control system is presented to estimate the loading torque during digging. The bucket forces (the digging force) are estimated through loading torques acting in the joints of the manipulator. A dynamic non-linear observer is developed to estimate the loading torques. Simulation results for a cycle of

digging operation is given to verify the performance of the control system. Also, to further validate the simulation results co-simulation experiments are preformed, and the results are presented.

A set of interactive haptic joysticks that render haptic feedback based on loading torque is developed. The haptic link design and the variable stiffness actuation method to render FFB are also presented. The technical and user evaluation of the proposed haptic joysticks is carried out in the virtual backhoe simulator platform. The haptic control is implemented with the dynamic observer and the motion controller. The tests are performed in two loading environments with 20 novice operators. Several metrics were used to evaluate the operator performances and the results are presented.

7.1 CONTRIBUTIONS

1. In Chapter 2, the mathematical modelling of robotic backhoe is presented. Dynamic modelling is presented using Lagrangian equations of motion. The dynamic equations are extensively used in the experimental studies and the technique can be used to obtain dynamic equations of any type of backhoe model .
2. Chapter 3 explains the significance of loading torque estimation and demonstrates a method to estimate the loading torque using a dynamic observer. The observer can be used estimate the loading torque arising from the bucket forces. Robustness to parameter variations is a significant advantage over other feedback controllers and can be used for sensor less joint torque estimation. Simulation and co-simulation results are presented to validate the proposed technique.
3. In Chapter 4, an innovative method of haptic feedback in joysticks is demonstrated for excavator control. The generation of haptic illusion in the device is explained with the concept of variable stiffness actuation mechanism. The force feedback (FFB) is rendered through ‘haptic links’, based on the effect of digging force at each joint. The stiffness in the

device varies dynamically with the load and restricts the operator motion with a resistive torque in the range of 0-0.9 Nm. The haptic joystick aims to render high fidelity kinesthetic feedback that can help to mitigate the operator error in loading operations

4. The development of dynamic virtual backhoe simulator as the test bed for the haptic framework is demonstrated. The modelling of contact forces is carried out using the equations of soil mechanics and simulator environment with rigid body dynamics. The simulator allows for the testing of controllers and haptic interfaces.
5. The haptic joysticks are evaluated through extensive user evaluation consisting of 20 novice operators. Force reflection enhances operator accuracy and maintains operator awareness. The user evaluation with the joystick showed an improvement of 40% in the volume of material removed and a significant drop in error rate related to force patterns and collisions.

7.2 FUTURE WORK

Based on the research reported, following are some of the areas suggested for future work

1. From design aspects, the material used for the design of haptic links could not maintain the rigidity after long uses. The lack of rigidity can affect the sensor magnet calibration and can give error in FFB. The material selection for haptic links is an area of future exploration. Also, the FFB sensitivity required to perceive variation in digging forces and force limits could be improved using high torque servo motors. Also, alternate variable stiffness feedback designs in FFB joysticks involving lesser actuation speed and design requirements and power consumption could be investigated in future.
2. From design aspects, the material used for the design of haptic links could not maintain the rigidity after long uses. The lack of rigidity can affect the sensor magnet calibration and can give error in FFB. This can be upgraded

by selecting improved materials. Also, the haptic links sometimes slipped when the operators used full strength to overcome the reactive torque. This can be improved by selecting improved materials. Also, the variation in the FFB sensitivity could be enhanced using high torque servo motor, which would impart stiffness perceptions and lead Alternate variable stiffness feedback designs in joysticks involving lesser actuation speed and design requirements and power consumption could be investigated in future

3. Through experiments, the DOB assisted control system proved to be effective in estimating the loading torque. However in the current study to reduce design complexity the actuator dynamics is ignored. The performance and stability of the control system is based on joint velocity. The backhoe is considered as a robotic manipulator and independent joint control is performed. The motion of the joystick is mapped to the position of the virtual backhoe. As the backhoe manipulator has slower dynamics and large workspace, position control is performed. Rate control with different haptic control schemes is open for further exploration.
4. To implement the haptic prototype in the mini backhoes suitable closed loop force control schemes may be implemented. The operator dynamics and device dynamics are not considered in the present study. The identification of the maximum forces that can be displayed to the operator without affecting the stability should be identified. Also learning based control schemes could be implemented to track the bucket forces to achieve better accuracy in operation.
5. The present work utilizes haptic modality to enhance operator performance. The real loading environments are less organized and hence may be affected with a lot of other factors like congestion, tight workplaces and even multiple tasks that may reduce the operator awareness. The slope of the terrain is also a major reason for excavator overturn. The future studies could involve alternate human machine interfaces (HMI), augmented

interaction techniques and also heads up displays to assess and evaluate the cognitive workload of operator.

REFERENCES

- [1] M. O. Ernst and M. S. Banks, “Humans integrate visual and haptic information in a statistically optimal fashion,” *Nature*, vol. 415, no. 6870, pp. 429–433, Jan. 2002.
- [2] J. Peck and T. L. Childers, “To have and to hold: The influence of haptic information on product judgments,” *J. Mark.*, vol. 67, no. 2, pp. 35–48, 2003.
- [3] D. J. Edwards and G. D. Holt, “Case study analysis of construction excavator H&S overturn incidents,” *Eng. Constr. Archit. Manag.*, vol. 17, no. 5, pp. 493–511, 2010.
- [4] A. E. R. Board, “Construction Safety – A Monograph,” 2019.
- [5] L. P. Gite, A. Khadatkar, and K. K. Tyagi, “Farm machinery accidents in Indian Farm Machinery Accidents in Indian agriculture,” *Ergon. Everyone- Proc. Int. Ergon. Conf. HWWE ity Calcutta, Kolkata*, vol. Volume: 1, no. January, pp. 283–290, 2009.
- [6] “OSHA (2009b), Trenching and Excavation, Sub-domain of the United States Department of Labor Occupational Safety and Health Administration,.”
- [7] HSE, “HSE(2005). ‘Workplace transport safety’ An employers’ guide, HSE Books, London,.” 2005.
- [8] D. Edwards, E. A. Parn, M. C. P. Sing, and W. D. Thwala, “Risk of excavators overturning: Determining horizontal centrifugal force when slewing freely suspended loads,” *Eng. Constr. Archit. Manag.*, vol. 26, no. 3, pp. 479–498, 2019.
- [9] H. Lingard, T. Cooke, and E. Gharaie, “A case study analysis of fatal incidents involving excavators in the Australian construction industry,” *Eng. Constr. Archit. Manag.*, vol. 20, no. 5, pp. 488–504, 2013.

- [10] Strategic Forum for Construction Good Practice Guide, “Lifting Operations with Excavators,” 2017.
- [11] “E55 Excavator Specs & Options - Bobcat Company.” [Online]. Available: <https://www.bobcat.com/excavators/models/e55/specs-options>. [Accessed: 12-Mar-2020].
- [12] “Safe load indicator.” [Online]. Available: <http://www.bojinlmi.com/en/product/product-12-560.html>
- [13] “BS EN ISO 9241-910:2011(en), Ergonomics of human-system interaction — Part 910: Framework for tactile and haptic interaction.” [Online]. Available: <https://www.iso.org/obp/ui/#iso:std:iso:9241:-910:ed-1:v1:en>.
- [14] A. El Saddik, “The potential of haptics technologies,” *IEEE Instrum. Meas. Mag.*, vol. 10, no. 1, pp. 10–17, Feb. 2007.
- [15] A. M. Okamura, “Methods for haptic feedback in teleoperated robot-assisted surgery,” *Ind. Rob.*, vol. 31, no. 6, pp. 499–508, 2004.
- [16] S. J. Breitschaft, S. Clarke, and C. C. Carbon, “A Theoretical Framework of Haptic Processing in Automotive User Interfaces and Its Implications on Design and Engineering,” *Front. Psychol.*, vol. 10, Jul. 2019.
- [17] C. Preusche and G. Hirzinger, “Haptics in telerobotics: Current and future research and applications,” in *Visual Computer*, 2007, vol. 23, no. 4, pp. 273–284.
- [18] C. Dando and C. Tranter, “Military and Defence Applications,” in *Applied Cyberpsychology*, Palgrave Macmillan UK, 2016, pp. 197–215.
- [19] N. Jafari, K. D. Adams, and M. Tavakoli, “Haptics to improve task performance in people with disabilities: A review of previous studies and a guide to future research with children with disabilities,” *J. Rehabil. Assist. Technol. Eng.*, vol. 3, p. 205566831666814, Jun. 2016.

- [20] M. Ostoja-Starzewski and M. Skibniewski, "A master-slave manipulator for excavation and construction tasks," *Rob. Auton. Syst.*, vol. 4, no. 4, pp. 333–337, 1989.
- [21] T. J. Cemenska, R. A., Schneider, M. P., and Buege, "'Force feedback lever " US Patent for Patent (Patent # 4,800,721,January 31, 1989)."
- [22] Anon, "A remotely operated excavator," *Nucl. Eng. Int.*, vol. 37, pp. 41–43.
- [23] N. P. M. Z. and R. F. P.D.Lawrence, S. E. Salcudean, N. Sepehri D. Chan, S. Bachmann, "Coordinated and Force-Feedback Control of Hydraulic Excavators," in *Fourth International Symposium on Experimental Robotics, ISER'95*, 1995.
- [24] N. R. Parker, S. E. Salcudean, and P. D. Lawrence, "Application of force feedback to heavy duty hydraulic machines," [1993] *Proc. IEEE Int. Conf. Robot. Autom.*, pp. 375–381, 1993.
- [25] J. M. Hadank, W. E. Allen, W. J. Bradbury, and P. D. Anderson, "Intuitive joystick control for a work implement US Patent Application Publication No. 5002454," 26-Mar-1990.
- [26] G. Danko, "Coordinated joint motion control System with position error correction US Patent Application Publication No. 20070168100," 03-Sep-2006.
- [27] S. E. Salcudean, N. M. Wong, and R. L. Hollis, "Design and Control of a Force-Reflecting Teleoperation System with Magnetically Levitated Master and Wrist," *IEEE Trans. Robot. Autom.*, vol. 11, no. 6, pp. 844–858, 1995.
- [28] S. Tafazoli, S. E. Salcudean, K. Hashtrudi-Zaad, and P. D. Lawrence, "Impedance control of a teleoperated excavator," *IEEE Trans. Control Syst. Technol.*, vol. 10, no. 3, pp. 355–367, May 2002.

- [29] A. Barrientos, O. Luengo, and A. Mora, "Teleoperated Backhoe Excavator with Haptic Control," in *Automation and Robotics in Construction*, 1999, pp. 491-496.
- [30] J. Frankel, "Development of a Haptic Backhoe Testbed," The Georgia Institute of Technology, 2004.
- [31] T. A. Faculty, M. E. Kontz, and I. P. Fulfillment, "HAPTIC CONTROL OF HYDRAULIC MACHINERY USING PROPORTIONAL VALVES HAPTIC CONTROL OF HYDRAULIC MACHINERY," no. December, 2007.
- [32] M. Elton, "An Efficient Haptic Interface for a Variable Displacement Pump Controlled Excavator," *Thesis*, no. May, 2009.
- [33] D. Kim, J. Kim, K. Lee, C. Park, J. Song, and D. Kang, "Automation in Construction Excavator tele-operation system using a human arm," *Autom. Constr.*, vol. 18, no. 2, pp. 173–182, 2009.
- [34] D. Kim, K. W. Oh, C. S. Lee, and D. Hong, "Novel design of haptic devices for bilateral teleoperated excavators using the wave-variable method," *Int. J. Precis. Eng. Manuf.*, vol. 14, no. 2, pp. 223–230, 2013.
- [35] L. Huang, H. Kato, T. Kawamura, and H. Yamada, "MASTER-SLAVE CONTROL FOR A CONSTRUCTION ROBOT TELEOPERATION SYSTEM (EVALUATION OF AN OPERATION SYSTEM WITH VIDEO CAMERAS AND FORCE FEEDBACK)," 2011.
- [36] A. A. Yusof, T. Kawamura, and H. Yamada, "Evaluation of construction robot telegrasping force perception using visual, auditory and force feedback integration," *J. Robot. Mechatronics*, vol. 24, no. 6, pp. 949–957, 2012.
- [37] A. A. YUSOF, T. KAWAMURA, and H. YAMADA, "Operational Evaluation of a Construction Robot Tele-operation with Force Feedback," *Trans. JAPAN FLUID POWER Syst. Soc.*, vol. 43, no. 1, pp.

8–15, 2011.

- [38] Y. J. Nam and M. K. Park, “Virtual excavator simulator featuring HILS and haptic joysticks,” *J. Mech. Sci. Technol.*, vol. 29, no. 1, pp. 397–407, 2015.
- [39] J. M. Jacinto-Villegas *et al.*, “A Novel Wearable Haptic Controller for Teleoperating Robotic Platforms,” *IEEE Robot. Autom. Lett.*, vol. 2, no. 4, pp. 2072–2079, Oct. 2017.
- [40] J. Yoon and A. Manurung, “Development of an intuitive user interface for a hydraulic backhoe,” *Autom. Constr.*, 2010.
- [41] M. D. Elton, A. R. Enes, and W. J. Book, “A virtual reality Operator Interface station with hydraulic hardware-in-the-loop simulation for prototyping excavator control systems,” in *2009 IEEE/ASME International Conference on Advanced Intelligent Mechatronics*, 2009, pp. 250–255.
- [42] H. Hayn, D. Schwarzmann, and R. B. Gmbh, “Control Concept for a Hydraulic Mobile Machine Using a Haptic Operating Device,” 2009.
- [43] H. Hayn and D. Schwarzmann, “A Haptically Enhanced Operational Concept for a Hydraulic Excavator,” in *Advances in Haptics*, InTech, 2010.
- [44] R. C. Winck, M. Elton, and W. J. Book, “Automation in Construction A practical interface for coordinated position control of an excavator arm,” *Autom. Constr.*, vol. 51, pp. 46–58, 2015.
- [45] F. Morosi, M. Rossoni, and G. Caruso, “Coordinated control paradigm for hydraulic excavator with haptic device,” *Autom. Constr.*, vol. 105, no. October 2018, p. 102848, 2019.
- [46] R. Van Der Linde, P. Lammertse, E. Frederiksen, and B., “The HapticMaster, a new high-performance haptic interface,” *Proc.*

EuroHaptic, Edinburgh, UK, pp. 1–5, 2002.

- [47] C. Carignan and K. Cleary, “Closed-loop force control for haptic simulation of virtual environments,” *Haptics-e*, vol. 1, no. 2, pp. 1–14, 2000.
- [48] S. P. DiMaio, S. E. Salcudean, C. Reboulet, S. Tafazoli, and K. Hashtrudi-Zaad, “A virtual excavator for controller development and evaluation,” *Proceedings. 1998 IEEE Int. Conf. Robot. Autom. (Cat. No.98CH36146)*, vol. 1, pp. 1–7, 1998.
- [49] H. I. Torres-rod, A. Excavator, and F. Motion, “Integration of Force-Position Control and Haptic Interface facilities for a Virtual Excavator Simulator,” pp. 761–768, 2005.
- [50] K. Wen, D. Neculescu, and J. Sasiadek, “Haptic force control based on impedance/admittance control aided by visual feedback,” *Multimed. Tools Appl.*, vol. 37, no. 1, pp. 39–52, Mar. 2008.
- [51] S. Suzuki and K. Furuta, “Adaptive Impedance Control to Enhance Human Skill on a Haptic Interface System,” *J. Control Sci. Eng.*, vol. 2012, 2012.
- [52] J. J. Gil, Á. Rubio, and J. Savall, “Decreasing the apparent inertia of an impedance haptic device by using force feedforward,” *IEEE Trans. Control Syst. Technol.*, vol. 17, no. 4, pp. 833–838, 2009.
- [53] A. Abdossalami and S. Sirouspour, “Adaptive control for improved transparency in haptic simulations,” *IEEE Trans. Haptics*, vol. 2, no. 1, pp. 2–14, 2009.
- [54] A. Abdossalami and S. Sirouspour, “Adaptive control of haptic interaction with impedance and admittance type virtual environments,” in *Symposium on Haptics Interfaces for Virtual Environment and Teleoperator Systems 2008 - Proceedings, Haptics*, 2008, pp. 145–152.

- [55] A. Frisoli, E. Sotgiu, C. A. Avizzano, D. Checcacci, and M. Bergamasco, “Force-based impedance control of a haptic master system for teleoperation,” *Sens. Rev.*, vol. 24, no. 1, pp. 42–50, 2004.
- [56] E. L. Faulring, J. E. Colgate, and M. A. Peshkin, “The Cobot Hand Controller: Design, Control and Performance of a Novel Haptic Display,” *Int. J. Rob. Res.*, vol. 25, no. 11, pp. 1099–1119, Nov. 2006.
- [57] M. H. Vu and U. J. Na, “A new 6-DOF haptic device for teleoperation of 6-DOF serial robots,” *IEEE Trans. Instrum. Meas.*, vol. 60, no. 11, pp. 3510–3523, Nov. 2011.
- [58] J. E. Speich, L. Shao, and M. Goldfarb, “Modeling the human hand as it interacts with a telemanipulation system,” *Mechatronics*, vol. 15, no. 9, pp. 1127–1142, Nov. 2005.
- [59] U. J. Na, “A new impedance force control of a haptic teleoperation system for improved transparency,” *J. Mech. Sci. Technol.*, vol. 31, no. 12, pp. 6005–6017, Dec. 2017.
- [60] M. Tavakoli, A. Aziminejad, R. V. Patel, and M. Moallem, “High-fidelity bilateral teleoperation systems and the effect of multimodal haptics,” *IEEE Trans. Syst. Man, Cybern. Part B Cybern.*, vol. 37, no. 6, pp. 1512–1528, Dec. 2007.
- [61] A. C. Smith, F. Mobasser, and K. Hashtrudi-Zaad, “Neural-network-based contact force observers for haptic applications,” *IEEE Trans. Robot.*, vol. 22, no. 6, pp. 1163–1175, Dec. 2006.
- [62] A. Gupta and M. K. O’Malley, “Disturbance-Observer-Based Force Estimation for Haptic Feedback,” *J. Dyn. Syst. Meas. Control*, vol. 133, no. 1, p. 014505, 2011.
- [63] S. Katsura, W. Iida, and K. Ohnishi, “Medical mechatronics - An application to haptic forceps,” *Annu. Rev. Control*, vol. 29, no. 2, pp. 237–245, Jan. 2005.

- [64] J. M. Daly and D. W. L. Wang, “Time-delayed bilateral teleoperation with force estimation for n-DOF nonlinear robot manipulators,” in *IEEE/RSJ 2010 International Conference on Intelligent Robots and Systems, IROS 2010 - Conference Proceedings*, 2010, pp. 3911–3918.
- [65] J. Gámez García, A. Robertsson, J. Gómez Ortega, and R. Johansson, “Generalized contact force estimator for a robot manipulator,” in *Proceedings - IEEE International Conference on Robotics and Automation*, 2006, vol. 2006, pp. 4019–4024.
- [66] K. Tadano and K. Kawashima, “Development of a master-slave system with force-sensing abilities using pneumatic actuators for laparoscopic surgery,” *Adv. Robot.*, vol. 24, no. 12, pp. 1763–1783, Sep. 2010.
- [67] M. Kontz, J. Beckwith, and W. J. Book, “Evaluation of a Teleoperated Haptic Forklift,” *Proceedings, 2005 IEEE/ASME Int. Conf. Adv. Intell. Mechatronics.*, pp. 295–300, 2005.
- [68] U. Wallersteiner, P. Lawrence, and B. Sauder, “A human factors evaluation of two different machine control systems for log loaders,” *Ergonomics*, vol. 36, no. 8, pp. 927–934, Aug. 1993.
- [69] C. Basdogan, S. De, J. Kim, M. Muniyandi, H. Kim, and M. A. Srinivasan, “Haptics in minimally invasive surgical simulation and training,” *IEEE Comput. Graph. Appl.*, vol. 24, no. 2, pp. 56–64, Mar. 2004.
- [70] C. Våpenstad *et al.*, “Lack of transfer of skills after virtual reality simulator training with haptic feedback,” *Minim. Invasive Ther. Allied Technol.*, vol. 26, no. 6, pp. 346–354, 2017.
- [71] P. Lamata, E. J. Gómez, F. Bello, R. L. Kneebone, R. Aggarwal, and F. Lamata, “Conceptual framework for laparoscopic VR simulators,” *IEEE Comput. Graph. Appl.*, vol. 26, no. 6, pp. 69–79, Nov. 2006.
- [72] M. Schijven and J. Jakimowicz, “Virtual reality surgical laparoscopic

- simulators: How to choose,” *Surg. Endosc. Other Interv. Tech.*, vol. 17, no. 12, pp. 1943–1950, Dec. 2003.
- [73] T. Ni, H. Zhang, C. Yu, D. Zhao, and S. Liu, “Design of highly realistic virtual environment for excavator simulator,” *Comput. Electr. Eng.*, vol. 39, no. 7, pp. 2112–2123, 2013.
- [74] A. F. Healy, J. A. Kole, L. E. Bourne, and G. Campitelli, “Training principles to advance expertise,” *Front. Psychol.*, 2014.
- [75] A. Vankipuram *et al.*, “Design and development of a virtual reality simulator for advanced cardiac life support training,” *IEEE J. Biomed. Heal. Informatics*, vol. 18, no. 4, pp. 1478–1484, 2014.
- [76] L. N. Boyle and J. D. Lee, “Using driving simulators to assess driving safety,” *Accid. Anal. Prev.*, vol. 42, no. 3, pp. 785–787, May 2010.
- [77] C. B. Tatum, M. Vorster, M. G. Klingler, and B. C. Paulson, “Systems Analysis of Technical Advancement in Earthmoving Equipment,” *J. Constr. Eng. Manag.*, vol. 132, no. 9, pp. 976–986, Sep. 2006.
- [78] S. P. DiMaio, S. E. Salcudean, and C. Reboulet, “A Virtual Environment for the Simulation and Programming of Excavation Trajectories,” *Presence Teleoperators Virtual Environ.*, vol. 10, no. 5, pp. 465–476, 2001.
- [79] X. Wang, P. S. Dunston, and M. Skibniewski, “Mixed Reality Technology Applications in Construction Equipment Operator Training,” *Proc. 21st Int. Symp. Autom. Robot. Constr.*, no. April 2018, 2017.
- [80] D. HOLZ, A. AZIMI, M. TEICHMANN, and J. KÖVECSES, “MOBILITY PREDICTION OF ROVERS ON SOFT TERRAIN: EFFECTS OF WHEEL- AND TOOL-INDUCED TERRAIN DEFORMATIONS,” in *Adaptive Mobile Robotics, Proceedings of the 15th International Conference on Climbing and Walking Robots and the*

- Support Technologies for Mobile Machines (CLAWAR 2012)*, 2012, pp. 647–654.
- [81] T. Makkonen, K. Nevala, and R. Heikkilä, “A 3D model based control of an excavator,” *Autom. Constr.*, vol. 15, no. 5, pp. 571–577, Sep. 2006.
- [82] Z. Towarek, “Dynamics of a single-bucket excavator on a deformable soil foundation during the digging of ground,” *Int. J. Mech. Sci.*, vol. 45, no. 6–7, pp. 1053–1076, Jun. 2003.
- [83] M. González, A. Luaces, D. Dopico, and J. Cuadrado, “A 3D Physics-Based Hydraulic Excavator Simulator,” in *ASME-AFM 2009 World Conference on Innovative Virtual Reality*, 2009, pp. 75–80.
- [84] D. Schmidt, M. Proetzsch, and K. Berns, “Simulation and control of an autonomous bucket excavator for landscaping tasks,” *Proc. - IEEE Int. Conf. Robot. Autom.*, pp. 5108–5113, 2010.
- [85] D. Schmidt and K. Berns, “Construction site navigation for the autonomous excavator Thor,” *ICARA 2015 - Proc. 2015 6th Int. Conf. Autom. Robot. Appl.*, pp. 90–97, 2015.
- [86] M. Choi, S. Ahn, and J. O. Seo, “VR-Based investigation of forklift operator situation awareness for preventing collision accidents,” *Accid. Anal. Prev.*, vol. 136, no. November 2019, 2020.
- [87] A. Dong, M. Lou Maher, M. J. Kim, N. Gu, and X. Wang, “Construction defect management using a telematic digital workbench,” *Autom. Constr.*, vol. 18, no. 6, pp. 814–824, Oct. 2009.
- [88] T. Kosch, R. Kettner, M. Funk, and A. Schmidt, “Comparing tactile, auditory, and visual assembly error-feedback for workers with cognitive impairments,” in *ASSETS 2016 - Proceedings of the 18th International ACM SIGACCESS Conference on Computers and Accessibility*, 2016, pp. 53–60.

- [89] A. Baddeley, "Working memory," *Science* (80-.), vol. 255, no. 5044, pp. 556–559, 1992.
- [90] A. J. Koivo, "Kinematics of excavators (backhoes) for transferring surface material," *J. Aerosp. Eng.*, vol. 7, no. 1, pp. 17–32, 1994.
- [91] S. Tafazoli, P. D. Lawrence, and S. E. Salcudean, "Identification of inertial and friction parameters for excavator arms," *IEEE Trans. Robot. Autom.*, vol. 15, no. 5, pp. 966–971, 1999.
- [92] M. E. Kontz and W. J. Book, *kinematic analysis of backhoes / excavators for closed-loop coordinated control*, vol. 39, no. 15. IFAC, 2006.
- [93] J. J. Craig, P. Prentice, and P. P. Hall, "Introduction to Robotics Mechanics and Control Third Edition," 2005.
- [94] A. J. Koivo, M. Thoma, E. Kocaoglan, and J. Andrade-Cetto, "Modeling and Control of Excavator Dynamics during Digging Operation," *Journal of Aerospace Engineering*, vol. 9, no. 1. pp. 10–18, 1996.
- [95] S. Tafazoli, S. E. Salcudean, K. Hashtrudi-Zaad, and P. D. Lawrence, "Impedance control of a teleoperated excavator," *IEEE Trans. Control Syst. Technol.*, vol. 10, no. 3, pp. 355–367, 2002.
- [96] S. T. Bilandi, "Identification of frictional effects and structural dynamics for improved control of hydraulic manipulators," no. January, 1997.
- [97] M. J. S. P.K. Vaha, "DYNAMIC MODEL OF EXCAVATOR By P. K. V~ih~i I and M. J. Skibniewski, 2 Member, ASCE," *J. Aerosp. Eng.*, vol. 6, no. 2, pp. 148–158, 1993.
- [98] C S Meera ;Gupta Mukul Kumar and M. Santhakumar, "Disturbance observer-assisted hybrid control for autonomous manipulation in a robotic backhoe," *Arch. Mech. Eng.*, vol. 66, pp. 153–169, 2019.
- [99] C S Meera ;Gupta Mukul Kumar, "Modelling & Position Control for Electro-hydraulic System," *Int. J. Recent Technol. Eng.*, vol. 8, no. 4,

2019.

- [100] H. E. Merritt, *Hydraulic control systems*. John Wiley, New York, 1967.
- [101] S. Tafazoli, C. W. De Silva, and P. D. Lawrence, "Tracking control of an electrohydraulic manipulator in the presence of friction," *IEEE Trans. Control Syst. Technol.*, vol. 6, no. 3, pp. 401–411, 1998.
- [102] Q. P. Ha, Q. H. Nguyen, D. C. Rye, and F. Durrant-Whyte, "Impedance control of a hydraulically-actuated robotic excavator," *J. Autom. Constr.*, vol. 9, no. 5, pp. 421–435, 2000.
- [103] K. Guo, J. Wei, J. Fang, R. Feng, and X. Wang, "Position tracking control of electro-hydraulic single-rod actuator based on an extended disturbance observer," *Mechatronics*, vol. 27, pp. 47–56, Apr. 2015.
- [104] D. Wang, L. Zheng, H. Yu, W. Zhou, and L. Shao, "Robotic excavator motion control using a nonlinear proportional-integral controller and cross-coupled pre-compensation," *Autom. Constr.*, vol. 64, pp. 1–6, 2016.
- [105] H. Feng *et al.*, "Robotic excavator trajectory control using an improved GA based PID controller," *Mech. Syst. Signal Process.*, vol. 105, pp. 153–168, 2018.
- [106] P. Saeedi *et al.*, "An autonomous excavator with vision-based track-slippage control," *IEEE Trans. Control Syst. Technol.*, vol. 13, no. 1, pp. 67–84, 2005.
- [107] A. Hemami and F. Hassani, "An Overview of Autonomous Loading of Bulk Material," no. ISARC, pp. 405–411, 2009.
- [108] S. Dadhich, U. Bodin, and U. Andersson, "Key challenges in automation of earth-moving machines," *Autom. Constr.*, 2015.
- [109] U. Andersson, *Automation and Traction Control of Articulated Vehicles*. 2013.

- [110] J. Han, "From PID to active disturbance rejection control," *IEEE Trans. Ind. Electron.*, vol. 56, no. 3, pp. 900–906, 2009.
- [111] S. Li, J. Yang, W. H. Chen, and X. Chen, *Disturbance Observer-Based Control Methods and Applications*. 2014.
- [112] C. P. Tan, Y. H. Zweiri, K. Althoefer, and L. D. Seneviratne, "Online soil parameter estimation scheme based on Newton-Raphson method for autonomous excavation," *IEEE/ASME Trans. Mechatronics*, vol. 10, no. 2, pp. 221–229, 2005.
- [113] H. Cannon and S. Singh, "Models for Automated Earthmoving," *Exp. Robot. VI*, pp. 163–172, 1999.
- [114] A. Mohammadi, M. Tavakoli, H. J. Marquez, and F. Hashemzadeh, "Nonlinear disturbance observer design for robotic manipulators," *Control Eng. Pract.*, vol. 21, no. 3, pp. 253–267, 2013.
- [115] G. J. Maeda, I. R. Manchester, and D. C. Rye, "Combined ILC and Disturbance Observer for the Rejection of Near-Repetitive Disturbances, with Application to Excavation," *IEEE Trans. Control Syst. Technol.*, vol. 23, no. 5, pp. 1754–1769, 2015.
- [116] S. Mohan, "Error analysis and control scheme for the error correction in trajectory-tracking of a planar 2PRP-PPR parallel manipulator," *Mechatronics*, vol. 46, pp. 70–83, 2017.
- [117] W. H. Chen, D. J. Ballance, P. J. Gawthrop, and J. O'Reilly, "A nonlinear disturbance observer for robotic manipulators," *IEEE Trans. Ind. Electron.*, vol. 47, no. 4, pp. 932–938, 2000.
- [118] A. B. Epenetus, M. CS, S. Mohan, and M. K. Gupta, "Development and motion control of spatial serial robotic manipulator under varying disturbances," *World J. Eng.*, vol. 16, no. 4, pp. 460–467, 2019.
- [119] M. Bodur *et al.*, "Dynamic cognitive force control for an automatic land

- excavation robot,” in *Proceedings of MELECON '94. Mediterranean Electrotechnical Conference*, pp. 703–706.
- [120] D. Sosa-Méndez, E. Lugo-González, M. Arias-Montiel, and R. A. García-García, “ADAMS-MATLAB co-simulation for kinematics, dynamics, and control of the Stewart-Gough platform,” *Int. J. Adv. Robot. Syst.*, vol. 14, no. 4, pp. 1–10, 2017.
- [121] J. Sudharsan and L. Karunamoorthy, “Path planning and co-simulation control of 8 DOF anthropomorphic robotic arm,” *Int. J. Simul. Model.*, vol. 15, no. 2, pp. 302–312, 2016.
- [122] A. Talvas, M. Marchal, and A. Lécuyer, “A survey on bimanual haptic interaction,” *IEEE Trans. Haptics*, vol. 7, no. 3, pp. 285–300, 2014.
- [123] R. Owen, G. Kurtenbach, G. Fitzmaurice, T. Baudel, and B. Buxton, “When it gets more difficult, use both hands - Exploring bimanual curve manipulation,” *Proc. - Graph. Interface*, no. January, pp. 17–24, 2005.
- [124] R. F. Dillon, J. D. Edey, and J. W. Tombaugh, “Measuring the true cost of command selection: Techniques and results,” in *Conference on Human Factors in Computing Systems - Proceedings*, 1990, pp. 19–25.
- [125] P. Kouřil, F. Liarokapis, and M. Potel, “Simulation of Underwater Excavation Using Dredging Procedures.”
- [126] R. Sekizuka, M. Ito, S. Saiki, Y. Yamazaki, and Y. Kurita, “System to Evaluate the Skill of Operating Hydraulic Excavators Using a Remote Controlled Excavator and Virtual Reality,” *Front. Robot. AI*, vol. 6, p. 142, Jan. 2020.
- [127] E. Strasnick, C. Holz, E. Ofek, M. Sinclair, and H. Benko, “Demonstration of haptic links: Bimanual haptics for virtual reality using variable stiffness actuation,” *Conf. Hum. Factors Comput. Syst. - Proc.*, vol. 2018-April, pp. 1–12, 2018.

- [128] M. Manti, V. Cacucciolo, and M. Cianchetti, “Stiffening in soft robotics: A review of the state of the art,” *IEEE Robot. Autom. Mag.*, vol. 23, no. 3, pp. 93–106, 2016.
- [129] C. H. B, J. Bilz, T. Fritzsche, and M. Kupnik, “Haptics: Perception, Devices, Control, and Applications,” vol. 9774, pp. 109–119, 2016.
- [130] M. Cianchetti, A. Licofonte, M. Follador, F. Rogai, and C. Laschi, “Bioinspired Soft Actuation System Using Shape Memory Alloys,” *Actuators*, vol. 3, no. 3, pp. 226–244, Jul. 2014.
- [131] Y. J. Kim, S. Cheng, S. Kim, and K. Iagnemma, “A novel layer jamming mechanism with tunable stiffness capability for minimally invasive surgery,” *IEEE Trans. Robot.*, vol. 29, no. 4, pp. 1031–1042, 2013.
- [132] J. Akyeampong, S. Udoka, G. Caruso, and M. Bordegoni, “Evaluation of hydraulic excavator Human-Machine Interface concepts using NASA TLX,” *Int. J. Ind. Ergon.*, vol. 44, no. 3, pp. 374–382, 2014.
- [133] “How many patterns are you competent on? | Heavy Equipment Forums. <http://www.heavyequipmentforums.com/showthread.php?9-How-many-pat-terns-are-you-competent-on/page4>.” [Online]. Available: <https://www.heavyequipmentforums.com/threads/how-many-patterns-are-you-competent-on.9>
- [134] J. C. Briggs, “The Promise of Virtual Reality ,” - *Futur.* , vol. 30, no. 5, Sep. 1996.
- [135] H. Benko, C. Holz, M. Sinclair, and E. Ofek, “NormalTouch and texturetouch: High-fidelity 3D haptic shape rendering on handheld virtual reality controllers,” in *UIST 2016 - Proceedings of the 29th Annual Symposium on User Interface Software and Technology*, 2016, pp. 717–728.
- [136] T. Carter, S. A. Seah, B. Long, B. Drinkwater, and S. Subramanian, “UltraHaptics: Multi-point mid-air haptic feedback for touch surfaces,”

UIST 2013 - Proc. 26th Annu. ACM Symp. User Interface Softw. Technol., pp. 505–514, 2013.

- [137] I. Choi, E. W. Hawkes, D. L. Christensen, C. J. Ploch, and S. Follmer, “Wolverine: A wearable haptic interface for grasping in virtual reality,” in *IEEE International Conference on Intelligent Robots and Systems*, 2016, vol. 2016-November, pp. 986–993.
- [138] J. L. C. Santiago, I. S. Godage, P. Gonthina, and I. D. Walker, “Soft robots and kangaroo tails: Modulating compliance in continuum structures through mechanical layer jamming,” *Soft Robot.*, vol. 3, no. 2, pp. 54–63, 2016.
- [139] X. Wang, P. S. Dunston, R. Proctor, L. Hou, J. Chung, and Y. So, “REFLECTIONS ON USING A GAME ENGINE TO DEVELOP A VIRTUAL TRAINING SYSTEM FOR CONSTRUCTION EXCAVATOR OPERATORS.”
- [140] A. J. P. Tixier, M. R. Hallowell, A. Albert, L. Van Boven, and B. M. Kleiner, “Psychological antecedents of risk-taking behavior in construction,” *J. Constr. Eng. Manag.*, vol. 140, no. 11, Nov. 2014.
- [141] C. H. Tang, W. T. Wu, and C. Y. Lin, “Using virtual reality to determine how emergency signs facilitate way-finding,” *Appl. Ergon.*, vol. 40, no. 4, pp. 722–730, Jul. 2009.
- [142] S. Bhandari, M. R. Hallowell, L. Van Boven, M. Golparvar-Fard, J. Gruber, and K. M. Welker, “Using augmented virtuality to understand the situational awareness model,” in *Construction Research Congress 2018: Safety and Disaster Management - Selected Papers from the Construction Research Congress 2018*, 2018, vol. 2018-April, pp. 105–115.
- [143] K. Kiili, “Digital game-based learning: Towards an experiential gaming model,” *Internet High. Educ.*, vol. 8, no. 1, pp. 13–24, Mar. 2005.

- [144] B. A. R. Reece, “The fundamental equation of earthmoving mechanics,” *J. Terramechanics*, vol. 2, no. 1, p. 99, 1965.
- [145] O. Luengo, S. Singh, and H. Cannon, “Modeling and identification of soil-tool interaction in automated excavation,” *Int. Conf. Intell. Robot. Syst.*, vol. 3, no. October, pp. 1900–1906, 1998.
- [146] M. D. Elton and W. J. Book, “Teleoperating Multi-DOF Hydraulic Manipulators,” 2011, pp. 395–400.
- [147] C. Y. So, “Acquisition, retention and transfer of heavy equipment operator skills through simulator training,” Purdue University, 2014.
- [148] L. E. Bernold, “Quantitative Assessment of Backhoe Operator Skill,” *J. Constr. Eng. Manag.*, vol. 133, no. 11, pp. 889–899, Nov. 2007.

APPENDIX A

A.1 DYNAMIC MODELLING OF ELECTROHYDRAULIC SYSTEM

Electrohydraulic systems (EHS) are widely known for the high-power density and high load bearing capacity. EHS are highly non-linear due to the presence of various plant uncertainties. The EHS model mainly includes the hydraulic actuator, servo valve, plant model uncertainty. Hydraulic cylinders in EHS are either, a symmetric hydraulic cylinder or an asymmetric hydraulic cylinder. The modelling and control of EHS with a symmetric hydraulic cylinder has been presented in Meera et.al.[99]. In excavator backhoes asymmetric cylinders are used commonly. The work presented here parallels similar works presented on modelling of EHS[100][101][102]. The study is presented here with an intension to obtain an insight into the non-linear nature of hydraulic systems.

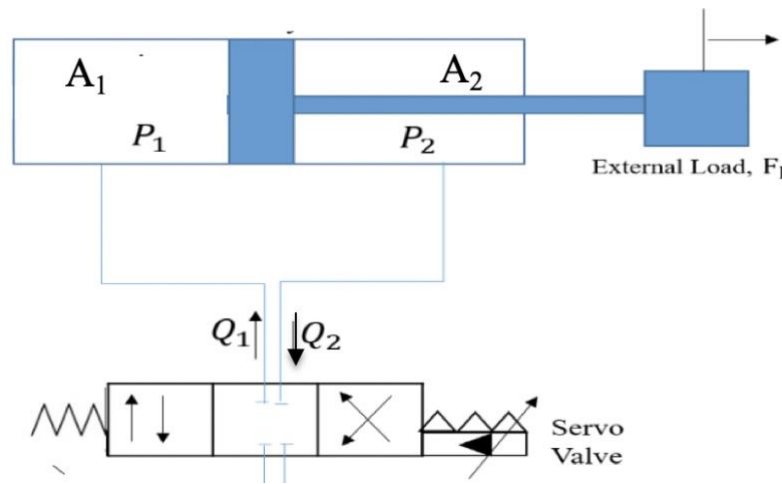


Fig A.1 The configuration of EHS.

A.1.1 HYDRAULIC CYLINDER MODEL

Fig A.1 shows the configuration of different elements present in an EHS. In a loaded system, the motion of cylinder occurs when the pressure applied overcomes the force applied by the external load. A single rod asymmetric hydraulic cylinder acts as the hydraulic actuator, where the piston motion is caused by the pressure difference across it. Applying the law of continuity to

both chambers of the hydraulic cylinder the load flows can be written as [100],

$$\left. \begin{aligned} (V_{01} + A_1 y) \frac{\dot{p}_1}{\beta_e} &= Q_1 - A_1 \dot{y} - C_{tl}(p_1 - p_2) \\ (V_{02} + A_2 y) \frac{\dot{p}_2}{\beta_e} &= Q_2 - A_2 \dot{y} - C_{tl}(p_1 - p_2) \end{aligned} \right\} \quad (\text{A.1})$$

where, y represents the cylinder displacement and A_1 and A_2 , the area of the head side and rod side of cylinder respectively. V_{01} , V_{02} denotes the initial total volume of two cylinder-chamber. β_e denotes the bulk-modulus, a measure of compressibility of hydraulic oil. Whilst coefficient of leakage is denoted by C_{tl} . p_1 and p_2 are the load-pressures of the hydraulic cylinder. Q_1 and Q_2 are the head side and rod side load flows to the cylinder respectively.

During the motion of piston, the spring force and viscous friction from oil are the two main resistance in EHS. The piston dynamics for the force F acting on piston can be given with Newton's second law as,

$$F = m\ddot{y} = p_1 A_a - p_2 A_2 - ky - b\dot{y} - F_i \quad (\text{A.2})$$

Here, the load mass of the piston is given by m , the opposing load (both external load and friction) on the cylinder by F_i , the load spring-constant by k and the co-efficient of viscous damping by b .

3.4.2 SERVO-VALVE MODEL

The servo-valve controls the fluid flow to the hydraulic cylinder. The valve model is a nonlinear function consisting of spool position dynamics and load-flow model. For a 4-way valve spool, load flow for the hydraulic cylinder can be expressed as,

$$\left. \begin{aligned} Q_1 &= C_d w x_v [sgn(x_v) \sqrt{p_s - p_1} + sgn(-x_v) \sqrt{p_1 - p_t}] \\ Q_2 &= C_d w x_v [sgn(x_v) \sqrt{p_2 - p_t} + sgn(-x_v) \sqrt{p_s - p_2}] \end{aligned} \right\} \quad (\text{A.3})$$

where, $sgn(\cdot) = \begin{cases} 1 & \cdot \geq 0 \\ 0 & \cdot < 0 \end{cases}$

p_s denotes the supply-pressure from the hydraulic pump and p_r denotes the return-pressure of tank. C_d , w and ρ represents the discharge co-efficient, area-

gradient of the servo-valve spool and hydraulic fluid density respectively. Variable Q_1 is the load-flow when $x_v \geq 0$ and Q_2 is the load-flow when $x_v < 0$, where x_v is the spool position. Considering both delay and damping in spool-position, a second order dynamic model is obtained for valve model. The relation between input control-voltage and the spool-position is given by,

$$x_v = K_s u \quad (\text{A.4})$$

where, K_s is the servo valve's gain constant and u represents the control voltage. The state variables can be defined as,

$$[x_1, x_2, x_3, x_4]^T = [y, \dot{y}, p_1, p_2]^T \quad (\text{A.5})$$

and considering,

$$\left. \begin{aligned} h_1 &= \frac{\beta_e}{A_1 x_1 + V_{01}} & h_2 &= \frac{\beta_e}{-A_2 x_1 + V_{02}}, \\ s_1 &= \text{sgn}(u) \sqrt{p_s - x_3} + \text{sgn}(-u) \sqrt{x_3 - p_t}, \\ s_2 &= \text{sgn}(u) \sqrt{x_4 - p_t} + \text{sgn}(-u) \sqrt{p_s - x_4} \end{aligned} \right\} \quad (\text{A.6})$$

The nonlinear state-space model of the EHS can be represented as,

$$\left. \begin{aligned} \dot{x}_1 &= x_2 \\ \dot{x}_2 &= \frac{1}{m} (A_1 x_3 - A_2 x_4 - b \dot{y} - F_l) \\ \dot{x}_3 &= h_1 (-x_2 A_1 - C_{tl} (x_3 - x_4) + K_s C_d w u s_1) \\ \dot{x}_4 &= h_2 (x_2 A_1 + C_{tl} (x_3 - x_4) + K_s C_d w u s_2) \end{aligned} \right\} \quad (\text{A.7})$$

In equation A.7 the EHS model is given with an asymmetric hydraulic cylinder as well as a simplified servo-valve model [103]. This non-linear state space model includes the effect of load dynamics and other parametric uncertainties and hence can be used in the controller designs for EHS.

APPENDIX B

The following are the dynamic equations derived in MATLAB for the robotic backhoe mechanism. The equations are derived following the Lagrangian equations of motion given by,

$$M(\theta)\ddot{\theta} + H(\theta, \dot{\theta})\dot{\theta} + G(\theta) + \tau_d = \tau$$

and the elements of inertia matrix (M) and the coriolis and centrifugal force (H) and gravity(G) matrix for the robotic backhoe

$$\begin{aligned} M_{11} = & I_{zz1} + m_2*(a_1 + a_2*\cos(q_2))^2 + m_4*\cos(q_1)^2*(a_1 + a_3*\cos(q_2 + q_3) \\ & + a_2*\cos(q_2) + a_4*\sin(q_2 + q_3 + q_4))^2 + m_4*\sin(q_1)^2*(a_1 + a_3*\cos(q_2 + q_3) \\ & + a_2*\cos(q_2) + a_4*\cos(q_2 + q_3 + q_4))^2 + m_3*\cos(q_1)^2*(a_1 + a_3*\cos(q_2 + \\ & q_3) + a_2*\cos(q_2))^2 + m_3*\sin(q_1)^2*(a_1 + a_3*\cos(q_2 + q_3) + a_2*\cos(q_2))^2 + \\ & a_1^2*m_1*\cos(q_1)^2 + a_1^2*m_1*\sin(q_1)^2; \end{aligned}$$

$$\begin{aligned} M_{12} = & m_4*\cos(q_1)*\sin(q_1)*(a_3*\sin(q_2 + q_3) + a_2*\sin(q_2) + a_4*\sin(q_2 + q_3 + \\ & q_4))*(a_1 + a_3*\cos(q_2 + q_3) + a_2*\cos(q_2) + a_4*\cos(q_2 + q_3 + q_4)) - \\ & m_4*\cos(q_1)*\sin(q_1)*(a_3*\sin(q_2 + q_3) + a_2*\sin(q_2) - a_4*\cos(q_2 + q_3 + q_4))*(a_1 \\ & + a_3*\cos(q_2 + q_3) + a_2*\cos(q_2) + a_4*\sin(q_2 + q_3 + q_4)); \end{aligned}$$

$$\begin{aligned} M_{13} = & m_4*\cos(q_1)*\sin(q_1)*(a_3*\sin(q_2 + q_3) + a_4*\sin(q_2 + q_3 + q_4))*(a_1 + \\ & a_3*\cos(q_2 + q_3) + a_2*\cos(q_2) + a_4*\cos(q_2 + q_3 + q_4)) - \\ & m_4*\cos(q_1)*\sin(q_1)*(a_3*\sin(q_2 + q_3) - a_4*\cos(q_2 + q_3 + q_4))*(a_1 + a_3*\cos(q_2 \\ & + q_3) + a_2*\cos(q_2) + a_4*\sin(q_2 + q_3 + q_4)); \end{aligned}$$

$$\begin{aligned} M_{14} = & a_4*m_4*\cos(q_2 + q_3 + q_4)*\cos(q_1)*\sin(q_1)*(a_1 + a_3*\cos(q_2 + q_3) + \\ & a_2*\cos(q_2) + a_4*\sin(q_2 + q_3 + q_4)) + a_4*m_4*\sin(q_2 + q_3 + \\ & q_4)*\cos(q_1)*\sin(q_1)*(a_1 + a_3*\cos(q_2 + q_3) + a_2*\cos(q_2) + a_4*\cos(q_2 + q_3 + \\ & q_4)); \end{aligned}$$

$$\begin{aligned} M_{21} = & m_4*\cos(q_1)*\sin(q_1)*(a_3*\sin(q_2 + q_3) + a_2*\sin(q_2) + a_4*\sin(q_2 + q_3 + \\ & q_4))*(a_1 + a_3*\cos(q_2 + q_3) + a_2*\cos(q_2) + a_4*\cos(q_2 + q_3 + q_4)) - \\ & m_4*\cos(q_1)*\sin(q_1)*(a_3*\sin(q_2 + q_3) + a_2*\sin(q_2) - a_4*\cos(q_2 + q_3 + q_4))*(a_1 \\ & + a_3*\cos(q_2 + q_3) + a_2*\cos(q_2) + a_4*\sin(q_2 + q_3 + q_4)); \end{aligned}$$

$$\begin{aligned} M_{22} = & I_{zz2} + I_{zz3} + I_{zz4} + a_2^2*m_2 + a_2^2*m_4*(\cos(q_2) + a_3*\cos(q_2 + q_3) + \\ & a_4*\cos(q_2 + q_3 + q_4))^2 + a_2^2*m_3*(\cos(q_2) + a_3*\cos(q_2 + q_3))^2 + \\ & m_4*\cos(q_1)^2*(a_3*\sin(q_2 + q_3) + a_2*\sin(q_2) + a_4*\sin(q_2 + q_3 + q_4))^2 + \\ & m_4*\sin(q_1)^2*(a_3*\sin(q_2 + q_3) + a_2*\sin(q_2) - a_4*\cos(q_2 + q_3 + q_4))^2 + \\ & m_3*\cos(q_1)^2*(a_3*\sin(q_2 + q_3) + a_2*\sin(q_2))^2 + m_3*\sin(q_1)^2*(a_3*\sin(q_2 + \\ & q_3) + a_2*\sin(q_2))^2; \end{aligned}$$

$$M23=Izz3 + Izz4 + m4*\sin(q1)^2*(a3*\sin(q2 + q3) - a4*\cos(q2 + q3 + q4))*(a3*\sin(q2 + q3) + a2*\sin(q2) - a4*\cos(q2 + q3 + q4)) + m4*\cos(q1)^2*(a3*\sin(q2 + q3) + a4*\sin(q2 + q3 + q4))*(a3*\sin(q2 + q3) + a2*\sin(q2) + a4*\sin(q2 + q3 + q4)) + a2^2*m4*(a3*\cos(q2 + q3) + a4*\cos(q2 + q3 + q4))*(\cos(q2) + a3*\cos(q2 + q3) + a4*\cos(q2 + q3 + q4)) + a2^2*a3*m3*\cos(q2 + q3)*(\cos(q2) + a3*\cos(q2 + q3)) + a3*m3*\sin(q2 + q3)*\cos(q1)^2*(a3*\sin(q2 + q3) + a2*\sin(q2)) + a3*m3*\sin(q2 + q3)*\sin(q1)^2*(a3*\sin(q2 + q3) + a2*\sin(q2));$$

$$M24=Izz4 + a2^2*a4*m4*\cos(q2 + q3 + q4)*(\cos(q2) + a3*\cos(q2 + q3) + a4*\cos(q2 + q3 + q4)) - a4*m4*\cos(q2 + q3 + q4)*\sin(q1)^2*(a3*\sin(q2 + q3) + a2*\sin(q2) - a4*\cos(q2 + q3 + q4)) + a4*m4*\sin(q2 + q3 + q4)*\cos(q1)^2*(a3*\sin(q2 + q3) + a2*\sin(q2) + a4*\sin(q2 + q3 + q4));$$

$$M31=m4*\cos(q1)*\sin(q1)*(a3*\sin(q2 + q3) + a4*\sin(q2 + q3 + q4))*(a1 + a3*\cos(q2 + q3) + a2*\cos(q2) + a4*\cos(q2 + q3 + q4)) - m4*\cos(q1)*\sin(q1)*(a3*\sin(q2 + q3) - a4*\cos(q2 + q3 + q4))*(a1 + a3*\cos(q2 + q3) + a2*\cos(q2) + a4*\sin(q2 + q3 + q4));$$

$$M32=Izz3 + Izz4 + m4*\sin(q1)^2*(a3*\sin(q2 + q3) - a4*\cos(q2 + q3 + q4))*(a3*\sin(q2 + q3) + a2*\sin(q2) - a4*\cos(q2 + q3 + q4)) + m4*\cos(q1)^2*(a3*\sin(q2 + q3) + a4*\sin(q2 + q3 + q4))*(a3*\sin(q2 + q3) + a2*\sin(q2) + a4*\sin(q2 + q3 + q4)) + a2^2*m4*(a3*\cos(q2 + q3) + a4*\cos(q2 + q3 + q4))*(\cos(q2) + a3*\cos(q2 + q3) + a4*\cos(q2 + q3 + q4)) + a2^2*a3*m3*\cos(q2 + q3)*(\cos(q2) + a3*\cos(q2 + q3)) + a3*m3*\sin(q2 + q3)*\cos(q1)^2*(a3*\sin(q2 + q3) + a2*\sin(q2)) + a3*m3*\sin(q2 + q3)*\sin(q1)^2*(a3*\sin(q2 + q3) + a2*\sin(q2));$$

$$M33=Izz3 + Izz4 + m4*\cos(q1)^2*(a3*\sin(q2 + q3) + a4*\sin(q2 + q3 + q4))^2 + m4*\sin(q1)^2*(a3*\sin(q2 + q3) - a4*\cos(q2 + q3 + q4))^2 + a2^2*m4*(a3*\cos(q2 + q3) + a4*\cos(q2 + q3 + q4))^2 + a2^2*a3^2*m3*\cos(q2 + q3)^2 + a3^2*m3*\sin(q2 + q3)^2*\cos(q1)^2 + a3^2*m3*\sin(q2 + q3)^2*\sin(q1)^2;$$

$$M34=Izz4 - a4*m4*\cos(q2 + q3 + q4)*\sin(q1)^2*(a3*\sin(q2 + q3) - a4*\cos(q2 + q3 + q4)) + a4*m4*\sin(q2 + q3 + q4)*\cos(q1)^2*(a3*\sin(q2 + q3) + a4*\sin(q2 + q3 + q4)) + a2^2*a4*m4*\cos(q2 + q3 + q4)*(a3*\cos(q2 + q3) + a4*\cos(q2 + q3 + q4));$$

$$M41=a4*m4*\cos(q2 + q3 + q4)*\cos(q1)*\sin(q1)*(a1 + a3*\cos(q2 + q3) + a2*\cos(q2) + a4*\sin(q2 + q3 + q4)) + a4*m4*\sin(q2 + q3 + q4)*\cos(q1)*\sin(q1)*(a1 + a3*\cos(q2 + q3) + a2*\cos(q2) + a4*\cos(q2 + q3 + q4));$$

$$M42=Izz4 + a2^2*a4*m4*cos(q2 + q3 + q4)*(cos(q2) + a3*cos(q2 + q3) + a4*cos(q2 + q3 + q4)) - a4*m4*cos(q2 + q3 + q4)*sin(q1)^2*(a3*sin(q2 + q3) + a2*sin(q2) - a4*cos(q2 + q3 + q4)) + a4*m4*sin(q2 + q3 + q4)*cos(q1)^2*(a3*sin(q2 + q3) + a2*sin(q2) + a4*sin(q2 + q3 + q4));$$

$$M43=Izz4 - a4*m4*cos(q2 + q3 + q4)*sin(q1)^2*(a3*sin(q2 + q3) - a4*cos(q2 + q3 + q4)) + a4*m4*sin(q2 + q3 + q4)*cos(q1)^2*(a3*sin(q2 + q3) + a4*sin(q2 + q3 + q4)) + a2^2*a4*m4*cos(q2 + q3 + q4)*(a3*cos(q2 + q3) + a4*cos(q2 + q3 + q4));$$

$$M44=m4*a2^2*a4^2*cos(q2 + q3 + q4)^2 + m4*a4^2*cos(q2 + q3 + q4)^2*sin(q1)^2 + m4*a4^2*sin(q2 + q3 + q4)^2*cos(q1)^2 + Izz4;$$

$$MM = [M11 M12 M13 M14;M21 M22 M23 M24;M31 M32 M33 M34;M41 M42 M43 M44];$$

$$H1= m4*(cos(q1)*(a2*q2d*sin(q2) + a4*sin(q2 + q3 + q4)*(q2d + q3d + q4d) + a3*sin(q2 + q3)*(q2d + q3d)) + q1d*sin(q1)*(a1 + a3*cos(q2 + q3) + a2*cos(q2) + a4*cos(q2 + q3 + q4)))*(sin(q1)*(a2*q2d*sin(q2) + a4*sin(q2 + q3 + q4)*(q2d + q3d + q4d) + a3*sin(q2 + q3)*(q2d + q3d)) - q1d*cos(q1)*(a1 + a3*cos(q2 + q3) + a2*cos(q2) + a4*cos(q2 + q3 + q4))) - (m2*(2*cos(q1)*(a1 + a2*cos(q2))*(sin(q1)*(a1 + a2*cos(q2))*q1d^2 + 2*a2*cos(q1)*sin(q2)*q1d*q2d + a2*cos(q2)*sin(q1)*q2d^2) - 2*sin(q1)*(a1 + a2*cos(q2))*(cos(q1)*(a1 + a2*cos(q2))*q1d^2 - 2*a2*sin(q1)*sin(q2)*q1d*q2d + a2*cos(q1)*cos(q2)*q2d^2) - 2*q1d*cos(q1)*(q1d*sin(q1)*(a1 + a2*cos(q2)) + a2*q2d*cos(q1)*sin(q2))*(a1 + a2*cos(q2)) + 2*q1d*sin(q1)*(q1d*cos(q1)*(a1 + a2*cos(q2)) + a2*q2d*sin(q1)*sin(q2))*(a1 + a2*cos(q2)) - 2*a2*q2d*cos(q1)*sin(q2)*(q1d*cos(q1)*(a1 + a2*cos(q2)) + a2*q2d*sin(q1)*sin(q2)*(q1d*sin(q1)*(a1 + a2*cos(q2)) + a2*q2d*cos(q1)*sin(q2)))))/2 - m4*(cos(q1)*(a2*q2d*sin(q2) - a4*cos(q2 + q3 + q4)*(q2d + q3d + q4d) + a3*sin(q2 + q3)*(q2d + q3d)) + q1d*sin(q1)*(a1 + a3*cos(q2 + q3) + a2*cos(q2) + a4*sin(q2 + q3 + q4)))*(sin(q1)*(a2*q2d*sin(q2) - a4*cos(q2 + q3 + q4)*(q2d + q3d + q4d) + a3*sin(q2 + q3)*(q2d + q3d)) - q1d*cos(q1)*(a1 + a3*cos(q2 + q3) + a2*cos(q2) + a4*sin(q2 + q3 + q4))) - m3*sin(q1)*(a2*q2d*sin(q2) + a3*sin(q2 + q3)*(q2d + q3d))*(cos(q1)*(a2*q2d*sin(q2) + a3*sin(q2 + q3)*(q2d + q3d)) + q1d*sin(q1)*(a1 + a3*cos(q2 + q3) + a2*cos(q2)))) - m4*sin(q1)*(cos(q1)*(a2*q2d*sin(q2) + a4*sin(q2 + q3 + q4)*(q2d + q3d + q4d) + a3*sin(q2 + q3)*(q2d + q3d)) + q1d*sin(q1)*(a1 + a3*cos(q2 + q3) + a2*cos(q2)))*(a2*q2d*sin(q2) + a4*sin(q2 + q3 + q4)*(q2d + q3d + q4d) + a3*sin(q2 + q3)*(q2d + q3d)) + q1d*sin(q1)*(a1 + a3*cos(q2 + q3) + a2*cos(q2))));$$

$$\begin{aligned}
& q4)*(q2d + q3d + q4d) + a3*\sin(q2 + q3)*(q2d + q3d) - \\
& m3*\cos(q1)*(\sin(q1)*(a1 + a3*\cos(q2 + q3) + a2*\cos(q2))*q1d^2 + \\
& 2*\cos(q1)*(a2*q2d*\sin(q2) + a3*\sin(q2 + q3)*(q2d + q3d))*q1d + \\
& \sin(q1)*(a3*\cos(q2 + q3)*(q2d + q3d)^2 + a2*q2d^2*\cos(q2)))*(a1 + \\
& a3*\cos(q2 + q3) + a2*\cos(q2)) + m3*\sin(q1)*(a1 + a3*\cos(q2 + q3) + \\
& a2*\cos(q2))*(\cos(q1)*(a1 + a3*\cos(q2 + q3) + a2*\cos(q2))*q1d^2 - \\
& 2*\sin(q1)*(a2*q2d*\sin(q2) + a3*\sin(q2 + q3)*(q2d + q3d))*q1d + \\
& \cos(q1)*(a3*\cos(q2 + q3)*(q2d + q3d)^2 + a2*q2d^2*\cos(q2))) + \\
& m4*\sin(q1)*(\cos(q1)*(a1 + a3*\cos(q2 + q3) + a2*\cos(q2) + a4*\cos(q2 + q3 + \\
& q4))*q1d^2 - 2*\sin(q1)*(a2*q2d*\sin(q2) + a4*\sin(q2 + q3 + q4)*(q2d + q3d + \\
& q4d) + a3*\sin(q2 + q3)*(q2d + q3d))*q1d + \cos(q1)*(a3*\cos(q2 + q3)*(q2d + \\
& q3d)^2 + a2*q2d^2*\cos(q2) + a4*\cos(q2 + q3 + q4)*(q2d + q3d + q4d)^2))* \\
& (a1 + a3*\cos(q2 + q3) + a2*\cos(q2) + a4*\cos(q2 + q3 + q4)) - \\
& m4*\cos(q1)*(\sin(q1)*(a1 + a3*\cos(q2 + q3) + a2*\cos(q2) + a4*\sin(q2 + q3 + \\
& q4))*q1d^2 + 2*\cos(q1)*(a2*q2d*\sin(q2) - a4*\cos(q2 + q3 + q4)*(q2d + q3d \\
& + q4d) + a3*\sin(q2 + q3)*(q2d + q3d))*q1d + \sin(q1)*(a3*\cos(q2 + q3)*(q2d \\
& + q3d)^2 + a2*q2d^2*\cos(q2) + a4*\sin(q2 + q3 + q4)*(q2d + q3d + \\
& q4d)^2))* \\
& (a1 + a3*\cos(q2 + q3) + a2*\cos(q2) + a4*\sin(q2 + q3 + q4)) + \\
& m4*\cos(q1)*(\sin(q1)*(a2*q2d*\sin(q2) - a4*\cos(q2 + q3 + q4)*(q2d + q3d + \\
& q4d) + a3*\sin(q2 + q3)*(q2d + q3d)) - q1d*\cos(q1)*(a1 + a3*\cos(q2 + q3) + \\
& a2*\cos(q2) + a4*\sin(q2 + q3 + q4)))*(a2*q2d*\sin(q2) - a4*\cos(q2 + q3 + \\
& q4)*(q2d + q3d + q4d) + a3*\sin(q2 + q3)*(q2d + q3d)) + \\
& m3*\cos(q1)*(a2*q2d*\sin(q2) + a3*\sin(q2 + q3)*(q2d + q3d) + \\
& q3d))*(\sin(q1)*(a2*q2d*\sin(q2) + a3*\sin(q2 + q3)*(q2d + q3d)) - \\
& q1d*\cos(q1)*(a1 + a3*\cos(q2 + q3) + a2*\cos(q2))) + \\
& m3*q1d*\sin(q1)*(\sin(q1)*(a2*q2d*\sin(q2) + a3*\sin(q2 + q3)*(q2d + q3d)) - \\
& q1d*\cos(q1)*(a1 + a3*\cos(q2 + q3) + a2*\cos(q2)))*(a1 + a3*\cos(q2 + q3) + \\
& a2*\cos(q2)) + m4*q1d*\cos(q1)*(\cos(q1)*(a2*q2d*\sin(q2) + a4*\sin(q2 + q3 + \\
& q4)*(q2d + q3d + q4d) + a3*\sin(q2 + q3)*(q2d + q3d)) + q1d*\sin(q1)*(a1 + \\
& a3*\cos(q2 + q3) + a2*\cos(q2) + a4*\cos(q2 + q3 + q4)))*(a1 + a3*\cos(q2 + q3) \\
& + a2*\cos(q2) + a4*\cos(q2 + q3 + q4)) + \\
& m4*q1d*\sin(q1)*(\sin(q1)*(a2*q2d*\sin(q2) - a4*\cos(q2 + q3 + q4)*(q2d + q3d \\
& + q4d) + a3*\sin(q2 + q3)*(q2d + q3d)) - q1d*\cos(q1)*(a1 + a3*\cos(q2 + q3) + \\
& a2*\cos(q2) + a4*\sin(q2 + q3 + q4)))*(a1 + a3*\cos(q2 + q3) + a2*\cos(q2) + \\
& a4*\sin(q2 + q3 + q4)) + m3*q1d*\cos(q1)*(\cos(q1)*(a2*q2d*\sin(q2) + \\
& a3*\sin(q2 + q3)*(q2d + q3d)) + q1d*\sin(q1)*(a1 + a3*\cos(q2 + q3) + \\
& a2*\cos(q2)))*(a1 + a3*\cos(q2 + q3) + a2*\cos(q2));
\end{aligned}$$

$$\begin{aligned}
H2 = & m2*((2*a2*q1d*\cos(q1)*\sin(q2) + \\
& 2*a2*q2d*\cos(q2)*\sin(q1))*(q1d*\cos(q1)*(a1 + a2*\cos(q2)) - \\
& a2*q2d*\sin(q1)*\sin(q2)) - (2*a2*q2d*\cos(q1)*\cos(q2) - \\
& 2*a2*q1d*\sin(q1)*\sin(q2))*(q1d*\sin(q1)*(a1 + a2*\cos(q2)) + \\
& a2*q2d*\cos(q1)*\sin(q2)) + 2*a2^2*q2d^2*\cos(q2)*\sin(q2));
\end{aligned}$$

$$\begin{aligned}
N3= & m4*\cos(q1)*(a3*\sin(q2 + q3) + a4*\sin(q2 + q3 + q4))*(\cos(q1)*(a1 + \\
& a3*\cos(q2 + q3) + a2*\cos(q2) + a4*\cos(q2 + q3 + q4))*q1d^2 - \\
& 2*\sin(q1)*(a2*q2d*\sin(q2) + a4*\sin(q2 + q3 + q4)*(q2d + q3d + q4d) + \\
& a3*\sin(q2 + q3)*(q2d + q3d))*q1d + \cos(q1)*(a3*\cos(q2 + q3)*(q2d + q3d)^2 \\
& + a2*q2d^2*\cos(q2) + a4*\cos(q2 + q3 + q4)*(q2d + q3d + q4d)^2)) - \\
& m3*(\sin(q1)*(a2*q2d*\sin(q2) + a3*\sin(q2 + q3)*(q2d + q3d)) - \\
& q1d*\cos(q1)*(a1 + a3*\cos(q2 + q3) + a2*\cos(q2)))*(a3*\cos(q2 + \\
& q3)*\sin(q1)*(q2d + q3d) + a3*q1d*\sin(q2 + q3)*\cos(q1)) - \\
& m4*(\cos(q1)*(a4*\cos(q2 + q3 + q4)*(q2d + q3d + q4d) + a3*\cos(q2 + q3)*(q2d \\
& + q3d)) - q1d*\sin(q1)*(a3*\sin(q2 + q3) + a4*\sin(q2 + q3 + \\
& q4)))*(\cos(q1)*(a2*q2d*\sin(q2) + a4*\sin(q2 + q3 + q4)*(q2d + q3d + q4d) + \\
& a3*\sin(q2 + q3)*(q2d + q3d)) + q1d*\sin(q1)*(a1 + a3*\cos(q2 + q3) + \\
& a2*\cos(q2) + a4*\cos(q2 + q3 + q4))) - m4*(\sin(q1)*(a4*\sin(q2 + q3 + q4)*(q2d \\
& + q3d + q4d) + a3*\cos(q2 + q3)*(q2d + q3d)) + q1d*\cos(q1)*(a3*\sin(q2 + q3) \\
& - a4*\cos(q2 + q3 + q4)))*(\sin(q1)*(a2*q2d*\sin(q2) - a4*\cos(q2 + q3 + \\
& q4)*(q2d + q3d + q4d) + a3*\sin(q2 + q3)*(q2d + q3d)) - q1d*\cos(q1)*(a1 + \\
& a3*\cos(q2 + q3) + a2*\cos(q2) + a4*\sin(q2 + q3 + q4))) - a2^2*m4*(a3*\cos(q2 \\
& + q3) + a4*\cos(q2 + q3 + q4))*(q2d^2*\sin(q2) + a3*\sin(q2 + q3)*(q2d + q3d)^2 \\
& + a4*\sin(q2 + q3 + q4)*(q2d + q3d + q4d)^2) - m3*(\cos(q1)*(a2*q2d*\sin(q2) \\
& + a3*\sin(q2 + q3)*(q2d + q3d)) + q1d*\sin(q1)*(a1 + a3*\cos(q2 + q3) + \\
& a2*\cos(q2)))*(a3*\cos(q2 + q3)*\cos(q1)*(q2d + q3d) - a3*q1d*\sin(q2 + \\
& q3)*\sin(q1)) + m4*\cos(q1)*(a4*\cos(q2 + q3 + q4)*(q2d + q3d + q4d) + \\
& a3*\cos(q2 + q3)*(q2d + q3d))*(\cos(q1)*(a2*q2d*\sin(q2) + a4*\sin(q2 + q3 + \\
& q4)*(q2d + q3d + q4d) + a3*\sin(q2 + q3)*(q2d + q3d)) + q1d*\sin(q1)*(a1 + \\
& a3*\cos(q2 + q3) + a2*\cos(q2) + a4*\cos(q2 + q3 + q4))) + \\
& m4*\sin(q1)*(a3*\sin(q2 + q3) - a4*\cos(q2 + q3 + q4))*(\sin(q1)*(a1 + a3*\cos(q2 \\
& + q3) + a2*\cos(q2) + a4*\sin(q2 + q3 + q4))*q1d^2 + \\
& 2*\cos(q1)*(a2*q2d*\sin(q2) - a4*\cos(q2 + q3 + q4)*(q2d + q3d + q4d) + \\
& a3*\sin(q2 + q3)*(q2d + q3d))*q1d + \sin(q1)*(a3*\cos(q2 + q3)*(q2d + q3d)^2 \\
& + a2*q2d^2*\cos(q2) + a4*\sin(q2 + q3 + q4)*(q2d + q3d + q4d)^2)) + \\
& m4*\sin(q1)*(\sin(q1)*(a2*q2d*\sin(q2) - a4*\cos(q2 + q3 + q4)*(q2d + q3d + \\
& q4d) + a3*\sin(q2 + q3)*(q2d + q3d)) - q1d*\cos(q1)*(a1 + a3*\cos(q2 + q3) + \\
& a2*\cos(q2) + a4*\sin(q2 + q3 + q4)))*(a4*\sin(q2 + q3 + q4)*(q2d + q3d + q4d) \\
& + a3*\cos(q2 + q3)*(q2d + q3d)) - a2^2*a3*m3*\cos(q2 + q3)*(q2d^2*\sin(q2) + \\
& a3*\sin(q2 + q3)*(q2d + q3d)^2) + m4*q1d*\cos(q1)*(\sin(q1)*(a2*q2d*\sin(q2) \\
& - a4*\cos(q2 + q3 + q4)*(q2d + q3d + q4d) + a3*\sin(q2 + q3)*(q2d + q3d)) - \\
& q1d*\cos(q1)*(a1 + a3*\cos(q2 + q3) + a2*\cos(q2) + a4*\sin(q2 + q3 + \\
& q4)))*(a3*\sin(q2 + q3) - a4*\cos(q2 + q3 + q4)) - \\
& m4*q1d*\sin(q1)*(\cos(q1)*(a2*q2d*\sin(q2) + a4*\sin(q2 + q3 + q4)*(q2d + q3d \\
& + q4d) + a3*\sin(q2 + q3)*(q2d + q3d)) + q1d*\sin(q1)*(a1 + a3*\cos(q2 + q3) + \\
& a2*\cos(q2) + a4*\cos(q2 + q3 + q4)))*(a3*\sin(q2 + q3) + a4*\sin(q2 + q3 + q4)) \\
& + a3*m3*\sin(q2 + q3)*\cos(q1)*(\cos(q1)*(a1 + a3*\cos(q2 + q3) + \\
& a2*\cos(q2))*q1d^2 - 2*\sin(q1)*(a2*q2d*\sin(q2) + a3*\sin(q2 + q3)*(q2d +
\end{aligned}$$

$$\begin{aligned}
& q3d)) * q1d + \cos(q1) * (a3 * \cos(q2 + q3) * (q2d + q3d)^2 + a2 * q2d^2 * \cos(q2))) + \\
& a3 * m3 * \sin(q2 + q3) * \sin(q1) * (\sin(q1) * (a1 + a3 * \cos(q2 + q3) + \\
& a2 * \cos(q2)) * q1d^2 + 2 * \cos(q1) * (a2 * q2d * \sin(q2) + a3 * \sin(q2 + q3) * (q2d + \\
& q3d)) * q1d + \sin(q1) * (a3 * \cos(q2 + q3) * (q2d + q3d)^2 + a2 * q2d^2 * \cos(q2))) + \\
& a3 * m3 * \cos(q2 + q3) * \cos(q1) * (\cos(q1) * (a2 * q2d * \sin(q2) + a3 * \sin(q2 + \\
& q3) * (q2d + q3d)) + q1d * \sin(q1) * (a1 + a3 * \cos(q2 + q3) + a2 * \cos(q2))) * (q2d + \\
& q3d) + a3 * m3 * \cos(q2 + q3) * \sin(q1) * (\sin(q1) * (a2 * q2d * \sin(q2) + a3 * \sin(q2 + \\
& q3) * (q2d + q3d)) - q1d * \cos(q1) * (a1 + a3 * \cos(q2 + q3) + a2 * \cos(q2))) * (q2d + \\
& q3d) + a3 * m3 * q1d * \sin(q2 + q3) * \cos(q1) * (\sin(q1) * (a2 * q2d * \sin(q2) + \\
& a3 * \sin(q2 + q3) * (q2d + q3d)) - q1d * \cos(q1) * (a1 + a3 * \cos(q2 + q3) + \\
& a2 * \cos(q2))) - a3 * m3 * q1d * \sin(q2 + q3) * \sin(q1) * (\cos(q1) * (a2 * q2d * \sin(q2) + \\
& a3 * \sin(q2 + q3) * (q2d + q3d)) + q1d * \sin(q1) * (a1 + a3 * \cos(q2 + q3) + \\
& a2 * \cos(q2)));
\end{aligned}$$

$$\begin{aligned}
N4 = & m4 * (\cos(q1) * (a2 * q2d * \sin(q2) + a4 * \sin(q2 + q3 + q4) * (q2d + q3d + q4d) \\
& + a3 * \sin(q2 + q3) * (q2d + q3d)) + q1d * \sin(q1) * (a1 + a3 * \cos(q2 + q3) + \\
& a2 * \cos(q2) + a4 * \cos(q2 + q3 + q4))) * (a4 * q1d * \sin(q2 + q3 + q4) * \sin(q1) - \\
& a4 * \cos(q2 + q3 + q4) * \cos(q1) * (q2d + q3d + q4d)) + \\
& m4 * (\sin(q1) * (a2 * q2d * \sin(q2) - a4 * \cos(q2 + q3 + q4) * (q2d + q3d + q4d) + \\
& a3 * \sin(q2 + q3) * (q2d + q3d)) - q1d * \cos(q1) * (a1 + a3 * \cos(q2 + q3) + \\
& a2 * \cos(q2) + a4 * \sin(q2 + q3 + q4))) * (a4 * q1d * \cos(q2 + q3 + q4) * \cos(q1) - \\
& a4 * \sin(q2 + q3 + q4) * \sin(q1) * (q2d + q3d + q4d)) + a4 * m4 * \sin(q2 + q3 + \\
& q4) * \cos(q1) * (\cos(q1) * (a1 + a3 * \cos(q2 + q3) + a2 * \cos(q2) + a4 * \cos(q2 + q3 + \\
& q4)) * q1d^2 - 2 * \sin(q1) * (a2 * q2d * \sin(q2) + a4 * \sin(q2 + q3 + q4) * (q2d + q3d + \\
& q4d) + a3 * \sin(q2 + q3) * (q2d + q3d)) * q1d + \cos(q1) * (a3 * \cos(q2 + q3) * (q2d + \\
& q3d)^2 + a2 * q2d^2 * \cos(q2) + a4 * \cos(q2 + q3 + q4) * (q2d + q3d + q4d)^2)) - \\
& a2^2 * a4 * m4 * \cos(q2 + q3 + q4) * (q2d^2 * \sin(q2) + a3 * \sin(q2 + q3) * (q2d + \\
& q3d)^2 + a4 * \sin(q2 + q3 + q4) * (q2d + q3d + q4d)^2) - a4 * m4 * \cos(q2 + q3 + \\
& q4) * \sin(q1) * (\sin(q1) * (a1 + a3 * \cos(q2 + q3) + a2 * \cos(q2) + a4 * \sin(q2 + q3 + \\
& q4)) * q1d^2 + 2 * \cos(q1) * (a2 * q2d * \sin(q2) - a4 * \cos(q2 + q3 + q4) * (q2d + q3d \\
& + q4d) + a3 * \sin(q2 + q3) * (q2d + q3d)) * q1d + \sin(q1) * (a3 * \cos(q2 + q3) * (q2d \\
& + q3d)^2 + a2 * q2d^2 * \cos(q2) + a4 * \sin(q2 + q3 + q4) * (q2d + q3d + q4d)^2)) - \\
& a4 * m4 * q1d * \cos(q2 + q3 + q4) * \cos(q1) * (\sin(q1) * (a2 * q2d * \sin(q2) - a4 * \cos(q2 \\
& + q3 + q4) * (q2d + q3d + q4d) + a3 * \sin(q2 + q3) * (q2d + q3d)) - \\
& q1d * \cos(q1) * (a1 + a3 * \cos(q2 + q3) + a2 * \cos(q2) + a4 * \sin(q2 + q3 + q4))) - \\
& a4 * m4 * q1d * \sin(q2 + q3 + q4) * \sin(q1) * (\cos(q1) * (a2 * q2d * \sin(q2) + a4 * \sin(q2 \\
& + q3 + q4) * (q2d + q3d + q4d) + a3 * \sin(q2 + q3) * (q2d + q3d)) + \\
& q1d * \sin(q1) * (a1 + a3 * \cos(q2 + q3) + a2 * \cos(q2) + a4 * \cos(q2 + q3 + q4))) + \\
& a4 * m4 * \cos(q2 + q3 + q4) * \cos(q1) * (\cos(q1) * (a2 * q2d * \sin(q2) + a4 * \sin(q2 + q3 \\
& + q4) * (q2d + q3d + q4d) + a3 * \sin(q2 + q3) * (q2d + q3d)) + q1d * \sin(q1) * (a1 + \\
& a3 * \cos(q2 + q3) + a2 * \cos(q2) + a4 * \cos(q2 + q3 + q4))) * (q2d + q3d + q4d) + \\
& a4 * m4 * \sin(q2 + q3 + q4) * \sin(q1) * (\sin(q1) * (a2 * q2d * \sin(q2) - a4 * \cos(q2 + q3
\end{aligned}$$

$$+ q4)*(q2d + q3d + q4d) + a3*\sin(q2 + q3)*(q2d + q3d) - q1d*\cos(q1)*(a1 + a3*\cos(q2 + q3) + a2*\cos(q2) + a4*\sin(q2 + q3 + q4)))*(q2d + q3d + q4d);$$

$$N=[N1;N2;N3;N4];$$

$$G1=0;$$

$$G2=a2*m2*\cos(q2) + a2*m4*(\cos(q2) + a3*\cos(q2 + q3) + a4*\cos(q2 + q3 + q4)) + a2*m3*(\cos(q2) + a3*\cos(q2 + q3));$$

$$G3= a2*m4*(a3*\cos(q2 + q3) + a4*\cos(q2 + q3 + q4)) + a2*a3*m3*\cos(q2 + q3);$$

$$G4= a2*a4*m4*\cos(q2 + q3 + q4);$$

$$G=[G1;G2;G3;G4];$$

APPENDIX C

PRE-TEST QUESTIONNAIRE

NAME:

AGE:

GENDER:

How many times have you used a VR simulator?

1. 0
2. 1-2 times
3. 2-5 times
4. 5-10 times
5. More than 10 times

How many times have you used a haptic device before?

1. 0
2. 1-2 times
3. 2-5 times
4. 5-10 times
5. More than 10 times

Area of application:

Do you have any touch impaired diagnosis?

- No
- Yes, please specify

POST TEST QUESTIONNAIRE

NAME:

Please rank and rate the interfaces (from 1-5) in context to the questions.

5-excellent 4-good 3-average 2-poor 1-very poor

What is the interface performance based on ease of operation during loading?

- Normal joystick control
- Haptic Feedback Joystick
- Haptic Joystick with audio cues

What is interface performance based on perception of risks?

- Normal joystick control
- Haptic Feedback Joystick
- Haptic Joystick with audio cues

What are the reliabilities of the interfaces in the loading operations?

- Normal joystick control
- Haptic Feedback Joystick
- Haptic Joystick with audio cues

How do you rate the interfaces for backhoe operations (based on your preference)?

- Normal joystick control
- Haptic Feedback Joystick
- Haptic Joystick with audio cues

Do you have any feedbacks/comments/suggestions regarding the experiments?

Do you have any suggestion for the improvement of the haptic joystick?

MEERA C S



EDUCATION

- | | | |
|-----------|---|---------|
| PG | M.Tech in Robotics Engineering
University of Petroleum and Energy Studies (UPES) | 2013-15 |
| UG | B.Tech in Electronics and Instrumentation Engineering
Cochin University of Science and Technology (CUSAT) | 2008-12 |

JOURNAL PUBLICATIONS

- **Meera C S**, Piniseti Swami Sairam, Adarsh Kumar, Mukul Kumar Gupta, “*Design and Analysis of New Haptic Joysticks for Enhancing Operational Skills in Excavator Control*”, Journal of Mechanical Design, ASME (Under Review)
- Alex Barre, **Meera C S**, Mukul Kumar Gupta and Santhakumar Mohan, “*Development and motion control of a spatial serial robotic manipulator under varying disturbances*”, World Journal of Engineering, vol. 16, no. 4, pp. 460–467, 2019.doi: 10.1108/WJE-02-2019-0052
- **Meera C S**, Mukul Kumar Gupta and Santhakumar Mohan, “*Disturbance observer-assisted hybrid control for autonomous manipulation in a robotic backhoe*” Archive of Mechanical Engg., vol. 66, no. 2, pp. 153–169, 2019. Doi: 10.24425/ame.2019.128442
- **Meera C S**, Mukul Kumar Gupta, “*Modelling & Position Control for Electro-Hydraulic System*”, International Journal of Recent Technology and Engineering, vol. 8, no:4, pp- 3841-3845.doi: 10.35940/ijrte.D8217.118419